

ARGONNE NATIONAL LABORATORY
9700 South Cass Avenue
Argonne, Illinois 60440

A MULTIPURPOSE NEUTRON DIFFRACTOMETER

by

Masao Atoji

Chemistry Division

July 1964

Operated by The University of Chicago
under
Contract W-31-109-eng-38
with the
U. S. Atomic Energy Commission

DISCLAIMER

This report was prepared as an account of work sponsored by an agency of the United States Government. Neither the United States Government nor any agency Thereof, nor any of their employees, makes any warranty, express or implied, or assumes any legal liability or responsibility for the accuracy, completeness, or usefulness of any information, apparatus, product, or process disclosed, or represents that its use would not infringe privately owned rights. Reference herein to any specific commercial product, process, or service by trade name, trademark, manufacturer, or otherwise does not necessarily constitute or imply its endorsement, recommendation, or favoring by the United States Government or any agency thereof. The views and opinions of authors expressed herein do not necessarily state or reflect those of the United States Government or any agency thereof.

DISCLAIMER

Portions of this document may be illegible in electronic image products. Images are produced from the best available original document.



TABLE OF CONTENTS

<u>Chapter</u>	<u>Page</u>
GENERAL INTRODUCTION	7
1. BASIC DIFFRACTOMETER	9
1-1. Introduction.	9
1-2. Graphite Collimator and Moderator	10
1-3. Primary Collimator	14
1-4. Monochromator Unit	17
1-5. Biological Shield	21
1-6. Secondary Collimators	23
1-7. Diffraction Turntable	24
1-8. Counter Shield	27
1-9. Counter Collimators and Beam Slits	30
1-10. Installation and Alignment	31
1-11. Basic Electronics.	34
1-12. Neutron Monitor and Detectors	40
2. AUXILIARY INSTRUMENTATION	44
2-1. Specimen Encasement.	44
2-2. Goniometric Devices.	46
2-3. Total Cross-section Experiment	47
2-4. Design of Diffraction Electromagnet	50
2-5. Magnet Experimental Data	56
2-6. Magnet Orienter.	60
2-7. Angular Dewar Assembly.	65
2-8. Angular Cryo-goniometer	69
2-9. Auxiliary Cryogenic Devices	76
2-10. Discussion of Cryogenic Instrumentation	80
2-11. Diffraction Furnaces.	84
APPENDIX I. Transmission Reference Data.	95
APPENDIX II. Neutron Filters	98
SPECIAL TOPIC. Symmetry Operators of Magnetic Groups	101
ACKNOWLEDGMENTS	108
REFERENCES	109
General References	109
Reference Books	116
Review Articles	118

LIST OF FIGURES

<u>No.</u>	<u>Title</u>	<u>Page</u>
1.	Plan View of the Neutron Diffractometer, Showing the Major Components in a Typical Setting.	11
2.	A Perspective Side View of the Diffractometer, Where the Secondary-collimator Axis is Assumed to be Parallel to the Primary-beam Direction for Illustrative Purpose	12
3.	Sub- and Epi-Cadmium Neutron Fluxes vs. the Graphite-moderator Length at the H-24 Beam Hole of the CP-5 Reactor Operated at 4.6 MW.	14
4.	Design Features of the Soller Collimator	16
5.	Block Diagram of the Basic Electronics	34
6.	Part of the Electronics Instruments.	35
7.	Schematic Drawing of the Drum-shaped Fission Counter with a Cadmium Diaphragm	41
8.	Neutron Diffraction Patterns of Nickel Powder	43
9.	A Compression Device for Preparing a Neutron Powder Sample Having Small Coherent-scattering and Low Capture Cross Sections.	45
10.	The Fine-slit Assembly with the Universal Goniometer Head Mounted on the Ω - and Height-adjustable Support.	46
11.	Typical Transmission-cell Setting in the Slit Box.	48
12.	Experimental Results for the Total Cross Section Obtained with Cu (111) Monochromatic Neutrons ($\lambda = 1.0683 \text{ \AA}$).	50
13.	Construction of the Diffraction Electromagnet.	51
14.	Block Diagram of the Cooling System and the Safety Devices for the Diffraction Electromagnet	55
15.	The Magnet-cooling System and the Auxiliary Safety Devices (below the Reactor Floor)	55
16.	The Magnetic Flux Density at the Center of the Gap as a Function of the Energizing Current	56
17.	The Magnetic Flux Density as a Function of the Air-gap Distance and Energizing Current.	56
18.	The Magnetic-field Homogeneity Curves.	57
19.	The Magnetic-field Homogeneity Curves.	57

LIST OF FIGURES

<u>No.</u>	<u>Title</u>	<u>Page</u>
20.	The Curves Representing the Field-homogeneity Dependency on the Air-gap Distance.	58
21.	The Liquid-Helium Angular Dewar with the Cryo-goniometric Device Mounted on the Diffraction Electromagnet.	59
22.	The Diffractometer Assembly with the Liquid-Helium Angular Dewar Mounted on the Electromagnet in the Setting for $X_{\parallel} = 0^{\circ}$	61
23.	The Setting at $X_{\parallel} = 45^{\circ}$	61
24.	The Side View at $X_{\parallel} = 45^{\circ}$	62
25.	The Setting at $X_{\parallel} = 90^{\circ}$	62
26.	The Design Detail of the Single-crystal Cryo-goniometer in the Liquid-Helium Angular Dewar	67
27.	Photographs of the Goniometer and Related Components for the Liquid-Helium Angular Dewar Assembly	70
28.	Design Features of the Remote-control Mechanism for the Cryo-goniometer	71
29.	The Cryo-goniometer in the Sample-aligning Assembly.	74
30.	The Sample-housing Construction in the Liquid-Helium Straight Dewar.	76
31.	Liquid-Helium Dewar Mounted on the Universal Goniometer Head	77
32.	A Variable-temperature Sample Holder for the Angular Dewar	82
33.	The High-temperature Diffraction Furnace (M-1) to be Mounted on the Large Goniometer Head	85
34.	The Low and Upper Inconel Bases and the Aluminum Mantle of the M-1 Furnace.	86
35.	Examples of Furnace Elements.	86
36.	The M-1 Diffraction Furnace with the Ion-getter Vacuum Pump Mounted on the Goniometer Head	87
37.	The Magneto-diffraction Furnace	88
38.	The Magneto-diffraction High-temperature Goniometer.	89

LIST OF FIGURES

<u>No.</u>	<u>Title</u>	<u>Page</u>
39.	Variations of Neutron Wavelength, Temperature, and Velocity with the Energy in Thermal and Near-thermal Regions	99
40.	A Reference Diagram for Selecting the α -Pu ²³⁹ Resonance Filter.	100
S-1.	Bravais-Shubnikov Lattices	101
S-2.	Bravais-Shubnikov Lattices (Continued)	102
S-3.	Symmetry Operators of the Axial-vector Space Groups	102
S-4.	Symmetry Operators of the Axial-vector Space Groups (Continued)	103
S-5.	Symmetry Operators of the Axial-vector Space Groups (Continued)	104
S-6.	Symmetry Operators of the Axial-vector Space Groups (Continued)	105
S-7.	Symmetry Operators of the Axial-vector Space Groups (Continued)	106

LIST OF TABLES

<u>No.</u>	<u>Title</u>	<u>Page</u>
I.	Input Tape Format	36
II.	Output Data Format	39
III.	Transmission Data for Selected Materials	95
IV.	Characteristics of the Resonance Filters Computed for the Naturally Occurring Elements Except for Pu ²³⁹	99

A MULTIPURPOSE NEUTRON DIFFRACTOMETER

by

Masao Atoji

GENERAL INTRODUCTION

The most unique application of neutron diffraction is in the study of the scattering phenomena due to interaction between the neutron magnetic moment and the magnetic moment of the atom, since neither X-ray nor electron diffraction can furnish information regarding the electronic spin structure. Crystal structure analysis is frequently a necessary preliminary to the magnetic study. Because of the scattering-amplitude characteristics, the neutron-diffraction technique has often played more than just a complementary role to X-ray and electron methods.

For pursuing these two major subjects, an automatic double-crystal neutron diffractometer, designed for both crystal and magnetic structure analyses at temperatures from 2°K to approximately 2000°K, and with a magnetic field of up to 18 kGauss for a 1.4-in. gap, has been constructed at the CP-5 reactor in the Argonne National Laboratory. The diffractometer is, primarily intended for study of thermal-neutron elastic scattering by poly- and single-crystal substances. Limited studies of the inelastic scattering, the total and related cross sections, and the small-angle scattering can also be accomplished. Nonpolarized beams of neutrons are used. Incorporation of the polarized-beam technique, on the other hand, would require some alterations of the beam-guide components and additional electronic control systems.

Our multiple objective was not satisfactorily fulfilled by any of the functioning diffractometers at various laboratories. Of course, exemplary design features originating from diffraction groups elsewhere were extensively incorporated. However, proper hybridization of the integral parts contrived for specific individual objectives in different environments required substantial modifications of most of the original designs. Consequently, even for those adequately developed by other groups, considerable engineering and instrumental studies were carried out with intention of improving their functional characteristics.

The engineering design was started late in 1960, and construction of the diffractometer was commenced early in 1961. The basic diffractometer components were assembled in mid-1962, and the first diffraction pattern was obtained through manual operation in June 1962. The electronic units for the four-angle automatic operation were tested in late 1962. At about this time the high- and low-temperature instruments

designed primarily for the crystallographic studies were completed. The electromagnet unit equipped for operation at high and low temperatures became operational in mid-1963. At the same time that diffraction experiments were being carried out, some improvements of various components were made during 1963 to 1964.

Besides outlining construction and instrumentation of our neutron diffractometer and its auxiliary equipments,* the present report includes a critical evaluation on the unit, the experimental results representing the instrumental characteristics, and tables, diagrams, and formulae which would be useful for practical neutron studies. A list of selected reference books and review articles are given. Caglioti et al. (1959) have also compiled bibliographies for neutron diffraction and scattering studies. In spite of our limited categorical selection, numerous additions in the present list reflect vividly the growth potential of the field.

*The construction and assembly drawings of the basic diffractometer and some of its auxiliary equipments have been designated by the Argonne National Laboratory as "Neutron Diffraction Spectrometer, MA, CS-2671 series," which are available upon request to the author.

1. BASIC DIFFRACTOMETER

1-1. Introduction

During the several-year period following construction of the first neutron diffractometer, pile neutrons were used at Argonne (Zinn, 1947), for only a few other high-flux neutron sources were available for diffraction studies. Other diffraction equipment was used by Wollan and Shull (1948) of Oak Ridge, Hurst et al. (1950) of Chalk River, and Bacon et al. (1950) and Lowde (1951) at Harwell. However, during the last decade, booming research-reactor construction throughout the world has accelerated diffractometer activity, and a wide variety of units are now in operation. A complete up-to-date review of this rapidly developing subject is difficult, and only those reports on the basic diffractometer are cited in the following.

Some progress reviews have been given in Pile Neutron Research in Physics (International Atomic Energy Agency, 1962, abbreviated IAEA hereafter). Two other Argonne diffractometers designed for the crystallographic analysis have been reported by Mueller et al. (1962), and a unit for powder and liquid studies by Clayton and Heaton (1961). The Brookhaven contributions are represented by Corliss et al. (1953), Pepinsky et al. (1954), Pepinsky and Frazer (1955), Langdon and Frazer (1959), and Prince and Abrahams (1959). The Livermore instrument was briefly introduced by Mead and Sparks (1960). Three MIT units have been described in detail by Shull (1960), and a diffractometer at the Naval Research Laboratory by Prince (1961). Compendia of the Oak Ridge diffractometers, distinctly divided into the crystallographic and magnetic categories, have been given by Peterson and Levy (1959) for the former and by Wollan et al. (1960) for the latter (see also IAEA-1962, pp. 53-55). Takei et al. (1960) constructed the Westinghouse apparatus. The details about the instruments at Los Alamos, Puerto Rico Nuclear Center, Washington State University, and several other locations have not been reported.

The Harwell designs have been well reported (Arndt and Willis, 1963; Bacon and Dyer, 1955, 1959; Bowes and Dyer, 1963; Lambe et al., 1961; Pattenden and Baston, 1957; Willis, 1962). The AEI unit has been described by Allenden and Winkworth (1963). The Chalk River instruments were outlined by Brockhouse (IAEA-1962, pp. 36-37) and McAlpin (1964), and the one at the McMaster University by Petch et al. (1960). The Australian center is also becoming active (see Sabine, 1962). A French diffractometer has been described by Breton et al. (1957). In Germany, the Munich units have been reported by Dachs and his co-workers (1961-1962), Lutz (1960), and a group at Maschinen Fabrik Augsburg-Nuremburg (1960). A diffractometer at Rossendorf, Dresden, has been described by Betzl and Kleinstück (1961) and Kleinstück (1961). Szabó et al. (1963) have reported their instrument in Hungary, and Caglioti et al. (1962) and Giacchetti et al. (1963) have summarized

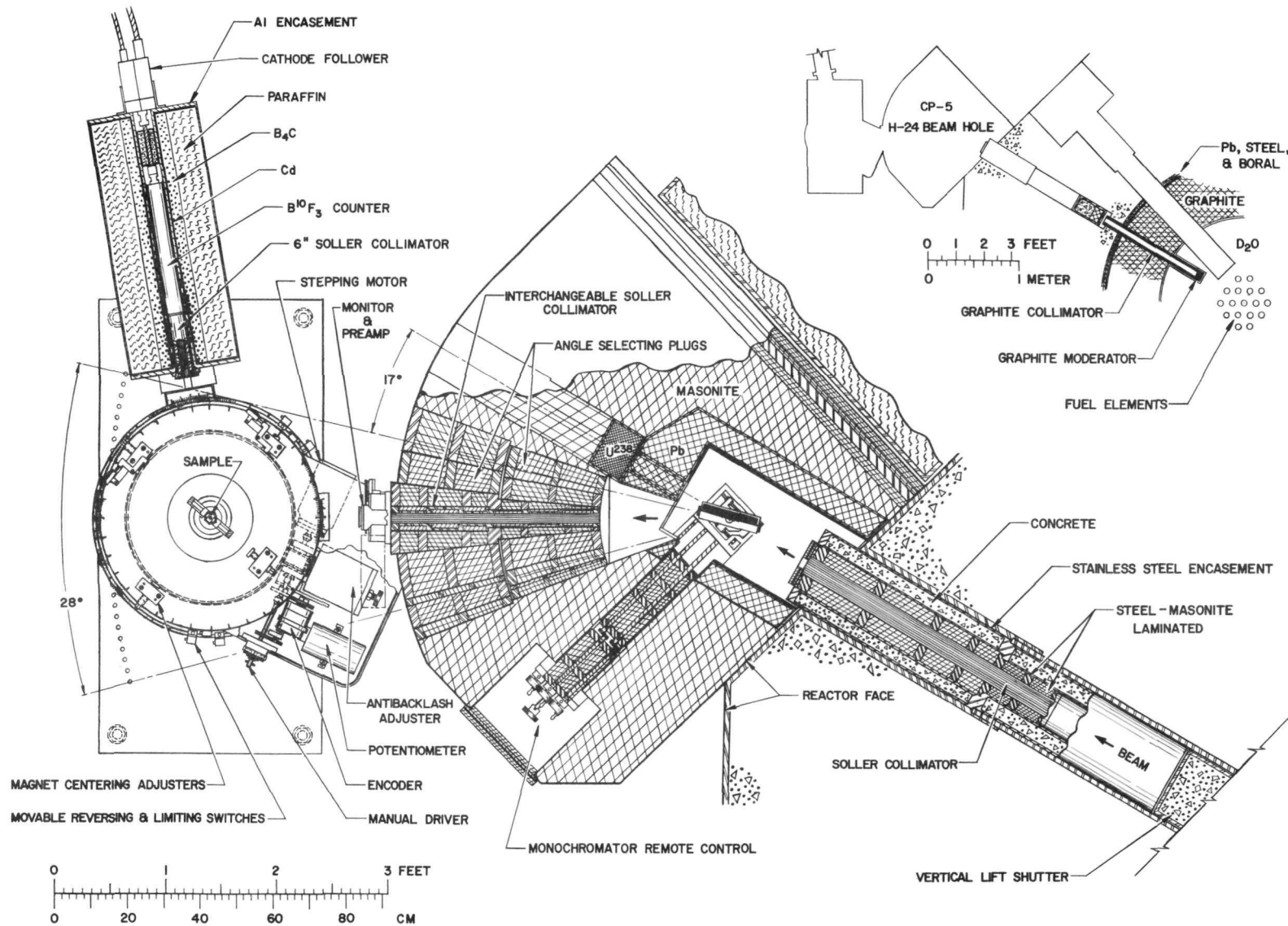
the Italian work. Loopstra (1962) has led Netherlands' neutron diffraction group, and the Norwegian units are delineated in papers by Barstad and Andresen (1957) and Goedkoop and Loopstra (1959). The Polish apparatus has been described by O'Connor and Bónkowski (1959) (IAEA-1962, pp. 369-378, and Krasnicki et al. (1962). The Spanish unit has recently been constructed by Ponce de Leon and Diaz (1962). The USSR activity is described in various publications (Bykov et al., 1957; Ozerov et al., 1960; Yamzin, 1959; Yamzin et al., 1962, 1963; Zivanović et al., 1961, of Czechoslovakia). Two diffractometers at Trombay, India, have been reported by Iyengar (1963). Japanese diffractometers were constructed by Hagihara et al. (1962), Kunitomi et al. (1962), and Miyake et al. (1962), and the one in China by Ang et al. (1961).

Assembly layouts of our diffractometer are shown in Figs. 1 and 2, which are referred to very frequently in the following chapters. The diffractometer follows a normal-beam equatorial mode. The design had to take into account geometrical restrictions arising from a limited working space and the assigned beam-hole configuration. These restrictions acted as a determining factor in some design-parameter calculations and, in a few cases, forced us to choose lower-degree parameters. Examples where unavoidable geometrical factors had to be taken are: the collimator length; locations of the monochromator and its remote-control device; the angular range for the monochromatic beam output and that for the detecting counter; and the shape of the biological shield.

Utilization of a single primary beam for two diffractometers has been adapted by several investigators (Bacon and Dyer, 1959; Miyake et al., 1962; Mueller et al., 1962; Peterson and Levy, 1959; Willis, 1962). However, the dual-diffractometer technique was found to be rather unsuitable for our case, because, in addition to the space limitation mentioned above, the interference between the second diffractometer and the large auxiliary instruments, such as the magnetic devices, is too severe to be tolerable in practice. Nevertheless, an auxiliary beam outlet was made to meet with a possible future development of a miniature diffractometer or a small neutron-diffraction camera.

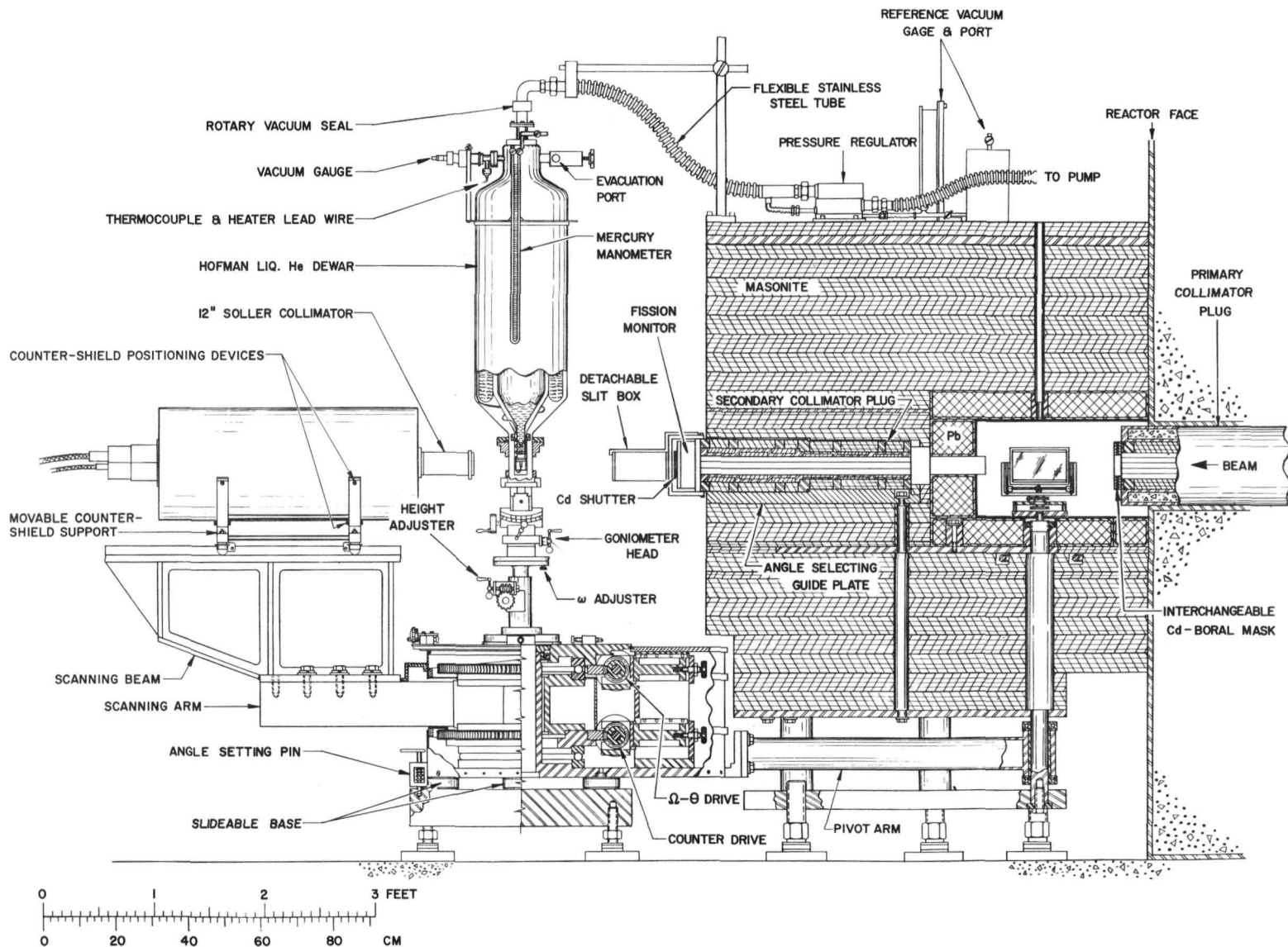
1-2. Graphite Collimator and Moderator

The in-pile collimator is separated by the vertical lift shutter into two parts, graphite and primary collimators. The graphite collimator, reinforced by an aluminum framework, is placed at the initial section of the beam port as a coarse, preliminary collimator. It starts at 21.25 in. from the reactor-core center and is a hollow cylinder, 48 in. long and 3.62 in. in diameter, with a rectangular through-opening of 2.01 x 2.74 in. (horizontal x vertical). The horizontal and vertical angular divergencies are 2°24' and 3°16' of arc, respectively. The first 14.75 in. section of the collimator lies within the core-tank interior. The center of the beam port is 42 in. from the reactor floor.



120-7767

Fig. 1. Plan View of the Neutron Diffractometer, Showing the Major Components in a Typical Setting. The single-crystal diffraction mode with the heavy-duty counter-shield is shown.



120-7769 Rev.

Fig. 2. A Perspective Side View of the Diffractometer, Where the Secondary-collimator Axis is Assumed to be Parallel to the Primary-beam Direction for Illustrative Purpose. Also shown are the liquid-helium straight-Dewar assembly with a vapor pressure controller for regulating the refrigerant temperature (cf. Fig. 31).

The average temperature of circulating D_2O in the core tank is about $44^\circ C$ (maximum fluctuation, $\pm 4^\circ C$)* and that at the graphite-reflector zone ranges from 75 to $100^\circ C$. However, some sections in the beam-port area within the graphite zone are occasionally heated to nearly $300^\circ C$, due partly to poor local dissipation of heat arising from exothermic nuclear and chemical reactions induced by neutrons and γ rays.

The neutron and γ -ray fluxes are high enough to produce, directly or indirectly, appreciable amounts of dissociated species of N_2 , O_2 , and H_2O in the atmosphere, and their corrosive action on the metal is by no means trivial in long-range operation. Consequently, with a safety factor of about 1.5 on the temperature scale, the in-pile collimator components, particularly those at the front half-section of the beam port, should satisfy the following conditions: melting point higher than $500^\circ C$; good thermal conductor in order to avoid further temperature rise; high corrosion resistance. In addition, relatively large thermal expansion of the collimator elements must be taken into consideration. Water cooling or other means of heat dissipation is rather impractical for our beam-port configuration.

The flux-vs.-energy distribution of the neutrons emerging through the beam port plays an important role in the diffractometer design.** Hence, at the initial stage of the project, a highly collimated neutron flux at 128.38 in. from the core center (2.75 in. outside of the reactor outer wall) was measured for varying thickness of the graphite block filling the entrance of the graphite collimator. A gold-foil detector, precalibrated with a standard pile, was placed at the exit of the port plug, 41.4 in. long, with a through axial hole, 0.0456 in.^2 in cross-sectional area. The tangential divergency of the beam was $20'$ of arc. The result shown in Fig. 3 indicates the cadmium-ratio maximum at about 24 in. of the graphite length, where the epi-cadmium contamination is less than 0.1% of the total flux but the sub-cadmium flux drops down to $2 \times 10^7 \text{ neutrons cm}^{-2} \text{ sec}^{-1}$. Since the double-crystal diffraction process selects out a large portion of the epi-cadmium neutrons, the condition for the highest thermal flux may be chosen, provided that: the fast-neutron shielding meets with the space limitation; neutrons scattered through the monochromatic beam-channel is a small fraction of the background in the diffraction pattern. The length of the moderator thus chosen is 4 in., which gives the sub-cadmium flux of 1.4×10^8 with 1% epi-cadmium contamination in the $20'$ -arc collimation. The sub- and epi-cadmium fluxes outside the graphite moderator are 1.5×10^8 and $7 \times 10^6 \text{ n cm}^{-2} \text{ sec}^{-1}$, respectively. Hence, we have practically no loss in the sub-cadmium flux due to the 4 in. graphite, which on the other hand reduces the epi-cadmium contamination from 4% to 1%. The maximum flux lies at about 1.2 \AA (corresponding to $420^\circ K$; see Fig. 39) in the Maxwellian distribution.

*The Maxwellian neutron temperature of $44 \pm 4^\circ C$ corresponds to a neutron energy of $0.0410 \pm 0.005 \text{ eV}$, and, to a wavelength of $1.413 \pm 0.009 \text{ \AA}$.

**Most diffractometers are designed for neutron wavelengths longer than about 0.5 \AA , i.e., not too far shorter than the cadmium-thermal-resonance wavelength, 0.6779 \AA .

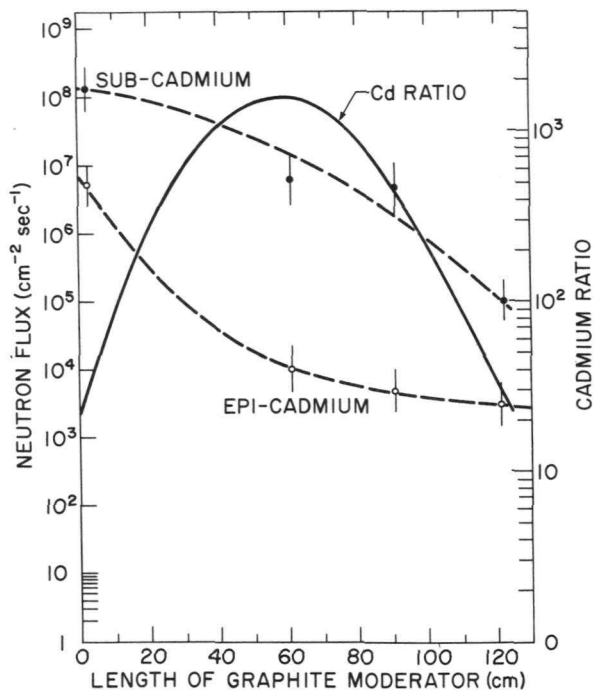


Fig. 3

Sub- and Epi-Cadmium Neutron Fluxes vs. the Graphite-moderator Length at the H-24 Beam Hole of the CP-5 Reactor Operated at 4.6 MW. The detector is placed at 326 cm (10.7 ft) from the reactor-core center and the beam divergence is 20' of arc. The cadmium-ratio values were obtained from the smoothed-out experimental curves.

120-8560

At the central region of the CP-5 reactor core operated at 4.6 MW, the sub- and epi-cadmium fluxes are approximately 5×10^{13} and $3 \times 10^{13} \text{ n cm}^{-2} \text{ sec}^{-1}$, in the 4π -counting geometry, respectively. At about 18 in. from the core center, where the cadmium ratio reaches its maximum, the sub-cadmium flux is nearly $10^{14} \text{ n cm}^{-2} \text{ sec}^{-1}$, while the epi-cadmium neutrons are moderated to $10^{12} \text{ n cm}^{-2} \text{ sec}^{-1}$. Near the core-tank wall encompassing the core with the 36-in. radius, fluxes of 2×10^{13} for sub-cadmium and of $4 \times 10^{11} \text{ n cm}^{-2} \text{ sec}^{-1}$ for the epi-cadmium have been recorded. Hence, the uncollimated flux at our beam-port entrance is estimated as 7×10^{13} for sub-cadmium and $7 \times 10^{11} \text{ n cm}^{-2} \text{ sec}^{-1}$ for epi-cadmium. The 20'-arc-collimated sub-cadmium flux without the graphite moderator is calculated to be $1.5 \times 10^8 \text{ n cm}^{-2} \text{ sec}^{-1}$, in excellent agreement with the observed value of $1.5 \times 10^8 \text{ n cm}^{-2} \text{ sec}^{-1}$; the calculated epi-cadmium flux is $1.5 \times 10^6 \text{ n cm}^{-2} \text{ sec}^{-1}$, considerably smaller than the observed flux $7 \times 10^6 \text{ n cm}^{-2} \text{ sec}^{-1}$. The disagreement between the fast-neutron flux and the experimental curves in Fig. 3 are not readily interpretable quantitatively, because of the complex geometry of the beam-port entry and because of far more complicated processes of diffusion, moderation, and absorption of the fast neutrons. Large preferred orientation of the microcrystals in the graphite block manufactured through an extrusion process makes, among other causes, the interpretation more ambiguous (Egelstaff, 1957).

1-3. Primary Collimator

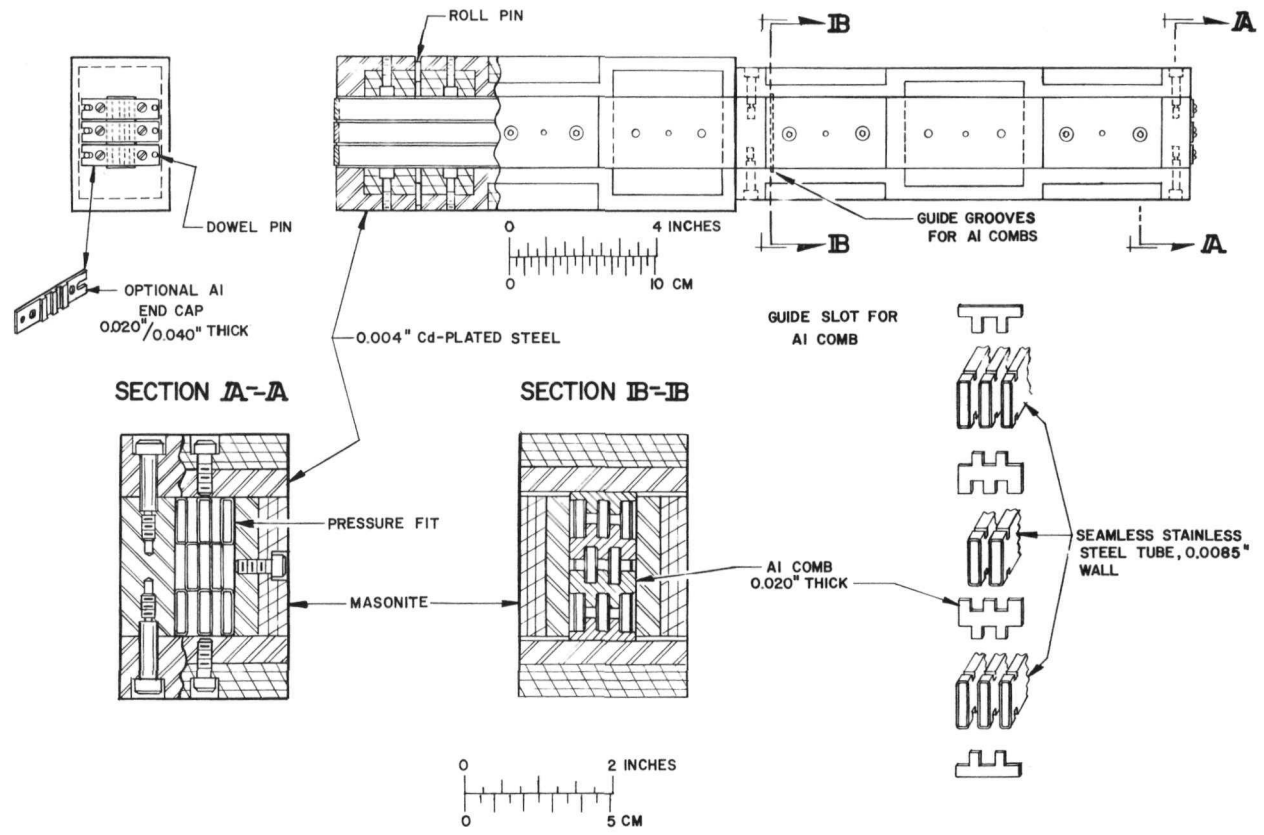
The quality of the diffraction data depends strongly on the choice of three major collimators (primary, secondary, and counter collimators). A number of authors has dealt with the thermal-neutron collimation problems

to various extents (Atoji, 1961b; Caglioti et al., 1958; Caglioti et al., 1960; Caglioti and Ricci, 1962; Dachs, 1961; Jones, 1962; Jones and Bartolini, 1963; Hase and Kleinstück, 1961; Sabine and Browne, 1963; Sailor et al., 1956; Schermer, 1960; Szabo, 1959, 1960a, 1960b; Willis, 1960a). The primary collimator, following the graphite coarse collimator and the vertical lift shutter, is not easily exchangeable in the present design. Hence, it has to accommodate all of the specific intensity-resolution requirements for current and conceivable future experiments, or a compromise design may be chosen. Hagihara et al. (1962) have constructed an elaborate primary-collimator unit consisting of three collimators of different horizontal divergence (5', 15', and 30' of arc), stacked normal to the collimator axes. A remote-control mechanism places a selected one into the beam. An arrangement of this sort is, however, unworkable with our beam-port configuration, and cumulative divergence variations can be attained by the secondary and counter collimators to a certain extent.

The primary-collimator unit is composed of two parts: the collimator and its adapter. The adapter is a 1.75-in.-wall, hollow cylinder which is contoured by 0.25-in.-thick stainless steel, and the wall cavity is filled with barytes concrete. The primary collimator, 45.497 in. long, with a rectangular aperture, 2.025 x 2.750 in., has its entry 61.625 in. from the beam-port entrance. It is partitioned by thin-walled, rectangular, stainless steel tubes into nine horizontal and five vertical Soller channels. The inner dimensions of the stainless steel tube (cold-drawn, seamless) are 0.216 x 0.540 in., and the wall thickness is 0.0085 in.* The horizontal and vertical angular divergencies are 16.3' and 40.6' of arc, respectively, assuming the tube wall to be an infinite absorber. Presently, all of our Soller collimators are constructed in accordance with the technique illustrated in Fig. 4, where the checker-board stacking scheme is employed for bundling the tubes. Except those adjacent to the collimator inner wall, the tubes support each other through pressure fitting at their corner shoulders. In addition, so as to insure the minimum tolerance for straightness and to increase the mechanical strength of the tube bundle, the end cap and the comb guide, both made of thin aluminum, are incorporated into the collimator construction. For the primary collimator, the aluminum combs were placed at two places, and the exit cap was replaced by the thinner aluminum cap after lining up the tubes. Total aluminum thickness in the beam path ranges from 0.040 to 0.080 in., which removes 1 to 2% of the thermal neutrons (ref. Appendix I). The resultant beam heterogeneity is about 1%, a completely negligible quantity in comparison with that due to the tube walls.

Although seemingly trivial, particular care was taken to make the entry cap dust-proof, since the vertical lift shutter creates very annoying dust during operation. The outer jacket of our collimators is of conventional steel-Masonite lamellar construction, for attenuating neutrons, strengthening the mechanical property, and compensating differences in the thermal expansion of the constituents.

*The manufacturer failed to meet the purchase stipulation on the wall thickness, less than 0.005 in. However, since further negotiation would have caused unnecessarily long delay of the project, no further action was taken.



120-7766 Rev.

Fig. 4. Design Features of the Soller Collimator

The fabrication of the fine collimator is one of the most critical problems in the nuclear instrumentation. Hence, numerous techniques have been developed. However, only a few cases have been described in detail in the literature: rubber-lamellae 10'-arc collimator by Caglioti and Casali (1962); nickel-foil (0.001 in. thick), 0.7'-arc collimator by Joki et al. (1956); steel-shim (0.002 in.) 2'-arc Soller by Sailor et al. (1956). Our design is relatively simple in its fabrication, and the checker-board packing cuts down the effective wall thickness to half of the closest-packing module which has been employed by various other investigators.

An interchangeable boral-cadmium mask (two 0.250-in.-thick borals* and 0.250-in. Cd) is used to stop down the incident thermal-beam profile. The mask with a rectangular aperture, 1.125 x 2.250 in., is commonly used for the parallel-beam technique and may be widened for the focusing-beam method. Also, the optimum aperture is dependent on the size of the monochromating crystal, as well as the diffraction mode of the monochromator, Bragg or Laue case (reflection or transmission). Interchange or removal of the mask is carried out with a remote-drive tool which can be operated from the outside of the biological shield through an opening for the angle-selecting plugs (Chapter 1-6).

1-4. Monochromator Unit

The goniometric center of the monochromator is 10.00 in. from the primary-collimator exit and is an alignment pivot for the subsequent parts of the diffractometer (see Chapter 1-10). The radiation-shielded remote-control unit for the monochromator is set either horizontally or vertically. The vertical insertion of the control unit is more suitable for adapting the 1:2 angular-coupling mechanism between the monochromating crystal and the turntable. However, simply because of the congested available space, the horizontal type developed by Mueller et al. (1962) was modified and was fitted into our shield without the 1:2 collateral mechanism. Anti-backlash gear-trains, larger crystal holder, elimination of the goniometer components in the beam path, and higher-accuracy goniometric read-out were incorporated into the previous model. The monochromating crystal, up to 6 in. x 3.5 in. x 3 in. thick, is mounted on an aluminum frame which possesses

*Boral: a mixture of B_4C and aluminum powder clad between aluminum sheets (Price et al., 1957).

Two types of stock boral are available: overall thicknesses of 3/16 and 1/4 in. for 50 and 30 w/o B_4C , respectively. In both types, the aluminum jacket is 0.036 in. thick (0.072 in. total), and the B_4C -Al core density is about 2.5 g cm^{-3} , which is very close to the average of the solid densities of B_4C (2.5 g cm^{-3}) and aluminum (2.7 g cm^{-3}). The boron contents are 0.98 and 0.59 g cm^{-3} for 3/16- and 1/4-in. thicknesses, respectively. The absorption coefficients, μ , in the transmission ratio $\exp(-\mu t)$, for 0.025- and 0.1-eV neutrons are, respectively, 12.0 and 6.12 for 3/16-in., and 11.1 and 5.68 for 1/4-in. thicknesses. The transmission ratios are correspondingly 6.0×10^{-6} and 2.2×10^{-3} for 3/16-in. and 1.5×10^{-5} and 3.5×10^{-3} for 1/4-in. thicknesses. The precision cutting of boral, with its hard and brittle core, is possible with the electric spark-discharge erosion cutter (Ch. 1-4). A thermally molded material, 200 mesh or finer, B_4C impregnated in Lucite in 1:1 weight ratio, is employed by some neutron groups. Other thermoplastics may also be used for this purpose.

2π rotational freedom for Ω and $\pm 30^\circ$ for the tilting adjustment. The assembly is subsequently set on cross slides, capable of ± 0.75 in. translations. Several flexible-cable linkages eliminate mutual interferences among four remote-control channels.

Ideally, three angular (Ω and two mutually orthogonal azimuths)* and two cross-sliding motions are essential for aligning a preadjusted crystallographic zone axis. Moreover, so as to minimize the intensity loss due to the parasitic diffraction process (Renninger or multiple Bragg scattering), a device permitting a wide-range Φ -variation at a given Ω -setting may also be adapted to the goniometer (Blinowski and Sosnowski, 1961). For a fixed monochromatic-beam output-channel technique, in which the wavelength change is carried out through selecting different diffracting planes of a crystal or changing the crystal (e.g., Willis, 1962), one may even execute a full-circle universal goniometry, which would, however, require a prohibitively elaborate device. Fortunately, in contrast with neutron spectrometry, the diffraction technique does not require frequent wavelength modulation, and precutting and presetting the crystal prior to the final mounting are usually adequate to compensate the deficiency in the goniometer-control multiformity. By the same token, the 1:2 coupling described above is not an absolute requirement in diffractometry. The parasitic diffraction effect can be minimized by preselecting an appropriate Φ orientation of the given reflecting plane. In any event, it is advisable to design the monochromator holder large enough to accommodate an uncut bulky crystal, the focusing flat or bent crystal, and those for the low-angle Bragg-case geometry. The remote control may be carried out by means of an electronic device such as the one constructed by Hagihara et al. (1962).

The neutron monochromating crystal requires some additional criteria to those for the X-ray case, where almost saturated advance has been made (e.g., International Tables for X-ray Crystallography, 1962, Vol. III, pp. 79-88; G. W. Brindley in Peiser et al., 1955, pp. 122-144). For neutrons, besides the common criteriasuch as large scattering amplitude and high Debye temperature, the crystal has to be grown to a large size and should possess a small effective absorption factor (including an often predominantly strong extinction effect). Moreover, because the incident neutron-energy spectra is continuous in contrast with the discrete spectra of an X-ray-tube beam, contamination due to the λ/n harmonics is usually higher for neutrons than for X rays. Hence, the incongruous-harmonics contamination in the crystal-monochromated neutrons is an inherent problem, and it should be small or be eliminated by an appropriate filter (see Appendix II). An endless effort to approach these conditions is apparent in numerous publications: an

*The Ω -axis is taken as the one normal to the incident beam and parallel to the detector axis. Other three-circle notations are: X-axis, normal to Ω -axis and to scattering vector; Φ -axis, goniometer-head axis and normal to X.

extensive Renninger-effect study on Cu (111) diffraction (Blinowski and Sosnowski, 1961); Pb (220), Quartz (10 $\bar{1}1$), and Al (111) monochromations (Caglioti and Ricci, 1962); flat and curved monochromators of lead and germanium, and the Fankuchen-cut crystals (Dachs and Stehr, 1962; Stehr, 1963); the second-order contaminations in NaCl (220) and (240), and in beryllium (1011) and (1231) (Haas and Shore, 1959); importance of the parasitic scattering, e.g., with beryllium (Hay, 1959); 2- and 4-Å neutrons from beryllium (0001)-zone (Hay *et al.*, 1958); aluminum (111) Fankuchen-cut (Henshaw, 1958); reflectivity tables and graphs for various beryllium and NaCl crystal-planes (Holm, 1953); Fe₃O₄ and germanium for 0.7- to 9-Å neutrons (McReynolds, 1952); proof of superiority of "92% Co/Fe" (111) over Fe₃O₄ (220) as polarizing monochromator (Nathans *et al.*, 1959); 4.7 to 9.3 Å from mica cleavage-planes with beryllium and BeO filters (Sabine *et al.*, 1962); calcite cleavage planes and beryllium (12 $\bar{3}1$) (Sailor *et al.*, 1956); the Cauchois-type bent-NaCl crystal for 0.25 to 1 Å (Sawyer *et al.*, 1947); detailed theoretical examinations on the Bragg-case and Laue-case monochromations and their higher-harmonics contaminations, and the experimental studies of Ge (111), Cu (111), and LiF (111) monochromators (Schermer, 1960); highly polarized neutrons, nearly 100%, from Fe₃O₄ (220) (Shull, 1951); Pb (111) and compression effect on its reflectivity and Ge (111) exhibiting the highest reflectivity (Shull 1960); very comprehensive work on germanium in comparison with silicon and NaCl (Wajima *et al.*, 1960); α -Fe₂O₃ (111) (rhombohedral) monochromation for 1 to 4 Å (Wanic and Riste, 1960); several planes of copper and lead for Bragg-angle 45° (Willis, 1962); fibrous-lineage texture in most of the crystals grown from the melt, Cu (111), Cu (100), Be, Mg, Ni, Pb, Bi, NaCl, and LiF (Weiss *et al.*, 1951). It should be noted that a number of other metals, alloys, and simple nonmetallic compounds satisfy closely the aforementioned criteria except that for growing to a large single crystal.

Our experience in this area is not significantly greater than those of other neutron groups. Single crystals of lead (2.5-in.-diameter cylinder, 6 in. long) and copper (2-in. diameter, 6 and 4 in. long), both of which were grown nearly parallel to the [110] axis, were mounted on a precision lathe. They were then machined to geometrically nearly perfect cylinders (± 0.0005 in.), and angular and axial fiducial hairlines were carefully scraped on the crystals. The crystal was placed on a large goniometer head (Chapter 2-2) with fine fiducial lines on its top platform. The crystal was then lined up with respect to these fiducial lines and also to the diffractometer axes by means of a theodolite capable of measuring angular differences of less than $\pm 0.002^\circ$ at our working distances. Through the rocking-curve analyses of the {110}-zone planes, the (111) planes were located in relation to the fiducial lines with the aid of the goniometer read-outs and the theodolite.

The first crystal was examined by X rays and subsequent crystals by neutrons. The resultant angular and axial specifications (with tolerances of $\pm 0.02^\circ$ and ± 0.001 in., respectively) were then transferred to the

micromanipulators attached to the electric spark-discharge erosion machine, for which there is an accuracy of ± 0.0003 in. in the dimensional setting. The spark-erosion process can prepare a strain-free single-crystal segment regardless of the specimen hardness, and is perhaps the most suitable technique for cutting and boring metallic and metalloid crystals.

The crystal was then sliced into halves along the $[110]$ axis and parallel to the (111) planes, and each segment was further cut to a rectangular parallelepiped, in some instances with two left-over round edges (e.g., $5.50 \times 1.55 \times 1.00$ in. for lead; $5.63 \times 1.60 \times 0.91$ in. for copper). These two slabs were then combined side by side to form a twin (111) mirror and were inserted into the aluminum frame equipped with set-screws. These micro-adjusting set-screws are used to line up two segments as equal as possible with regard to their reflectivities. This final adjustment must be carried out by use of diffraction methods, because of possible errors incurred during the cutting processes. Any relative adjustment which opens up the closely contacting midsection of the combined segments is prohibitive; hence, for these specific directions, high accuracy must be emphasized or repeated cutting processes may be needed.

In order to remove dislocated or recrystallized portions, which might have formed during the cutting procedures, heavy chemical etching was applied to the lead crystals. However, no effect due to the etching process was observed upon examination of the reflectivity and the rocking-curve profiles in the neutron examination. The combined segments in the aluminum frame were then slid into the outer aluminum frame, whose orientations are governed by the remote-control device described previously.

Certain low-melting-point crystals, e.g., of lead and zinc, can be grown into a large rectangular-parallelepiped shape, but such growing technique becomes more involved for other crystals. The segment-conjoin technique for the Bragg-case monochromator may be unnecessary in the Laue case, for which considerably smaller crystals can be employed. An X-ray adapter for lining up the neutron monochromator-crystal has been described by Szabó and Krén (1959). Wood (1963) has published an excellent manual for the crystal-orientation experiment.

The transmission absorption coefficients of our copper and lead crystals were not more than 15% off the calculated values, exclusive of the extinction effect. For crystals of this size, this result is rather unbelievable. However, as also found by Weiss *et al.* (1951), Shull (1960), and others, reflectivity inhomogeneity was also apparent in our crystals, as much as $\pm 25\%$ in the pin-hole beam examination. Abrupt cooling-warming techniques with liquid nitrogen and hot water did not change appreciably either the integrated reflectivity or the transmission value. Other known techniques for inducing mosaic structure, e.g., compression, bending, bending-unbending, or ultrasonic-wave applications, in some instances at elevated temperatures,

were not applied to our crystals. These processes may increase the integrated reflectivity appreciably, but to a lesser degree as regards the peak intensity. In other words, they increase the rocking-curve width more than proportional to the integrated intensity. Moreover, a uniform induction of mosaic structure by means of the stress techniques is exceedingly difficult and is not worth trying on expensive single crystals unless needs are well-justified.

Our crystal holder can be used for both the Bragg and Laue cases, and can readily be replaced by other types without modifying the remote-control section.

1-5. Biological Shield

The monochromator area is completely enveloped by the biological shield for neutrons and γ rays, except where allowance is made for the primary-beam lead-in and the monochromated beam lead-out. The term "biological shield" may be misleading, because the neutron background suitable even for the routine diffraction experiment is far lower than a limit imposed through the radiation-protection guide (see Chapter 1-8). Numerous shielding techniques are described in the book of Price et al., (1957), and the physical properties of some potential shielding materials are summarized in books edited by Blizard and Abbott (1962) and by Tipton (1960). In Appendix I, the thermal-neutron transmission data are given for commonly employed materials.

The monochromator is set at about the center of a γ -ray shielding housing: 12 x 10 x 10-in. inner hollow space; 6-in. lead-cast clad in 0.3-in. steel jacket for the primary-beam projected area and 3 in. elsewhere excluding the reactor-wall portion; 2.25-in.-high pie-shaped opening for monochromatic beam output and another opening for the monochromatic remote controller. In the primary-beam-impinging section, a rectangular through-hole, 2.25 in. high, 1.5 in. wide and 6 in. along the beam path, is made as an auxiliary beam lead-out, which is normally closed with a lead port-plug. Right behind the port plug, 72% depleted uranium metal (0.042 kg U^{235} in 21.0 kg total) is placed as an additional γ -ray absorber. The uranium stopper is 3.50 in. high, 5.25 in. wide, and 3.75 in. along the beam direction, and is clad in an 0.25-in. steel jacket. By means of this auxiliary beam lead-out and with the use of a 45° Bragg-angle monochromation, a small diffractometer or a film camera may be installed on the top platform of the biological shield, provided that they do not interfere with the main installation, as stated in Chapter 1-1. This straight-through beam port is also used for the instrumental alignment. The inner faces of the monochromator housing are covered with a sandwiched cadmium-boral liner to decrease aberrantly scattered neutrons and subsequently to cut down the background due especially to fast neutrons escaping through the secondary collimator. Lithium compounds, such as Li_2CO_3 , are often used for this purpose, but were not

adopted because of constructional difficulty. The space allocated for the monochromator is large enough to accommodate a permanent magnet and magnetic shieldings for the polarized-beam technique. The total weight of the Pb-U γ -ray shield is approximately 600 kg (0.66 short ton). A combination of lead and tungsten alloy J is used by Bacon and Dyer (1959).

For diffusing and moderating fast neutrons* and absorbing slow neutrons, a layer pile composed of 2-in.-thick Masonite die-stocks** surrounds the monochromator housing. The hydrogen content of our Masonite is 5.3×10^{22} atoms cm^{-3} , about 79% of the hydrogen content of water and 67% of that of paraffin or polyethylene (see book by Price et al., 1957, p. 292). Paraffin intermixed with one or more thermal-neutron attenuators† is superior to water and to Masonite as regards both neutron- and γ -ray-removal cross sections. However, as stressed by Bacon and Dyer (1959), Mueller et al. (1962), and Shull (1960), the Masonite shield is more advantageous as regards fabrication, installation, and modification procedures.

The average thickness of our Masonite shield is about 24 in. from the Pb-U shield, and the dimensions measured from the primary-collimator exit are roughly 48 in. along the main beam and 30 in. along other directions. A peculiar notch on the right-hand side of the shield (see Fig. 1) was made to accommodate auxiliary installations of other experimentalists at CP-5. The Masonite layers are interlocked rigidly to the steel polystyrene-framework. The monochromator unit and housing, the secondary-collimator components, and other alignment-sensitive components are supported entirely by the steel construction. As a part of the steel framework, several steel plates are interleaved into the Masonite layers so as to enforce the alignment stability. A section following the lead plug and the uranium block is filled with a vertically inserted Masonite segment which can be removed without disturbing the instrumental and tectonic alignments of the shield. The total weight of our biological shield, including the secondary collimator assembly and the monochromator unit, is estimated to be approximately 4×10^3 kg (4 short tons), which is supported by a steel base with six large jack-screws for adjusting height and leveling (see Fig. 2).

*The average total cross sections for neutrons with energies above 10 eV of practically all of naturally occurring elements lie around 10 b and seldom exceed 50 b. Hence, in the absence of an efficient absorber, the fast neutrons have to be moderated down to thermal energy.

**Benelex 70 of Masonite Corp. is used. Cellulose fibers, prepared by exploding wood chips by giant guns, are bonded together under high pressure, utilizing wood's natural binding agent, lignin. No chemical is added in the process and, hence, an average atomic ratio C:H:O = 6:10:5 of cellulose may be applicable to Benelex 70. The density of 2-in. Benelex is 1.43 g cm^{-3} , approaching pure fiber density of about 1.6 g cm^{-3} (see also Table III of Appendix I).

†Relatively economical materials for this purpose are B_4C , $\text{Na}_2\text{B}_4\text{O}_7 \cdot 10\text{H}_2\text{O}$ (borax) and CaB_6 . Calomel (Hg_2Cl_2), having a relatively large capture cross section for thermal neutrons, may be added for increasing the γ -ray-removal cross section (ref. Appendix I).

At various points just outside of the biological shield, differences in the neutron and γ -ray fluxes when the beam-port shutter was closed as compared with those when the shutter was open were less than the statistical fluctuation of the measurements at the 4.6-MW operation of the reactor. It is expected that this effectiveness will hold even at the proposed 10-MW operation. Further discussion regarding the room background is given in Chapter 1-8.

1-6. Secondary Collimators

The secondary collimator, a beam-guiding channel between the monochromator and the diffraction sample, is at 13.500 in. from the monochromator pivot and is 23.000-in. in length. Three types of collimators, two with Soller and a collimator-jacket module, have been constructed. The design features of the Soller type are similar to the primary collimator and are illustrated in Fig. 4.

The collimator designated as type I has five horizontal and three vertical Soller channels composed of seamless stainless steel rectangular tubes, 0.142 in. by 0.613 in. in ID and with a 0.0085-in. wall. These tubes fill an opening 0.765 x 1.874 in., and the horizontal and vertical divergencies are, respectively, 21.2' and 1°31.5' of arc, if the wall is assumed to be an infinite absorber. The Soller type-II collimator has an opening, 0.599 x 1.741 in., which is partitioned to three horizontal and three vertical sections by cadmium-plated steel tubings, 0.186 in. by 0.566 in. in ID, and with a 0.009-in. wall, including 0.0015-in. cadmium plating on all surfaces. The horizontal and vertical divergencies are, therefore, 27.7' and 1°24.6' of arc, respectively. These Soller collimators are primarily designed for the powder diffractometry, and, for the single-crystal case, the beam emerging through the central Soller channel is employed. Since the homogeneous intensity in the beam cross section is a more critical requirement for the monochromatic beam than for the primary beam, the end caps (see Fig. 4) were removed after lining up the Soller tubes and the tube end-shoulders were soldered together by a special fusing flux.

The third type has a through opening of 1.127 x 2.252 in., which may take insertion of the collimator of any type, for instance, a Masonite non-Soller collimator of dimensions 0.393 x 0.393 in. (58.8' divergence) for the single-crystal study. This collimator jacket is also used for experimental development of the Soller construction. A pair of sectional hollow plugs inserted at both ends of the collimator jacket are sometimes used to obtain various beam profiles. A pair of cadmium masks are set at the collimator mouths, and the following 0.094-in.-thick cadmium masks have currently been employed: 0.307 x 1.625 in., 0.461 x 1.625 in., and 0.606 x 1.625 in., and, for the single-crystal study only, 0.160 x 0.630 in. and 0.207 x 0.587 in.

Two major techniques, fixed and variable Bragg-angle settings, are available for the angular setting of the secondary collimator. The fixed-setting module simplifies the instrumentation and may be sufficient for the crystallographic study, although the wavelength variation is relatively cumbersome (Willis, 1962; see also Chapter 1-4). Some examples of use are: 45° Bragg-angle (Peterson and Levy, 1959; Willis, 1962), 21° (Hagihara et al., 1962) and 11° or 13° (Bacon and Dyer, 1959; Bykov et al., 1957; review article by Goedkoop, 1961, 1962).

The majority of the diffractometers use the variable Bragg-angle technique, which may further be divided into (A) rotatable double cylindrical-drum type and (B) interchangeable wedge construction. With the former continuous wavelength modulation can be carried out; the latter technique gives a discrete change but is simpler in view of precision engineering.

Ours is of wedge type and the Bragg-angle selection spans from 8.5° to 22.5° in 0.5° intervals. The radial guiding grooves with 1° intervals are made on the pie-shaped angle-selecting guide-plate. All of the secondary collimators are fitted into one master adapter with a protrusion on its base along the collimator axis, and this protrusion is set into the radial guiding groove of the angle-selecting guide-plate. The remaining opening is shielded off by the Masonite-steel laminated wedges. Two wedge sets, front and rear, are used, and each set is composed of the pie-shaped wedges for 1°, 2°, 4°, 5°, and two 8°'s. The height of the master adapter is 5.5 in. at the front section and steps down to 5.3 in. at the rear portion. These height dimensions, which are considerably larger than at other installations similar to ours, are aimed at flexible accommodation of various collimation techniques.

1-7. Diffraction Turntable

The major components of the diffraction turntable described here are the specimen table, and the driving and encoding mechanisms, but the counter shield and collimators, which are described in the following chapters, are not included.

In X-ray diffractometry, the diffraction turntable, customarily called a "diffraction goniometer," constitutes the major instrumentation. The X-ray diffraction goniometer, steadily developed during the past two decades, can readily be adapted for single-crystal neutron crystallography, see, e.g.: General Electric unit (Pepinsky and Frazer, 1955; Peterson and Levy, 1959; Shull, 1960); Hilger (Arndt and Willis, 1963); Picker X ray (Mueller et al., 1962). However, the X-ray turntable can hardly accommodate our massive auxiliary instruments, such as the magnet and the Dewar. Some dimensional characteristics of the horizontal turntable described by Mueller et al. (1962) meets with our specifications and therefore they were partially incorporated into our engineering designs. The key components, their correlative modes

with the driving and encoding mechanisms and the counter-unit construction are, however, substantially different from the model of Mueller et al. Consequently, extensive engineering and instrumental work was needed.

The spindle axis of the turntable, coinciding with the crystal (Ω) and the counter (2θ) axes, is set at 56.00 in. from the monochromator pivot, i.e., 19.50 in. from the secondary-collimator exit. The turntable assemblage, which is slidable on a steel base-platform, 48 x 24 in. and 4 in. thick, is connected to the pivot arm for the 28° -range setting with the fixed radius of 56 in. The platform is supported by six jack-screws which level up the platform upper surface to 7.5 in. and the top surface of the specimen-table (Ω -table) to 22.7 in. from the reactor floor. The distance between the center of the neutron beam and the Ω -table top is 19.3 in., which is large enough to accommodate all of the conceivable auxiliary devices.

One of the unique features of our designs lies on the $\Omega:2\theta$ drive mode. No mechanical or magnetic 1:2 gear coupling is used, and the $\theta:2\theta$ scanning is accomplished by 1:2 electronic-pulse feeding to the driving motors. This $\Omega:2\theta$ driving mechanism is assembled on a carriage base, 1- to 1-1/2-in.-thick steel, with a spindle post, of 4.5-in. OD and 3.25-in.-reamed ID. This base is set on several brass pads with a web-like oil-retaining groove for lubricating the sliding process, and is connected to the pivot arm through a joint at which small mutual alignments can be made. The spindle post of the carriage base carries, from bottom to top: a large ball bearing; the main gear component for 2θ (360 teeth and 18-in. OD); the counter scanning arm fastened to the lower gear; the ball bearing and the gear for the Ω -drive identical to those for 2θ ; the Ω -table. Stacking of these components is guided by their respective center-aligning fittings, which are preloaded by means of the retainer and a thrust bearing located at the Ω -table center. The Ω -table is 23.6 in. in diameter and about 1 in. in the average thickness. These assemblies have shown no shortcoming for long-range operation, even with the magnetic device weighing nearly 2000 lb (1.5 short tons, see Chapter 2-6). However, as described in Chapter 1-10, our turntable assembly imposes certain limitations on the counter-shield weight, particularly in the instrumentation without the magnet.

Resemblance between the Ω and 2θ drive mechanisms mentioned above is further emphasized in the driving shaft, where the following components and their assembly are identical in Ω and 2θ : a worm-gear for 1° main-gear rotation per one revolution of the driving shaft; Slo-Syn (type 400) motor on one end of the shaft (see Chapter 1-11); use of the other end of the shaft for adapting the manual-drive crank-handle and for a drum dial for 1° to 0.01° reading; an electronic shaft-encoder connected to the shaft through an antibacklash gear-train; metal-spring antibacklash adjuster for the worm-gear mesh. The drive shaft may be divided into two sections. The primary linkage, the motor \rightarrow the shaft coupling \rightarrow the worm-gear \rightarrow the encoder, is mounted on a journal bracket which is slidable on the carriage base

normal to the mesh between the worm and main gears. This arrangement enables one to adjust the antibacklash spring tension without disconnecting the driving and encoding components. The secondary section with the components for the manual mode of operation is mounted on the carriage wall and is connected to the primary linkage through a shaft coupling. A helipot for the X-Y recorder (see Chapter 1-11) is attached to the secondary section of the 2θ shaft. Whenever adjustment of the antibacklash spring is required, although the shaft coupling absorbs small misalignment, the coupling between these two sections is usually disconnected and then readjusted.

The outer framework of the carriage base is used for attaching the following various devices: sectional dust covers including the Lucite sections for visual inspection of the gear components; crescent protractor for 2θ (0.1° reading with a vernier on the counter scanning arm); electronic switches and connectors for the drive control. The counter scanning range is -85° to 130° at any of the monochromator angular settings. A 360° graduation is inscribed on the Ω -table for the Ω -angle and a 0.1° vernier for Ω is attached to the top dust cover.

The counter scanning arm is extended out 28 in. from the turntable center, and the scanning beam is bolted onto the arm in either one of two alternative settings for variation of the sample-to-counter distance. Because of the heavy counter-shield that the arm and beam have to support, the following criteria were sought: least possible moment of force acting upon the turntable-aligning and driving mechanisms; least warping and fast libration-damping characteristics under heavy loading and in the momentum-transfer process during the counter drive. Accordingly, the cantilever section of our scanning arm is of steel-box construction, 4.75 in. x 4.75-in. OD in cross section, and a 0.25-in. wall. The scanning beam has an aluminum I-beam construction with thin aluminum fringe enforcements, and the shape of the scanning beam is such that the weight distribution is roughly reciprocally proportional to the distance from the turntable center. The total weight of the scanning beam is only about 30 lb. The top platform, 32 in. long, is equipped with a steel guiding rail for the counter-shield support and also a reference scale for the counter setting. In extended operation with the counter-shield, weighing about 150 lb, there has been observed no significant mutual interferences among the turntable components. The "upper" powder diffractometer of Bacon and Dyer (1959), the unit built by Maschinen Fabrik Augsburg-Nuremberg (1960), and the Chalk River spectrometer (McAlpin, 1964) employ a large steel platform to support the counter-shield assembly, overcoming difficulties involved in the cantilever-type support. A further improved model has been described by Allenden and Winkworth (1963). In comparison with what is required for powder diffractometry, the restriction is much relaxed for the single-crystal case, where a smaller counter and correspondingly a lighter counter-shield may be used, and the counter can be set much closer to the specimen.

1-8. Counter Shield

One of the most annoying problems in neutron experiments is due to fluctuating room-neutron background that increases the statistical error in the resultant data. In general, the room-background variance is larger for higher background. Moreover, it is not unusual in a reactor experiment that the variance is a dominant error factor and in turn has a strong influence on the quality and efficiency of the experiment.* Consequently, all conceivable efforts should be expended in achieving the lowest possible background level with the least fluctuation. Foreign thermal neutrons can easily be shielded off. Hence, in the BF_3 -counter technique with an appropriate pulse discriminator, the problem is confined to the fast-neutron background. Schermer (1960) has also discussed this subject rather extensively.

With regard to the self-originated background, the effectiveness of the biological shield and the fast-neutron contamination in the monochromatic beam are readily controllable. Particular attention should be paid to the latter which could amount to from 10 to $10^3 \text{ n cm}^{-2} \text{ sec}^{-1}$, although these figures represent seemingly negligible percentage contaminations, about 0.1 to 0.01% in the typical monochromatic fluxes, 10^5 to $10^6 \text{ n cm}^{-2} \text{ sec}^{-1}$. Thus, the design of the beam catcher should not be handled carelessly, as was pointed out in the book by Hughes (1953, pp. 340-341) and also by Schermer (1960). With the proper instrumentation, the diffractometer beam is highly collimated and small in aperture, so that there is seldom a significant build-up of room background.

On the other hand, the foreign fast-neutrons bouncing around in the reactor area are hard to subdue. As stated in Chapter 1-5, the radiation safety control** is of little help in abating the background to a low level. Congestion with a variety of installations, involving fast neutrons and γ rays, is not unusual in the reactor area. Correspondingly, individual requirements as regards the background species and level are different; moreover, the reactor shielding itself is not adequate for the low-level requirement. The counter-shield design has to be based on the flux and spectrum of the background neutrons, both of which change from time to time. Nevertheless, a rough estimate of the average background properties should be obtained at the earliest stage of the diffraction instrumentation, since the shield for the

*Let us compare two simplified yet typical cases for which we assume identical experimental parameters except for the background variances: the first case, background count, 10 ± 1 (10%); the second case, 100 ± 5 (5%). A repetition of 25 experiments of the latter case is required to obtain the accuracy of the former.

**Maximum permissible radiation dose is around $100 \text{ mrem week}^{-1}$ (40 hr), about three-quarters of which may be assumed to be attributed to γ rays. The time-averaged neutron flux to cause a 25-mrem week^{-1} dose is roughly 170, 125, 75, 20, and $5 \text{ n cm}^{-2} \text{ sec}^{-1}$ for neutron energies, thermal, 0.1 keV, 10 keV, 0.1 MeV and 1 MeV, respectively (National Bureau of Standards, 1957). The conventional B^{10}F_3 counter with a light-duty radiation shield would count, conservatively, more than $500 \text{ counts min}^{-1}$ in the highest permissible-dose background.

counter and possible installation of partition walls have strong correlation with the basic design and layout of the diffractometer.

The beam-port experimental area of the CP-5 reactor is highly infested with aberrant neutrons and γ rays, largely because of vigorous research activities and overutilization of the assigned space. The current average neutron-background flux at about 6 ft from the reactor wall and 2 ft above the floor is 25 ($\pm 50\%$ or larger) $n\text{ cm}^{-2}\text{ sec}^{-1}$ for the epi-cadmium and about equal amount for the sub-cadmium. The total neutron-background corresponds to about 4 ± 2 mrem hr^{-1} and, with the γ -ray background, it is equivalent to 12 ($\pm 50\%$) mrem hr^{-1} . Although the background level decreases rapidly with increasing distance from the reactor wall, a 40-hr/week personal stay near the reactor wall is definitely not permissible, unless additional protection is provided.

The neutron counter requires much stronger protection against the background neutrons. Before the project-design work was commenced, counter-shield mockup experiments were undertaken with various thicknesses and combinations of paraffin, paraffin impregnated with B_4C , B_4C , boral, Masonite, and cadmium. Better materials, such as high B^{10} -content material, are conceivable, but their costs or fabrication difficulties are prohibitive in practice. Here again, we have to choose a proper compromise between highest effectiveness and least weight as regards the counter shield. The counter shield should cut down the high background flux by a factor of about 10^{-4} , but the proposed diffractometer design would be more involved if the weight of the counter shield exceeds about 200 lb. Composite shields with Masonite were, as expected, far inferior to those with paraffin or equivalent material (see Chapter 1-5). A circular layer, of paraffin- B_4C -Cd, along the inward direction, was found to be most appropriate for our background. Two types of counter-shield have been constructed. (1) A light-duty module (70 lb including the support): shielding factor of 10^{-3} , and 10 to 5% variance contribution to the sample intensity data; 6.5-in.-OD cylinder with a 2-in.-diameter opening along the axial center for the counter; 36 in. long with a 10-in. cathode-follower-adapting cavity; layer composed of 1.5-in. paraffin-0.5-in. B_4C -0.060-in. cadmium encased in a 0.094-in. aluminum envelope. (2) Heavy-duty, 150-lb shield: shielding factor of 10^{-4} , and 5 to 0.5% variance contribution; 12-in.-OD with a 2-in. central opening; 28 in. long; layer of 3.25-in. paraffin-1.4-in. B_4C -0.060-in. cadmium encased in 0.125-in. aluminum. The light-duty shield is used for certain coherent-scattering and related experiments, e.g. three-dimensional single-crystal data collection, where fast automatic counter drive is allowed on account of strong scattering from the sample. The heavier counter shield is indispensable for high-precision work, e.g., for paramagnetic, satellite-peak, and other background-sensitive studies.

The B_4C hollow-cylinder segments, 4 to 5 in. long, were prepared by means of hydraulic compression and molding (4000 lb in.^{-2} , nominal) at room

temperature, with a mixture, 200 mesh or finer, of B_4C and 10 to 20 w/o elementary boron. Elementary boron, readily available in finely powdered form, was used to fill intergranular spaces among the coarse B_4C particles. Plastic binder (cellulose or vinyl cement solution) was soaked into the compressed mixture in the hydraulic setting. Air hardening with sodium silicate or chemical binding with magnesium oxychloride may also be employed for this purpose. The final packing density of our B_4C -B segments was about 1.8 to 2.0 $g\ cm^{-3}$.* (Manual packing provides densities less than 1.3 $g\ cm^{-3}$.) The segments were bonded together by use of a boron-vinyl cement mixture. Elementary boron is slightly better than B_4C in the neutron absorption efficiency per unit volume, but it is too costly to use in a large quantity. For adapting the 1-in.-diameter counter, a hollow, aluminum-enveloped cylinder containing manually packed elementary boron (0.354 in. thick) and cadmium (0.020 in.) was inserted into the 2-in.-central hole.

On the outer surface of the counter shield, fine fiducial lines were inscribed to aid in the manual and optical lining-up procedures. These fiducial lines were correlated with a set of dowel pins around the counter-adapting opening of the shield, and these pins were used for aligning the following counter attachments: the counter collimators and slits (see Chapter 1-9); the slit box; the double pin-hole transmission-cell supporter (see Chapter 2-3). The counter support is equipped with the following: height and lateral centering set screws for the counter-shield alignment; the counter support with height-adjustable ball casters which slide on the platform of the scanning beam; laterally adjustable slide-guide along the central rail on the platform.

Unfortunately, it was found later that our counter-shield mockup experiment was carried out at probably the lowest room-background level, for some installations which have been largely responsible for the background buildup were inactive. It was first observed that the experiment, particularly that with the light counter shield, had occasionally been disturbed by a burst of foreign fast neutrons, the origin of which could not immediately be determined. With the help of the radiation-safety group, level-contour maps for the room neutrons in our area were prepared so as to locate the neutron-leakage sources and, in turn, to supply the data to efficient shield construction within the limited available space. The result was virtually fruitless, because neutrons from widely spread 4π -sources were being multiply scattered and their directional nature was more or less completely smeared out. Through the kind cooperation of the reactor groups, measurements were then made of the room neutrons when the in-pile

*A hot-pressed B_4C developed by Norton Company of Worcester, Mass., possesses a density of 2.5 $g\ cm^{-3}$.

beam-port shutters in CP-5 were opened, one at a time. The results showed our biological shield was satisfactory. Subsequently, several aluminum-sheet-encased borated-paraffin* walls were erected around our area.

Under certain circumstances, leaking neutrons may sometimes give little disturbance to immediate neighbors, but may strongly interfere with an experiment on the opposite side of the reactor. Variation of the ceiling crane position gave small, but measurable, background change in high-precision counting with an insufficient counter shield. In an ideal installation, the whole diffractometer assembly should be completely enclosed, not only by the side walls, but also by the ceiling shield. If this were practicable, the counter shield and the related instrumentations could have been greatly simplified. The ceiling shield was, however, not easily adaptable to the diffractometer area, and our counter shields with aids of the shielding walls have thus far proven to be satisfactory for most of the precision experiments.

1-9. Counter Collimators and Beam Slits

Three counter collimators of the Soller type that are currently in use differ in their lengths, 6, 9, and 12 in., but possess an identical aperture construction: five horizontal and three vertical Soller channels in a rectangular overall opening of 0.640 x 1.641 in.; Soller construction with the use of seamless steel tubes of 0.118 in. x 0.537-in. ID and 0.0075-in. wall plus 0.0015-in. cadmium plating on all surfaces. The construction principles here are similar to those used for the primary and secondary collimators, except that no aluminum comb is used and, after lining up the tubes, aluminum end caps were substituted by soldered joints as applied to the secondary collimators. A dowel-pin-guided connector was used to combine two collimators so that collimations 15, 18, and 21 in. in lengths could be carried out. The horizontal and vertical angular divergencies are, respectively: 1°7.3' and 5°6.6' for the 6-in. collimator; 44.9' and 3°24.7' for the 9-in. collimator; 33.7' and 2°33.6' for the 12-in. collimator; 26.9' and 2°2.9' for the 15-in. collimator; 22.4' and 1°42.4' for the 18-in. collimator; 19.2' and 1°27.8' for the 21-in. collimator.

A number of beam slits have been prepared for the multipurpose instrumentation. The slits of sandwich construction, Al (0.125 in.)-Cd (0.093 in.)-boral (0.188 in.), are placed either at the secondary-collimator exit or at the counter-collimator entry. The slits are also fitted into slots in the slit box (see Fig. 11), which is mountable on either the secondary-collimator exit or the counter-collimator entry. In a majority of the experiments, these slits are used at the secondary-collimator exit to confine the

*Steam-melted paraffin was cooled to slightly above its solidifying point and mixed with 20 w/o sodium metaborate (borax). Paraffin of low quality and low solidifying point is best suited for this intermixing process for preventing dehydration of borax at 75°C. Polyethylene or its few-percent borated product possesses a shielding effect about equal to paraffin-borax, and they are employed for patching up small sections because of their ease of handling; yet they are costly (about 10 times as expensive as paraffin).

profile of the beam impinging on the sample. Hence, their apertures are chiefly based on the neutron sample size or its holder dimensions. They are, in rectangular coordinates (in cm): 1.20 x 4.45, 1.65 x 3.81, 1.27 x 3.81, 1.02 x 3.81, 0.76 x 3.81, 1.02 x 2.54, and 1.02 x 1.02. These slits possess access screw holes for adapting the resonance filters (see Appendix II), and the slit-filter combination is often mounted on the counter-collimator entry so as to eliminate the scattering effect from the filtering material.

Another set of beam slits, made of 0.094-in. cadmium, is designed solely for the counter collimators. The horizontal apertures of the slits are integrals of the Soller-channel dimensions, and the vertical apertures are integrals of the Soller opening or 1.5 in., the latter of which is related to the effective cross-sectional area of the 2-in.-diameter counter. Those currently in use possess the following sizes (in cm): 1.59 x 4.13, 0.97 x 3.81, 0.32 x 3.81, 0.97 x 1.39, 0.32 x 1.39, 1.30 x 3.81, 0.65 x 3.81, 1.59 x 1.39, 1.30 x 1.39, 0.65 x 1.39, 2.38 x 4.45, 1.91 x 4.45, 1.27 x 4.45, 0.96 x 4.45, and 0.64 x 4.45. Wide-open counter collimation is frequently employed in single-crystal diffractometry. Here, the counter Soller-collimator is removed and only the counter-front slit is used. Also constructed for this purpose is a Masonite cylinder, 6 in. long and 2 in. in diameter, with a rectangular hole, 1 cm x 2 cm; the cadmium slits can be set at the basal faces of this cylinder.

The counter entry-window is routinely set at 15.7 cm, slightly larger than 6 in., from the counter-shield front face. The workable distance between the Ω -tube center to the counter-entry window can be set from 25 cm to 68 cm and from 36 cm to 75 cm, for the light and heavy counter shields, respectively. These distances, measured at the inward setting of the scanning beam on the arm, could be increased by 8.89 cm in the outward setting. Typical distances between the specimen and the counter entry are: 41.22 cm for powder diffractometry; 30 cm for single-crystal study; up to 75 cm for the high-resolution work, such as for small-angle-scattering experiments.

1-10. Installation and Alignment

Precision installation and alignment of the massive collimation system and the heavy-duty turntable required exceptionally tedious efforts. Schermer (1960) has described a commendable technique, and other neutron groups have developed individually suited methods to the subject matter. Our case is outlined as follows.

Firstly, the beam-port centerline was located. Glass plates inscribed with cross hairlines were placed at both ends of the central hole of the port plug, and a small battery-lamp unit was set at the inner end of the hole. Following a rough survey with simple instruments, the high-precision theodolite was used to determine the centerline more exactly and the reference fiducial lines were subsequently marked down around the beam-port exit

and on other stationary items, such as the reactor building wall. The process was repeated for different angular positions of the port plug in order to compensate for its eccentricity and other setting errors. Finally, average fiducial lines were made permanent markings.

The port plug was then replaced by the primary collimator, and the biological shield was installed up to the beam height. By use of a pointer at the monochromator pivot point as an additional reference, the angle-selecting guide plate and the monochromator goniometer were aligned with the aid of the theodolite and a spirit level capable of detecting ± 0.0002 in. in 12 in. In spite of the rigid construction as described in Chapter 1-5, the alignment at half-piling of the Masonite shield had to be readjusted after full stacking of the Masonite, because of level shifting of about 0.002 in./12 in. This small shift is by no means negligible in large-scale instrumentation, e.g., corresponding to as much as 0.02° error in our diffraction geometries.

Similar successive lining-up procedures were applied to the turntable installation through use of the multiple adjusting devices described in Chapter 1-7. The alignment problem was associated with precise driving and positioning of the heavy counter shield. The maximum allowable angular error in our diffractometry has been set at 0.01° . The corresponding sample eccentricity is $0.875 \times 10^{-4} R$, where R is the distance between the sample and the counter. For example, the centering deviation of the sample should be kept below 0.026 mm or 0.001 in. for $R = 30$ cm; otherwise, the eccentricity correction may become an additional major factor in the data processing. In particular, vibrations of the turntable components must be kept at a minimum during the driving mode, since there exists no simple systematic correction for them. For the counter setting and drive, in spite of the relaxation factor of two, the above criteria must be overcautiously enforced.

Alignment of turntable vs. the counter unit implies two separate subjects: the retaining stability of the spindle post against the scanning arm; and the first-class lever balance between the turntable and the counter shield. The former, discussed in Chapter 1-7, was attained through a conventional technique of preloading the bearing components. Our simple spindle assembly upholds a preloading equivalent to about 4000 lb-in. at the counter arm. As the load exceeds this, increasing friction among the bearing elements tends to interfere with the $\Omega-2\theta$ independent drive and to make the torque above the optimum limit. A more elaborate preloading design has been described by Bacon and Dyer (1959), and various devices for this procedure have been developed by other groups. Our loading limit is relatively low and suffices our current requirement with a very close tolerance.

An elementary problem, the first-class lever-poise, arises because our turntable assembly sits on the base platform. The turntable weighs

about 1000 lb and possesses a balancing moment of force ranging from 3000 to 5000 lb-in., depending on the position of the counter arm. This barely counterpoises the counter unit with the heavy-duty shield that creates about 3000 lb-in. or more. The pivot arm was originally designed to relieve this but was not satisfactory because of the following reason. The fitting precision at the pivot shaft can hardly be made better than 0.0005 in./12 in., which is a least requirement deduced from our angular tolerance, 0.01° . In fact, our pivot arm cannot counteract the sample centering shift of less than 0.003 in. Fortunately, the problem was solved rather readily. Lead bricks were placed on the stationary section of the carriage assembly, and this increased the balancing moment to 5000 lb-in. A further large safety factor was gained by means of two large, removable clamps binding the turntable and the base platform, the latter of which weighs about 1300 lb.

The driving-torque requirement for the counter arm with the heavy-duty counter shield is nearly 200 oz-in. at the motor shaft for the antibacklash coupling of less than $\pm 0.005^\circ$. Hence, a Slo-Syn motor generating about 400 oz-in. was mounted. The output torque of the motor decreased as the motor speed increased. Our optimum slow-speed of the heavily loaded counter arm is around $50^\circ \text{ min}^{-1}$. After numerous correlative adjustments, the sample eccentricity of less than 0.0005 in. was obtained under the most severe scanning condition.

As also stated in Chapter 1-7, the Ω drive is far simpler than the counter drive and, because of the preloading thrust-bearing design, no appreciable torque change was observed by mounting the heaviest auxiliary instrument, i.e., the electromagnet assembly, weighing nearly 2000 lb. Actually, the aforestated balancing and libration problems are greatly relaxed when the massive auxiliary instrument is mounted on the Ω -table. Nevertheless, because of the electronics circuitry, an oversized Slo-Syn 400 motor is used also for the Ω drive.

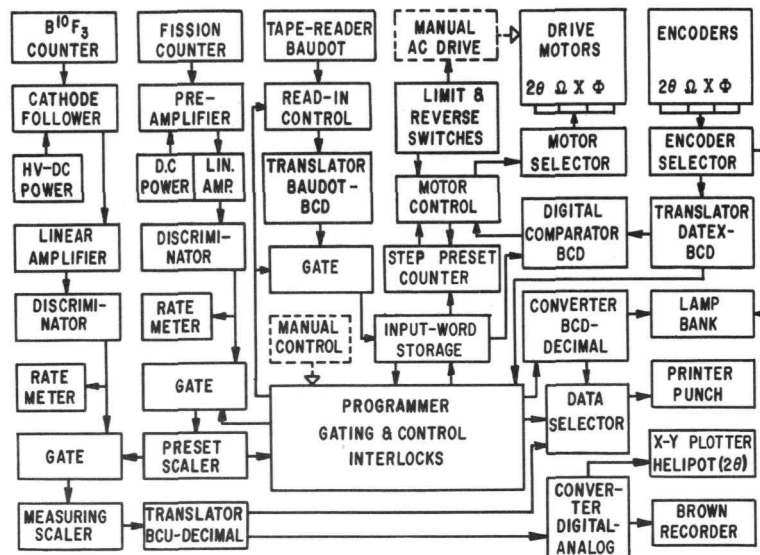
Other possible disturbances of the alignment were examined as follows. The heavy-duty crane operation in the CP-5 building vibrates the floor level in the order of 10^{-5} in./ft, which is detectable on a high-sensing bull's eye spirit level but can be ignored for our case. The floor shifting, due probably to seasonal alteration of the building foundation, is sometimes considerably higher than that due to the crane and associated disturbances; hence, occasional checking has been enforced. Upon completion of all this tedious lining-up work, additional fiducial marks were inscribed on the outer faces of the secondary collimators, the angle-setting plugs, and also on the reactor wall.

During the monochromation-angle variation, the pivot arm serves excellently in keeping the monochromator-to-sample distance to a high degree of constancy. However, in spite of the careful alignment, the angle-indexing holes on the base platform were found to be usable only as a

reference. The refined line-up process using the diffraction patterns of the standard samples often results in slight off-setting of the turntable from these index holes. However, the turntable is heavy enough to sit stationarily without using the angular-setting pin and the aforementioned clamps to enforce this stability.

1-11. Basic Electronics

The basic electronics* for the diffractometer may be divided into two groups: those for the counting and recording subroutines, and the automatic control equipment. The former consists of standard accessories, and the latter becomes necessary because of lengthy data-gathering processes and high radiation hazard. The system is represented in the block diagram of Fig. 5 and the photograph of Fig. 6. In the following chapter the neutron-counter characteristics are outlined.



120-8562

Fig. 5. Block Diagram of the Basic Electronics

The main counting channel consists of the following: a cathode follower directly connected to the $B^{10}F_3$ counter; a regulated DC high-voltage power supply feeding 0 to 5 kV to the counter; a packaged assembly consisting of a linear amplifier (x100 to x1600 in gain), a DC power supply, a discriminator (0 to 40 V in base discrimination), a rate meter in counts-per-second scale (60 to 20,000 counts sec^{-1}), and a pulse generator for standardization (1, 1/2, and 1/4 of the input-line pulse); a measuring scaler, Beckman/Berkeley 7060 (6 decimal digits). The monitoring channel

*Although, needless to say, it is important that the input power lines be free from electronic noise, inclusive of very low-level disturbance, a high-efficiency noise suppressor must be incorporated. For instance, our input power is being delivered from a transformer which is isolated from high-power equipment, such as the crane motor and the electromagnet. In a remote-control arrangement for eliminating possible indirect inductive interference, the power lines for the magnet and the furnaces are laid on the right-hand side of the diffractometer, whereas heavily shielded signal and counting cables are in the left-hand conduit run.

starts with a fission counter, which is followed by a preamplifier, the linear-amplifier assembly, and a preset scaler, Beckman/Berkeley 7416 (6 decimal digits). The counting operations are normally controlled through the programmer, and the measured counts are fed into the recording units through a translator which converts Beckman/Berkeley voltage-output in 1224 binary-coded decimal (BCD) code to decimal-coded relay-contact closures. In his book Gillespie (1953) has discussed specific problems regarding the noise and resolution in the nuclear-counter amplifiers.



120-6555

Fig. 6. Part of the Electronics Instruments. Left to right: the X-Y recorder; a console containing the measuring scaler, the amplifier unit (including the rate-meter, the discriminator for the $B^{10}F_3$ counter, and the DC power supply), Brown recorder, the preset scaler, the amplifier unit for the fission counter, the power supply for the potentiometer and the recorders, the high-voltage power supply for the $B^{10}F_3$ counter, the power supply for the high-temperature furnace; the automatic control unit.

Numerous automatic-control electronics have recently been reported* and are now available commercially, but this was not the case in 1960.

*Allenden and Winkworth (1963), Arndt and Willis (1963), Betzl and Kleinstück (1961), Cole et al. (1963), de Agostino (1963), Hagihara et al. (1962), Langdon and Frazer (1959), Miyake et al. (1962), Ozerov et al. (1960), Prince (1961), Prince and Abrahams (1959), and Wooster et al. (1963).

Our automatic instrumentation, obtained in collaboration with the Datex Corporation, is designed for the most general goniometry in the three-circle cone method, i.e., four independent angular settings with the θ - 2θ scanning mode. A full-circle X - Φ goniometer for this purpose is briefly described in Chapter 2-2. The drive motors for Ω and 2θ are Slo-Syn synchronous SS400 (three-leads) (see Chapter 1-7). For χ and Φ , Slo-Syn SS250, producing a torque (max 250 oz-in.) of nearly five times the required amount, is used, since SS400 and SS250 can be controlled through the same circuitry in both DC and AC modes. The maximum error in the crystal and counter angular settings is 0.01° , which is also the minimum stepping angle controllable through our motors in a DC operation. Our unit is mostly transistorized.

The single-crystal mode of operation is outlined as follows. The input tape with 5-hole Baudot code is prepared in the format shown in Table I, and the tape is fed into the Friden motorized tape-reader. Each of six characters representing the title information (e.g., Miller indices h , k , and l) is sequentially translated from the Baudot code to the 8421 BCD code which will enter into the transistorized input-word storage. When the title-information storage is completed, this is forwarded to the BCD-decimal converter at which the BCD data will be stored and translated into the decimal data in contact closure form. The decimal data will then be presented to the printer-punch unit.

Table I

INPUT TAPE FORMAT

Number of Characters	Data (single crystal)	Number of Characters	Data (powder)
1	Begin of cycle code (Figure key)*	1	Beginning of cycle code
6	Title information	6	Title information
1	End of word code (Space bar)*	1	End of word code
5	Φ (xxx.xx $^\circ$)	1	Powder code (Slash key)*
1	End of word code	1	End of word code
5	X	5	Initial 2θ
1	End of word code	1	End of word code
5	Initial Ω	1	Fixed 0
1	End of word code	1	Direction of counter rotation
5	Initial 2θ	2	Counter stepping angle
1	End of word code	1	End of word code
1	Direction of crystal rotation	5	Final 2θ
1	Direction of counter rotation	1	End of word code
2	Counter stepping angle (.xx $^\circ$)		
1	End of word code		
5	Final 2θ		
1	End of word code		

*5-hole Baudot code specification

As soon as the title information is stored at the BCD-decimal converter, the input-word storage will be cleared and the tape reader will start extracting the Φ -angle information. The input-tape Φ -angle (COMMAND) in the general storage will then be sent to the digital comparator for coincidence examination with the encoder Φ -angle (FEEDBACK), which has been translated into the 8421 BCD code from the Datex-coded encoder out-put. The comparator generates the positioning commands to the DC motor control, RUN for non-coincidence and STOP for coincidence between COMMAND and FEEDBACK. The comparator also provides the motor direction commands, forward if $\text{COMMAND} > \text{FEEDBACK}$, reverse if $\text{COMMAND} < \text{FEEDBACK}$. Moreover, in order to prevent the overshoot in the coincidence process, the slow-down command is given by the comparator when the difference between COMMAND and FEEDBACK becomes less than 1° during the RUN mode. The slow-down speed is variable and is usually about one-third of the normal RUN speed. Upon completion of the Φ setting, the final encoder Φ -angle is recorded on the printer-punch unit through the converter (BCD to decimal) and the data selector. As soon as the final Φ -angle is stored in the BCD-decimal converter, the input-word storage will again be cleared for the X cycle, which will proceed on the subroutine identical with the Φ -cycle.

The process is repeated for the initial Ω and 2θ angles in succession. In other words, the storage, the comparator, and related electronics are employed in sequence. In view of the construction and trouble-shooting, this sequence scheme is much simpler and economical than the simultaneous settings of two or more angles by means of electronics of larger capacity. The former is more time consuming in the coincidence setting than the latter, but proper arrangement of the input data makes the problem trifling, particularly in comparison with the time required for the counting process. Our motor-speed control is common for all four angles and is virtually determined by the 2θ drive requiring the largest torque. Regarding the direction command of the comparator, suppose that the input angle is 1° but the encoder angle has been 359° . The motor will then have to travel 358° instead of the shorter cut of 2° . As mentioned before, this situation can be avoided by a proper programming on the input-tape. In addition, movable reverse switches (microswitches) are provided for variable maximum and minimum angle settings. If the coincidence were not met during the reversed drive due to the error in the input-tape, another reverse switch would subsequently be energized. However, this second switch-contact does not reverse the motor direction, but forwards the program to the next cycle. The reversing switches are absolutely required in the counter drive, because of the limited scanning range. The diffractometry with the magnet or the furnace often requires the reversing switches on the Ω -drive, for avoiding interference among the instruments. Several microswitches connected in series are also used as the limit switches so as to protect the instrument from accidental failure of the reversing switches. When any one of the limit-switch sensors is pushed down, the motor control stays at the STOP command.

Completion of the coincidence positioning for all four angles is followed by extraction of the direction of the crystal rotation, the direction of the counter rotation, and the step angle. The clockwise rotation is represented by the numeral "1" in the Baudot code and the counterclockwise rotation by "2." Of course, in the $\theta:2\theta$ scanning mode, both the crystal and the counter should rotate in the same direction. The counter stepping angle can vary from 0.02° to 0.98° in 0.02° intervals and, correspondingly, the crystal from 0.01° to 0.49° in 0.01° intervals. The direction and step-angle values will be stored in an auxiliary section of the input-word storage. The final- 2θ angle will then be extracted from the input-tape and will be stored in the input-word storage until the counter reaches this angle. The counter stepping angle ($\Delta 2\theta$) will enter into the step preset-counter, which will advance the counter by $\Delta 2\theta$ in increments of 0.01° . Every other pulse will drive the Ω -stepping motor in the same direction. When the step is completed, that is, the step preset-counts decrease down to zero, the STOP commands will be given to the 2θ and Ω motors, and the preset and measuring scalers will be gated to operate. The neutron-counting process ceases when the monitor counts become equal to the present counts, and subsequently the measured neutron counts will be sent to the printer-punch unit with a subtotaling facility. The neutron counts, the subtotal, and the counter angle will be printed out on the recording paper, and subsequently they will be perforated on the tape. Simultaneously, the neutron counts will be fed into the X-Y recorder or the Brown recorder through the digital-analog converter.

The subtotal routine can be suppressed by means of the panel control. Repetition of the counting sub-routine will be followed. Upon completion of the cycle, the read-out records will be made on total counts, final 2θ , Φ , X and Ω as a part of the self-checking procedures. All storage will then be cleared, and if the system is under the continuous-cycle command, the input-tape will be forwarded to the next cycle.

In the powder mode of operation, a powder code replaces the crystal angles in the input-tape format and interlocks the crystal motors. Continuous rotation of the powder sample is carried out by the AC drive of the Slo-Syn Ω -motor ($72^\circ/\text{min}$ for 60-cycle input) or by a separate induction motor of 1 to 2 rpm. The AC-drive-motor control, which is completely isolated from the programming circuitry, is also used for adjusting all four angles in the single-crystal alignment, since the tape preparation or the manual drive using the crank handle is rather troublesome in such non-routine processes. The counter step-increment in the powder mode can take any angle between 0.01° and 0.99° because of the absence of the $\theta:2\theta$ scanning mode.

The printer-punch assembly is composed of two units, a Datex modification of the Monroe 400 printer with adding and storage facilities, and a Friden tape-punch. The printer possesses eleven printing bars. The first

is used for lettering, asterisk for the reset and the total counts, "S" for the subtotal, and "N" for the counter angle. The following ten bars are assigned for the numeral recording, and the tenth bar also prints letter "P" for the powder code. The output tape is in the 8421 BCD code. The Y-axis of the XY plotter (Electro Instrument Model 223) represents the 2θ angle which is potentiometrically supplied from a 40-turn helipot (see Chapter 1-7). Additional circuitry extends the Y-range settings to $0^\circ - \pm 15^\circ$, $0^\circ - \pm 30^\circ$, $0 - \pm 45^\circ$, $0^\circ - \pm 60^\circ$, $0 - \pm 75^\circ$, $0^\circ - \pm 150^\circ$, and $-85^\circ - +140^\circ$. With this and other self-contained range regulators, a precision rocking curve can be recorded on the X-Y recorder. For extended operation, the Brown recorder with auxiliary full-scale and zero-point adjusters is employed in place of the X-Y recorder, since the latter is strongly restricted in the recording chart space (10 x 15 in.). The Brown chart, however, is run on the time base (1/2, 1, 2, 4, 6, 8, 12, 16 in./hr). However, the fluctuation in the input neutron flux is usually less than several %, and hence the Brown recorder often plays a role more than just a qualitative display of the data. Of course, a large portion of the data processing is carried out from the printer-punch output (see Table II). The visual display of any one of four angles can be made on the lamp bank. During the operation with the printer-punch recording, the lamp bank shows all of the numerical data flowing into the printer-punch unit. This display in the follow-mode lasts about a half second* for each datum.

Table II

OUTPUT DATA FORMAT

Number of Characters	Data (single crystal)	Number of Characters	Data (powder)
6	Title information	6	Title information
5	Φ	1	Letter "P"
5	X	5	Initial 2θ
5	Initial Ω	7	Neutron counts at $2\theta_j$
5	Initial 2θ	10	Count subtotal
7	Neutron counts at $2\theta_j$	5	$2\theta_j$
10	Count subtotal	7	Neutron counts at $2\theta_k$
5	$2\theta_j$	5	$2\theta_k$
7	Neutron counts at $2\theta_k$	10	Count subtotal
10	Count subtotal	⋮	⋮
5	$2\theta_k$	10	Total counts
⋮	⋮	5	Final 2θ
10	Total counts		
5	Final 2θ		
5	Φ		
5	X		
5	Final		

*The displaying time is correlated to the time-interlocking settings of all other sequence controls in the system. These timing settings are variable to a certain extent.

The automatic control panel consists of the following: a selection switch for single cycle or continuous cycle; start and reset push-button switches; a subtotal in-out switch. Other panel-board controls include a selection switch for automatic or manual mode of operation, a switch for follow or non-follow display on the lamp-bank, and a display selection switch for one of four angles. The manual mode of operation is carried out through the panel-board control switches. A push-button switch is provided for "RUN-STOP" operation of each of four motors. A common step-slew switch and four directional switches for clockwise or counterclockwise complete the manual control of the motor drive. The manual-print push button activates a single cycle of the neutron-count record process at the given angular settings.

Finally, it would readily be noticed that a confused usage of the digital codes is apparent in our automatic control system, i.e., Baudot, Datex, 8421 BCD, and 1224 BCD codes are employed. This is due to the availability of the instruments and the computers when the system was designed. It is advised that the input and output tapes, the encoder, the scaler output, and related control-storage units should be coded on the same binary code, preferably on 8421 BCD, which is a direct representation of the BCD unit.

1-12. Neutron Monitor and Detectors

For monitoring the monochromatic neutron input, a drum-shaped low-efficiency fission counter (see Fig. 7) is placed at the exit of the secondary collimator. The active counting area, 3 in. in diameter, is currently reduced down to 2 in. by means of the cadmium shield. This large active area accommodates a wide variety of collimation techniques. The fission counter is a parallel-plate type with a fissile U^{235} layer on both the positive and negative electrodes. The U^{235} coating was made by the painting technique (see the book by Allen, 1960, p. 62). A dilute alcohol solution of uranium nitrate (97% enriched in U^{235}) was brushed on the electrode and converted to the oxide by subsequent heating in air. Four repetitions were required to obtain a firm coating of 0.1 mg cm^{-2} of U^{235} . The U^{235} layers remove 2.5% of thermal neutrons from the collimated beam, and the fission counting efficiency (see the book by Price, 1958, p. 263) ranges from 0.026% to 0.060% for 0.1- to 0.025-eV neutrons. For instance, 3.8×10^7 neutrons at 0.1 eV produce 10^4 fission counts. With a preamplifier gain of 10^2 and an amplifier gain of about 2×10^2 , the plateau length in the counting-rate characteristics spans from 50 to 900 V of the counter voltage. Our applied voltage across the electrodes was selected at 250 V. This fission counter is better than a low-efficiency BF_3 monitoring counter in several aspects: longer plateau length, higher counting stability, and less electronics required on account of much lower plateau voltage.

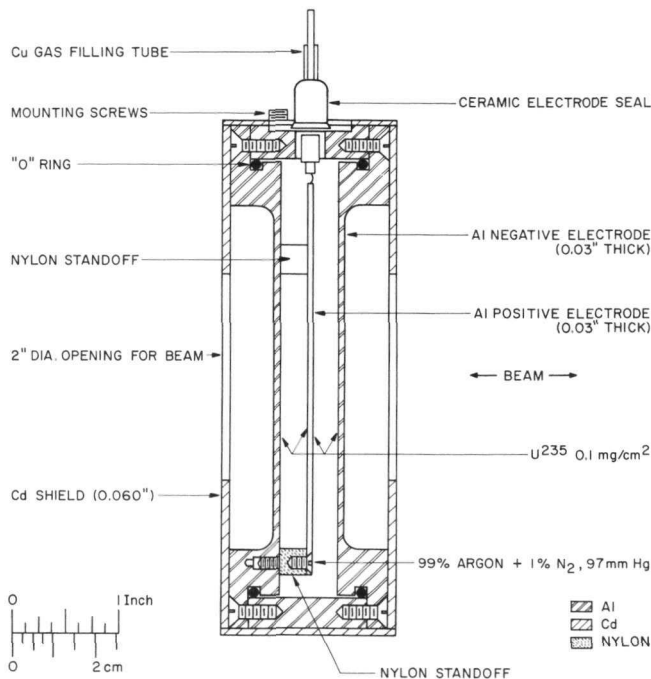


Fig. 7

Schematic Drawing of the
Drum-shaped Fission Counter
with a Cadmium Diaphragm

120-8156

The main neutron detector, a conventional BF_3 (96% B^{10} , 40 to 70 cm Hg in gas pressure) end-window proportional counter, 2 in. in OD with ceramic (usually fused Al_2O_3) or nickel entrance window, is currently used both for single-crystal and powder studies. These counters, possessing about 60 to 80% absorption efficiency for thermal neutrons, were constructed by the Reuter-Stokes Electronic Components, Inc. and the Nancy Wood Counter Laboratory under the specifications for minimizing the dead-counting space due to the tungsten-anode wire (<0.002 in.) and its insulator in the metal-window type. The high-voltage insulator isolating the anode from the metal window is usually a boron-free glass, but the dimensions may run up to 0.1 in. diameter and 1 in. long in some models. Currently, the metal-window counter is being replaced by the ceramic module, particularly for the single-crystal work. Nevertheless, our counter-shield supporter is designed to accommodate the commonly employed technique for the metal-window counter, i.e., offsetting the counter axis so that the beam avoids the insulator entirely.

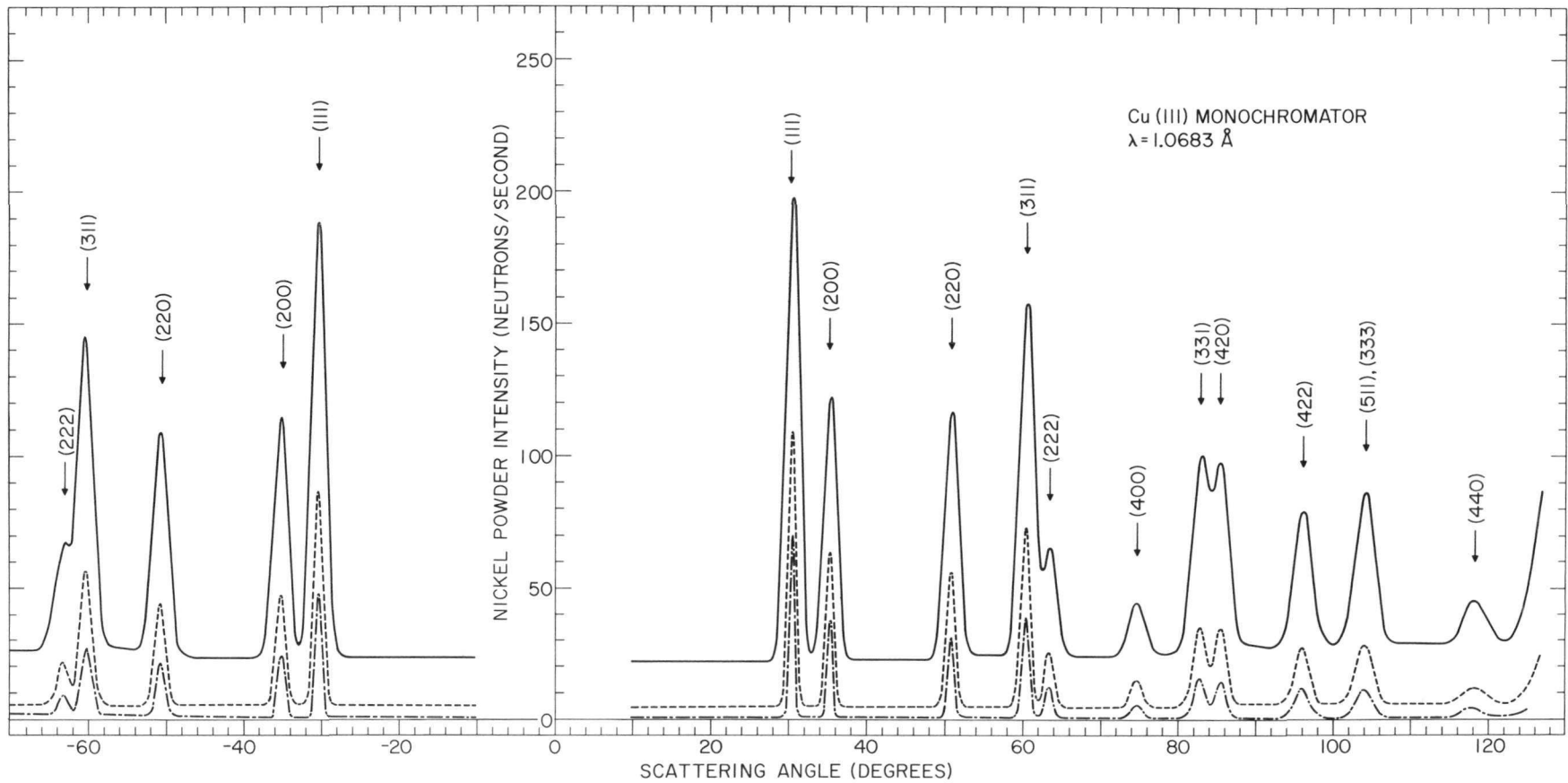
A novel technique for eliminating the end effects in the proportional counter has been described by Sikkema (1957). The B^{10}F_3 counters with the cathode-follower are operated at 2 to 3 kV for an amplifier gain of about 10^3 . The plateau length is, although not unusual, disappointingly short for all of our counters, being about 100 to 200 V.* In our current electronics, the pulse pair-resolution is about $10 \mu\text{sec}$, corresponding to $10^5 \text{ pulse sec}^{-1}$ in the detecting counter. For higher neutron fluxes, as described in Chapter 1-2, a precalibrated gold-foil detector is routinely employed.

*The plateau voltage and length, and the discriminator setting of a given counter, are dependent on the following: the distance between the counter and the preamplifier or the cathode follower; the gain setting and other characteristics of the amplification; the energy of the incoming neutrons.

The photographic technique is generally inferior to the counter method in the quantitative evaluation of intensity. However, the former gives, effortlessly, a time-averaged diffraction pattern inherent from the background fluctuation. Very often, the diffraction peak is distorted due to macroscopic imperfection of the sample crystal, and localized diffuse scattering is parasitic on the background. Moreover, spurious reflections may also exist because of diffraction effects from the sample container and holder. The routine counter technique with a linear scanning mode may not detect this and hence may be followed by the film method.

Since Wollan et al. (1948) took the first neutron Laue picture with an indium screen, neutron radiography has been improved to a great extent, particularly in shortening the exposure time. Thewlis (1956) has described general principles, Smith (1962), Smith and Holcomb (1963), and Wang et al. (1962) have developed a ZnS(Ag)-Li⁶F phosphor. Berger (1962a, 1962b, 1963, 1964) has further quantitatively investigated the measurement of intensity. We have utilized the photographic technique for checking the beam-intensity profile and the sample alignment in the low- and high-temperature enclosures. Also, a precession camera is being installed behind the main monochromatic-beam catcher having a small neutron-guiding center-hole. The scintillation and solid-state counters lessen the counter-shield size and weight and, hence, greatly simplify the instrumentation. Brief reviews on this subject have been given by Bacon and Lonsdale (1953) and King (1964). However, the efficiency and noise characteristics of these counters have to be improved substantially so as to substitute the B¹⁰F₃ counter (see also Allen, 1960).

As an example, diffraction patterns of nickel powder are shown in Fig. 8. The three experimental curves were taken under the same conditions except for varying the counter collimation, i.e., using 6-in. or 12-in. Soller-collimator, or without Soller collimator. The common experimental conditions are: the secondary collimator, type II; the beam slit at the secondary-collimator exit, 1.27 x 3.81 cm²; the slit at the counter-collimator entry or at the counter-shield front-face, 0.97 x 3.81 cm²; specimen-to-counter-distance, 41.22 cm; Nancy-Wood 2-in.-diameter counter; the sample holder, 1-cm ID. The resolution-collimation correlation is exemplarily demonstrated in Fig. 8. Although the diffraction intensity decreases rapidly with increasing collimation, the signal-to-noise ratio is considerably better for the higher collimation. The analyses of the peak width and intensity suggest incompleteness in all of the reported formulations on the subject (Chapter 1-3). Theoretical interpretations on our elaborate data for the powder and single-crystal collimations are now in progress.



120-8043

Fig. 8. Neutron Diffraction Patterns of Nickel Powder. The solid, dotted, and broken diffraction curves were obtained with the counter collimations, no Soller, and 6-in. and 12-in. Soller collimators, respectively.

2. AUXILIARY INSTRUMENTATION

2-1. Specimen Encasement

Our specimen encasing and related preparation techniques for routine experiments are briefly described here. The materials for encasing the neutron sample should satisfy general requirements for the beam-path component, i.e., their capture and scattering cross sections, including the magnetic contribution, should be as small as possible. Their scattering effects should easily be subtracted from the experimental data. Of course, for specific experiments, such as those at high and very low temperatures and those under an external magnetic field, we have additional criteria, which will be discussed in Chapters 2-7 to 2-11.

Our materials for enclosing the powder specimen are $Ti_{2.13}Zr$ (disordered alloy), Al, and V, among which $Ti_{2.13}Zr$ is most frequently used since $Al < Ti_{2.13}Zr < V$ and $0 = Ti_{2.13}Zr \lesssim V < Al$ in the total cross section and the coherent scattering cross section, respectively (ref. Table III in Appendix I). For enveloping the reactive specimen, fused silica, nickel, Monel-alloy, and Teflon are used; other encasing materials may be selected from Table III.*

The standard dimensions of our cylindrical holders are: 2.5 to 3 in. in height; 1.0, 0.8, and 0.6 cm in ID; 0.005 to 0.004 in. in wall thickness. The holder is equipped with a tectorial cap with O-ring or thin neoprene-diaphragm gasket. Fused-silica tube, of 1-cm ID and 0.5-cm wall, is used for some specific experiments.

A powder specimen is uniformly packed into a holder by means of a Lucite stick, and the packing height is measured with another Lucite stick, graduated in mm. For samples having low coherent-scattering cross section and relatively small capture cross section, in order to increase signal-to-background ratio, the powder is compressed by means of the device shown in Fig. 9. The device is placed in a small laboratory hydraulic press (maximum pressure of 5000 lb in.⁻²), and the compressed specimen may be used with or without the holder. For reactive samples, the whole device is enclosed in a Lucite glovebox in which a positive pressure of dry inert gas is kept during the compressing and transfer processes. When the preferred-orientation problem arises, the sample may be intermixed with fillings of $Ti_{2.13}Zr$ or vanadium and, for simultaneous absolute-intensity determination, with

*Note that the scattering effect could be relatively large even for large transmission ratio if the capture cross section is very small.

the standard substance* (e.g., fillings of Al, Mg, Ni, Si, Zn, or dendritic NaCl**). The absorption correction for the thin-walled cylindrical tube with an absorbing medium is given by Levy and Sharrah (1955) and Boutron and Mériel (1960).

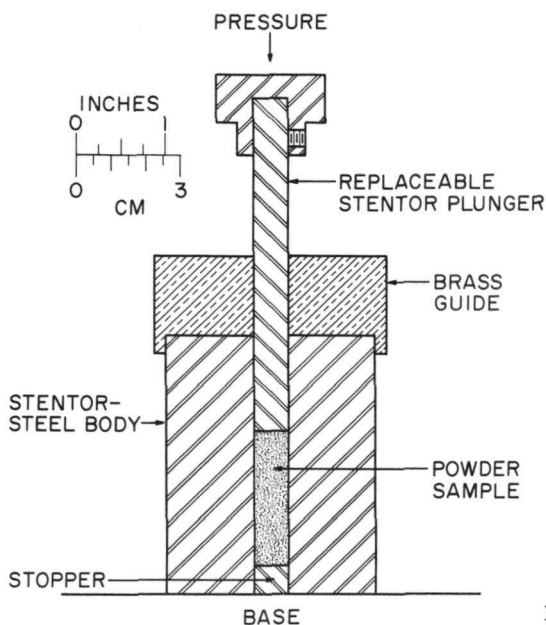


Fig. 9

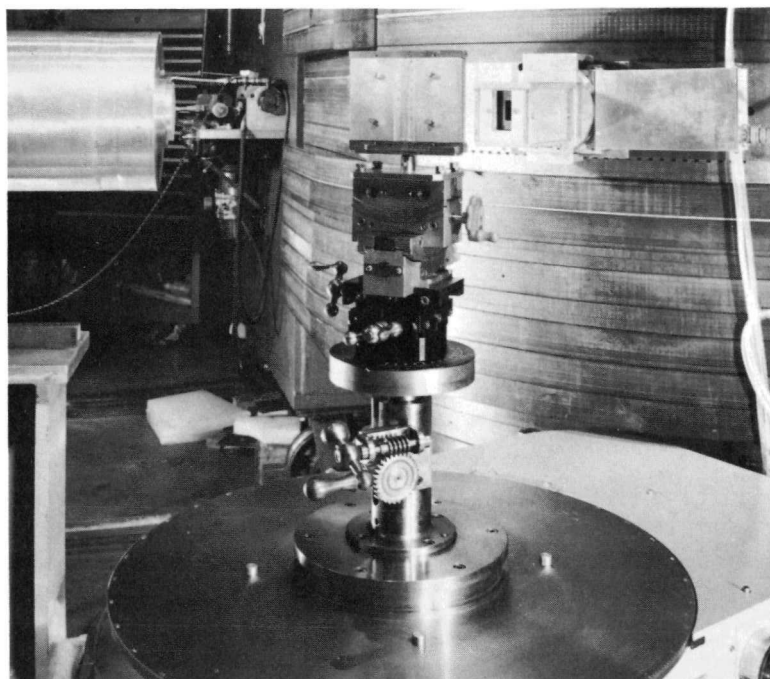
A Compression Device for Preparing a Neutron Powder Sample Having Small Coherent-scattering and Low Capture Cross Sections

Our flat powder-sample holder is a rectangular aluminum box with an exchangeable window 5.5 x 2.25 in. (horizontal x vertical), for which 0.015-in.-thick aluminum or 0.04-in.-thick fused silica is frequently employed. The maximum sample thickness is 1 in., and the sample dimensions may be varied by means of movable partition walls. The holder is gasket-tight and is set on the fine-slit "T" holder which is in turn mounted on the large goniometer head (see Fig. 10). Our flat folder is useful for diffractometry with highly absorbing specimens or weak coherent scatterers, but is not designed for small-angle scattering studies.

The powder-sample encasing techniques described above are readily applicable to the single-crystal specimen. Here, the fused quartz capillary is a favorite encasing material. The use of a Pyrex capillary should be avoided because of an appreciable content of boron (see Appendix I). The single crystals are often shaped into sphere, cylinder, or plate. For preparing the spherical crystal, besides the well-known Bond technique, Heintzelman *et al.* (1962) and Belson (1964) have developed unique methods. The melt-and-blow technique, if applicable, can be used to prepare spherical crystals extemporaneously from the polycrystalline substance.

*Total cross section and coherent intensity per unit volume should not be too far different between the specimen and standard substances. The absorption correction in the method of mixtures would be greatly simplified by sieving out proper particle sizes (see book by Peiser *et al.*, 1955, pp. 338-340).

**Pulverized high-cleavaging substances are not recommended.



120-6564

Fig. 10. The Fine-slit Assembly with the Universal Goniometer Head Mounted on the Ω - and Height-adjustable Support. The slit box and the fission counter are seen at the secondary-collimator exit.

2-2. Goniometric Devices

The full two-circle goniometer in use was constructed by the Picker X-ray Corporation, and the Datex encoders and Slo-Syn 250 motors are attached to the Picker unit for automatic control of X and Φ angles. Arndt and Willis (1963), Mueller *et al.* (1963), Peterson and Levy (1959) have described their full-circle goniometers, and Alexander and Smith (1962), Sabine (1963), Santoro and Zocchi (1964), and Willis (1960b, 1961) have discussed the geometric properties and the aligning procedures.*

The normal-beam nonequatorial technique has been adapted to the neutron goniometry by Maschinen Fabrik Augsburg-Nuremburg (1960) and Takei *et al.* (1960). The equi-inclination and other techniques developed for X-ray methods have not been used in the neutron-counter diffractometry. In comparison with the four-circle diffractometry, these techniques suffice with lesser degree of accuracy in the specimen alignment and require two- to three-angle automation instead of the four-angle control. However, the wide-open collimation virtually eliminates the difference in the alignment requirements, and the sequent usage of the control electronics

*Although it is written for the quarter X-circle goniometer and essentially for the X-ray application, Furnas' manual (1956) for the three-circle cone method is very useful in the neutron single-crystal study.

(Chapter 1-11) makes the second problem trifling. The normal-beam non-equatorial and related techniques have some shortcomings in the large-scale instrumentation and also in the data processing (Wooster, 1963).

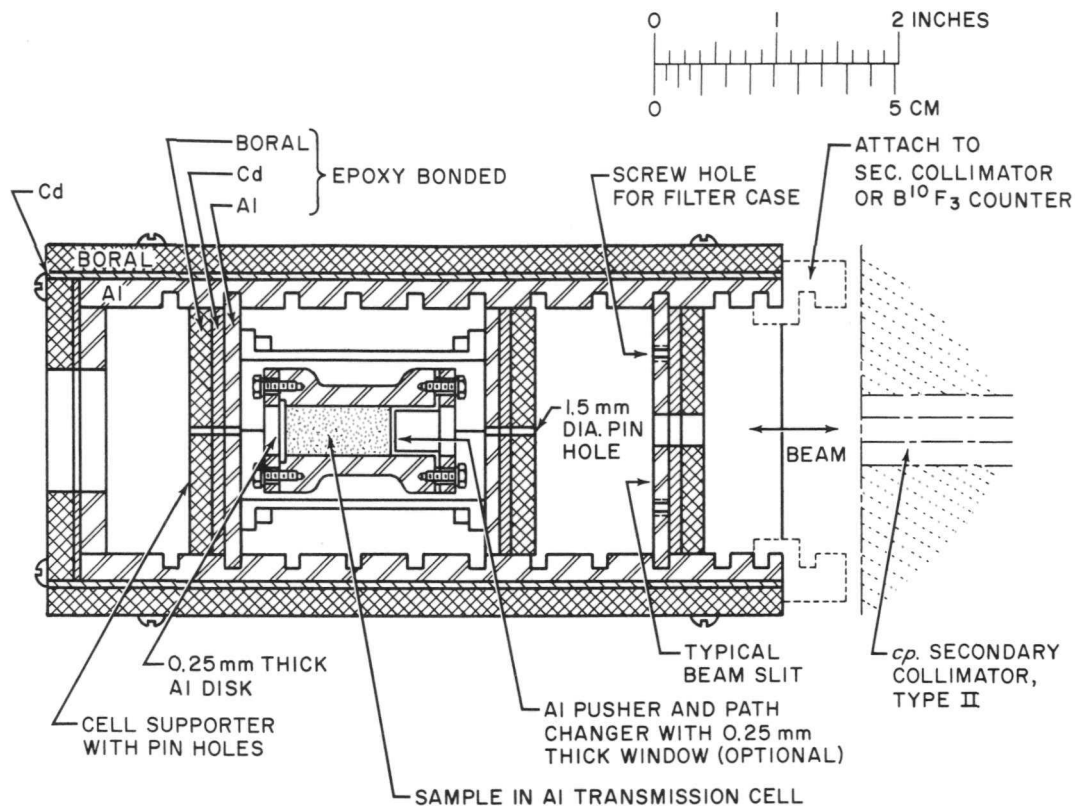
A large, universal goniometer head with mesh-tension, adjustable gear trains was constructed based on the following design specifications: cross slides for ± 0.5 -in. translation; azimuth inclination, $\pm 20^\circ$ with 0.1° vernier reading; the lower-rocker reading circle, 11.692 in. in diameter; the upper-rocker reading circle, 7.942 in. in diameter; the common center of the azimuth rocking circles, 2.375 in. from the center of the top platform. This goniometer head has been used as a supporting base for almost all of the auxiliary instruments, as well as for direct specimen mounting.

The goniometer-head unit is equipped with a 2π Ω -adjuster which is very useful in crystal aligning, since the zero-adjusting of the encoder needs skillful decoupling and coupling procedures of the precision gear trains. The goniometer unit is supported by the height-adjustable post which can set the top platform of the goniometer down to 7.25 in. from the beam center. When the specimen position deviates from the common center of two orthogonal rockers, both azimuth reading and cross-slide centering have to be recalibrated and readjusted. Hence, the specimen position in the Dewar and the furnace (Chapters 2-9 and 2-11), both of which are mountable on the goniometer head, are designed to coincide with the azimuth-circle centroid. Nevertheless, the wide-range height adjuster relaxes the limitation in the size of a possible future instrument mountable on the goniometer head. This goniometer head is also employed in the precision alignment of the powder-specimen holder.

The fine-slit assembly is shown in Fig. 10. A pair of boral-cadmium-aluminum plates (ref. Chapter 1-9) is set on the "T"-shaped holder in a sliding-door manner. The scales on two movable plates and the one on the "T" holder define the slit position and its aperture width, and the aperture height is confined by pasting strips of cadmium plate over the part of the slit opening. The fine-slit assembly is used for studying the homogeneity and divergency of the monochromatic beam. It is also used for mounting lamelli-powder or metal-foil specimens in the Bragg-case geometry.

2-3. Total Cross-section Experiment

The total cross-section measurement with our diffractometer is based on the transmission-cell technique which is illustrated in Fig. 11.



120-8569

Fig. 11. Typical Transmission-cell Setting in the Slit Box

The transmission cell is made of aluminum, and has a bobbin-like shape for reducing the weight and for easy handling. The specimen is filled into the cylindrical through-opening, 1 cm in diameter and 3.05 cm in length. The end windows are a pair of aluminum disks, 0.25 mm thick, and the cover caps are placed with or without O-rings. An optional aluminum pusher with the 0.25-mm-thick window is used for reducing the beam path-length of the high-capturing specimen (see Fig. 11). The cell can be employed for both solid specimens and liquid samples. For a specimen which reacts with aluminum, a thin-walled Teflon tube of 1-cm OD is inserted into the specimen cavity, and thin Teflon disks replace the aluminum windows. The total cross section is obtainable without knowing the specimen length along the beam direction, since $n = N_A W / (MS)$, where W is the weight of the specimen and S is the basal area of the specimen cylinder (Appendix I for other notations).

The transmission cell is placed onto the V-shaped bridge of the cell supporter. The beam-guiding pinholes, 0.15 cm in diameter, are made on the boral-cadmium-aluminum end plates of the supporter. The outer distance between two pinholes is 7.14 cm; hence the corresponding beam divergency is $1^\circ 12'$ of arc. The cell supporter is mountable either on the exit of the secondary collimator or on the entrance of the counter

collimator. Usually the cell supporter is placed in the boral-cadmium-shielded slit box so as to reduce the spurious effect due to strayed neutrons.

For suppressing the unwanted neutron contamination, the filter technique (see Appendix II) may be employed and the secondary monochromator may be incorporated into the transmission experiment. For this purpose, a laid-off monochromator crystal is placed on the large goniometer head at the Ω -table center. The divergency and aperture of the beam in the transmission experiment are determined from those of the secondary and counter collimators, the counter-slit aperture, and the double-pinhole geometry. The solid angle subtended by the $B^{10}F_3$ counter at the specimen can then be made to be 10^{-4} to 10^{-5} of 4π . Hence, the "in-scattering effect" (Egelstaff, 1958) is usually negligibly small, and the small-angle scattering correction, if any, will be found most effectively by interchanging the position of the transmission cell between the secondary-collimator exit and the counter-collimator entry.

A practical technique for obtaining the total cross section is given as follows. A singly or even doubly monochromated beam is not entirely free of unwanted neutrons. Subsequently, the transmitted neutron intensity is expressed as

$$I = \int I_0(E) \exp[-n\sigma_t(E)] dE,$$

where $I_0(E)$ is the incident beam intensity, which may be separated into three terms: the component for the principal monochromatic neutrons, $I_0(E_1)$; the second-order contamination, $I_0(E_2)$; and the residual term, $I_0(\langle E \rangle)$. The energy spread of the first two terms can be neglected unless E_1 or E_2 is near a sharp resonance. The $I_0(\langle E \rangle)$ component originates from the incoherent elastic scattering and inelastic scattering from the monochromating crystal, and also from the scattering due to other collimating components. The amounts of $I_0(E_1)$, $I_0(E_2)$, and $I_0(\langle E \rangle)$ may be determined from the double-crystal or pair-transmission method or a combination of both (Wajima et al., 1960). Our method, based on incorporation of the cadmium plate in the single-transmission technique, is considerably simpler than other methods.

The transmission equation is now expressed as follows:

$$\begin{aligned} I = & I_0(E_1) \exp[-n\sigma_t(E_1) - n\alpha_{Cd}(E_1)] \\ & + I_0(E_2) \exp[-n\sigma_t(E_2) - n\alpha_{Cd}(E_2)] \\ & + I_0(\langle E \rangle) \exp[-n\sigma_t(\langle E \rangle) - n\alpha_{Cd}(\langle E \rangle)], \end{aligned}$$

where α_{Cd} is the total cross section of cadmium. Firstly, the empty transmission cell, i.e. $n = 0$, is placed in the beam, and the neutron counts

vs. varying thickness of cadmium are recorded ($n_{\text{Cd}} = 0.4632 \times 10^{23} \text{ t cm}^{-2}$). Since $\sigma_{\text{Cd}}(E_1)$ and $\sigma_{\text{Cd}}(E_2)$ are far larger than $\sigma_{\text{Cd}}(\langle E \rangle)$, $\sigma_t(E_1)$, or $\sigma_t(E_2)$, the first two terms in the above equation are neglected for thick cadmium filters with which $I_0(\langle E \rangle)$ and $\sigma_{\text{Cd}}(\langle E \rangle)$ are determined. As shown in Fig. 12, a straight line obtained with large cadmium thicknesses supports our assumption that a single $\sigma_{\text{Cd}}(\langle E \rangle)$ value is sufficient to obtain a representation of the residual term. With the aid of $\sigma_{\text{Cd}}(E_1)$ and $\sigma_{\text{Cd}}(E_2)$ (see review article of Hughes and Schwartz, 1958), $I_0(E_1)$ and $I_0(E_2)$ are subsequently obtained from a simple curve-fitting method.

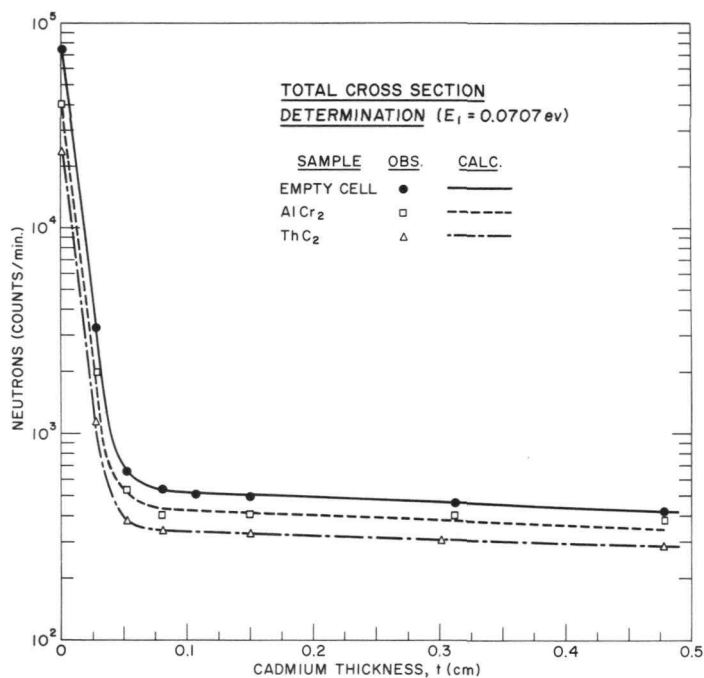


Fig. 12
Experimental Results for Total Cross
Section obtained with Cu(111) Mono-
chromatic Neutrons ($\lambda = 1.0683 \text{ \AA}$)

120-8131

The transmission data obtained with the sample are similarly analyzed; examples are shown in Fig. 12, where we have $I_0(E_1) = 7.47 \times 10^4$; $I_0(E_2) = 72$; $I_0(\langle E \rangle) = 533$ in relative count units and $\sigma_{\text{Cd}}(\langle E \rangle) = 10.8 \text{ b}$. The resultant cross sections of AlCr₂ and ThC₂ indicated in Fig. 12 are in excellent agreement with the values calculated by means of the atomic cross sections.

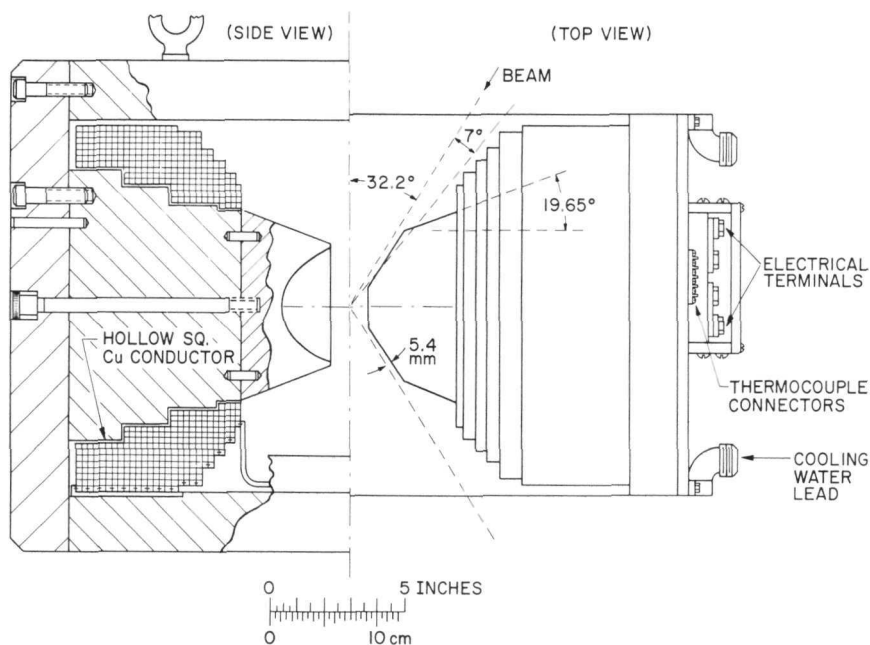
2-4. Design of Diffraction Electromagnet

The general principles and the practical procedures in the design of the high-field electromagnet have been very thoroughly discussed by Ishikawa and Chikazumi (1962), although their formulations are not directly applicable to our case. A good review has been given by E. Mendza in the book by Hoare *et al.* (1961, pp. 173-180). An electromagnet to be used for diffraction studies has to admit the incident and scattered beams in a large range of angles, which introduces additional problems in the design and fabrication. Since the spin-coupling interaction in the magnetic substance is strongly temperature dependent, the magnet should also be able to

accommodate the Dewar and the furnace. Moreover, there exist obvious restrictions in the dimensions and weight of the magnet on the diffraction turntable.

The superconductor magnet has potential usage in the diffraction, for attaining very high magnetic field (see book of Kolm *et al.*, 1962), but it is not suitable for use in a high-temperature experiment.

Diffraction magnets have been constructed by various neutron groups, but no design details have appeared in the literature. Our electromagnet, designed and constructed in cooperation with Spectromagnet Industries, California, is depicted in Fig. 13.



120-8155

Fig. 13. Construction of the Diffraction Electromagnet. On the left-hand side, the cross section parallel to the yz -plane is shown, and on the right-hand side, the xz schematic is given. Pole pieces with 1.4-in.-gap are employed. The short horizontal bars in the coil conductors indicate the electrical connections between adjacent subcoils. The inlet-outlet water channels for cooling individual subcoils have been omitted.

In the earliest stage of the diffractometer design, a maximum magnetic field of about 20 kGauss* was assumed for the proposed magnet. The physical volume of an electromagnet is roughly proportional to the cube of

*Practically all of ferromagnetic substances (except, e.g., iron and Fe-Co alloys) possess saturation magnetization values less than about 20 kOe. Likewise, in general, in ferromagnetic and antiferromagnet substances, completion of domain growth or boundary displacements takes place at an external magnetic field of below 20 kOe. This is followed by the magnetization-orientation of the magnetic spins, for which the saturation field however frequently exceeds 20 kOe.

the air-gap distance for a given magnetic field. A limited survey of 20-kGauss magnets revealed this proportionality constant to be about 2×10^3 . The weight of the magnet is about 45 to 65% of the weight for the whole volume of the magnet being occupied by the yoke material. These approximate rules were considered in the preliminary design of the diffractometer.

Further prerequisites were later specified or determined as follows:

(A) The straight double-yoke type was chosen to attain sufficient mechanical strength* and for a simple adaption of the magnet orienter described in Chapter 2-6.

(B) The air gap has to be 3 to 4 cm, or wider, in order to permit insertion of the thermal envelopes for the specimen.

(C) The air-gap variation is attained by means of interchanging pole pieces, because of simplicity in the fabrication of the magnet orienter.

(D) The maximum scattering angle (2θ) admissible through the magnet was selected to be between 60 and 70°. Although the magnetic-scattering intensity decreases rapidly with increasing scattering angle, it is obvious that the wider admissible angle is by all means better, for instance, in the Fourier transform of the magnetic data for eliminating the series-of-termination effect. However, the magnetic-flux leakage tends to increase considerably in the magnet-pole configuration, allowing scattering angles larger than about 70°.

(E) At the maximum magnetic flux, the field homogeneity should be less than $\pm 0.5\%$ within the specimen volume, for which the largest dimensions were selected as follows: 1 cm x 4.5 cm (horizontal x vertical) in the cross-sectional area normal to the field direction; 1 cm along the third axis (orthogonal coordinates). The above dimensions are implied by the size of the powder holders; the corresponding field homogeneity becomes much higher for the smaller volume of a single-crystal specimen. Because the specification (D) interferes severely with the pole-piece design, the field-homogeneity requirement here is set considerably lower than for nondiffraction magnets ($\pm 0.1\%$ or better).

The details of the calculations and the improved pole-piece designs will be published elsewhere. The resultant design characteristics are described below. The dimensions of the yoke were determined not only from the magnetic-saturation requirements, but also from non-steric-hindrance conditions between the magnet with its orienter and the diffractometer

* The magnetostatic force in kg/cm^2 between the pole pieces is $0.04 B^2$, where B is the air-gap flux density in kGauss. For 20 kGauss, this attracting force is $16 \text{ kg}/\text{cm}^2$ or $228 \text{ lb}/\text{in}^2$ and the integrated force is equivalent to about 1500 lb for our 1.4-in. gap pole pieces.

components in the scanning mode. The outer dimensions of the yoke (forged Armco-ingot iron) are 25.238 in. along the field direction in the air gap, 18.011 in. high and 14.012 in. wide.* The thickness of the yoke is 2.206 in. throughout; hence, the flux-propagation cross section of the yoke is $2 \times 30.91 \text{ in.}^2$ (399 cm^2), which is smaller than the cross section of the pole base. This conflicts with the general principle that the yoke cross section should be about 1.2 to 1.4 times the pole-base area, for sufficing the saturation sequence, pole-piece face \rightarrow pole piece \rightarrow pole \rightarrow yoke, or for simultaneous saturation of these components. However, our maximum field can be attained without saturating the pole-base area, and further validation of our yoke cross section is given below.

The shape of the pole is of circular stairs so as to approximate the logarithmic condition for the least flux leakage and to have a compact coil winding within our yoke environment. The dimensions of the pole are, from the pole base to the top of the circular stairs: 10 in. in diameter and 1.75 in. in riser height; 8.75 in. in diameter and 1.75-in. riser; 7.5 in. and 1.75 in.; 7 in. and 1.186 in. The total length of the pole is 6.436 in. The optimum diameter of the pole base may be obtained from the following approximation:

$$\text{maximum magnetic field (kOe)} = 28 \log\left[\frac{\text{(diameter of pole base)}}{\text{(air gap distance)}}\right].$$

For 20 kOe and a 1.4-in. air gap, we obtain 7.2 in., the diameter of the pole base, which may be compared with our diameter of 10 in. for the non-saturation condition. The cross-sectional area of the 7.2-in. base is 263 cm^2 , which is considerably smaller than the yoke cross section. When the circular stair is approximated by the frustum of a right cone, the vertical half-angle of the cone is about 19.7° , which is an important value required for obtaining the maximum field with the least fringe flux. The pole material is also of Armco-ingot iron forgings.

The pole piece is the frustum of a right cone whose near-tip area has been shaved off in order to admit the incident and scattered neutrons. The diameter of the base of the pole piece is 6.898 in., and the vertical half-angle of the cone is 19.65° . The height of the cone frustum is 4 in. minus one-half of the air-gap distance. The profile of the xz cross section** is represented by the axial cross section of a pile of two cone frustums with the following dimensions: vertical half-angles of 19.65° and 57.8° , and frustum heights of 2.02 in. and 1.98 in. minus one-half of the air-gap, for the base and top cone frustums, respectively; the diameter of the base of the top cone frustum is 5.454 in. These dimensions are designed to allow scattering angles (2θ) up to 64.4° , for which the neutron beam width is taken as 0.423 in. (1.07 cm).

*Conventionally, these are often taken as follows: the width of the yoke equals the diameter of the pole base; the yoke thickness equals half of the yoke width.

**The z-axis is parallel to the pole axis, and the y-axis is parallel to the straight-cut direction of the pole piece. The x-axis is then chosen in the orthogonal system with the origin at the center of the air gap.

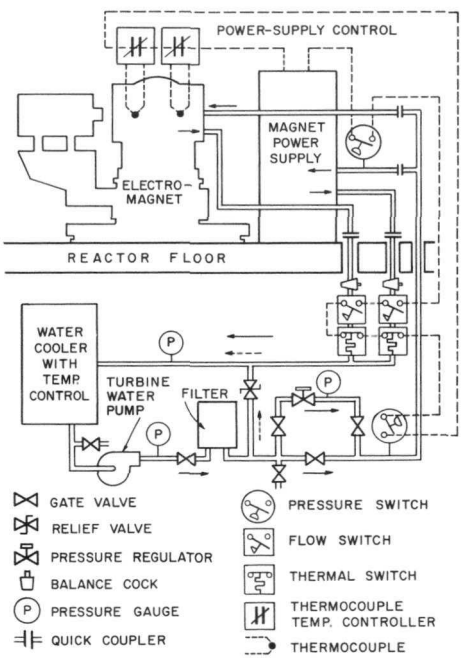
The air-gap variation is attained by cutting off the gap section of the pole piece of the same dimensions. Subsequently, the pole-piece face approaches the circular form as the gap distance increases. Also, the effect of the top cone frustum on the gap field becomes smaller for larger air gaps. The dimensions of the base cone frustum are unchanged by the gap variation. Four pairs of the pole pieces for air gaps of 1.4, 1.5, 2, and 3 in. have been prepared. The 1.4-in. air gap has been used for most of the neutron experiments. The shape of the pole-piece face is confined by two arcs signified by the top cross section of the base cone frustum and two chords parallel to the y direction. The radii of the arcs, the lengths of the chords, and the distances between two chords (the x-widths of the pole-piece faces) are, respectively: 2.27, 4.31, and 1.44 in. for the 1.4-in. gap; 2.29, 4.29, and 1.59 in. for the 1.5-in. gap; 2.38, 4.13, and 2.37 in. for the 2-in. gap; 2.56, 3.30, and 3.92 in. for the 3-in. gap. The pole-face areas are 41.3, 46.0, 69.5, and 115.3 cm² for the 1.4-, 1.5-, 2-, and 3-in. air gaps, respectively. The cone angles of the poles and the pole-piece dimensions for the smaller air gaps (1.4 and 1.5 in.) are approximately equal to the optima or maxima obtained from the field calculations. However, the pole-piece dimensions for larger air gaps deviated slightly from the values recommended by the calculations. The pole-piece material is also forged Armco iron with a saturation value of about 21.6 kOe. An obvious improvement from use of Fe₂Co (34.5 w/o Co) having the saturation value of 24.2 kOe has not been carried out. Several attempts with Fe₂Co Rose shims for obtaining higher field homogeneity were not fruitful with our pole configuration.

The coils should be designed so that they produce the largest possible field in the air gap. However, steric factors associated with the neutron beam and the yoke interfere. As a result, the shape of the coils is also one of circular stairs, and the differential ampere-turn varies along the pole axis. The coil contour allows a neutron-scattering angle up to $2\theta = 74.4^\circ$. The coils are wound with hollow-core copper conductor which is water-cooled internally. The hollow copper-wound coils lend themselves to efficient cooling and exhibit a compactness of the coil packing. The conductor is insulated by Mylar tape, and is imbedded in an epoxy resin to increase the dielectric and mechanical properties of the coils. The numbers of the winding are: eight seven-turns around the first riser of the pole; eight ten-turns for the second riser; the turn sequence, 13-12-12-12-12-9-9-7 toward the air gap for the third riser; 8-6-6-4 for the top riser. The total winding per coil is 246 turns. It should be noted that the coils around the third riser of the pole produces the largest magnetomotive force, and the ampere-turn distribution along the pole axis does not deviate too much from the optima from the field calculations.

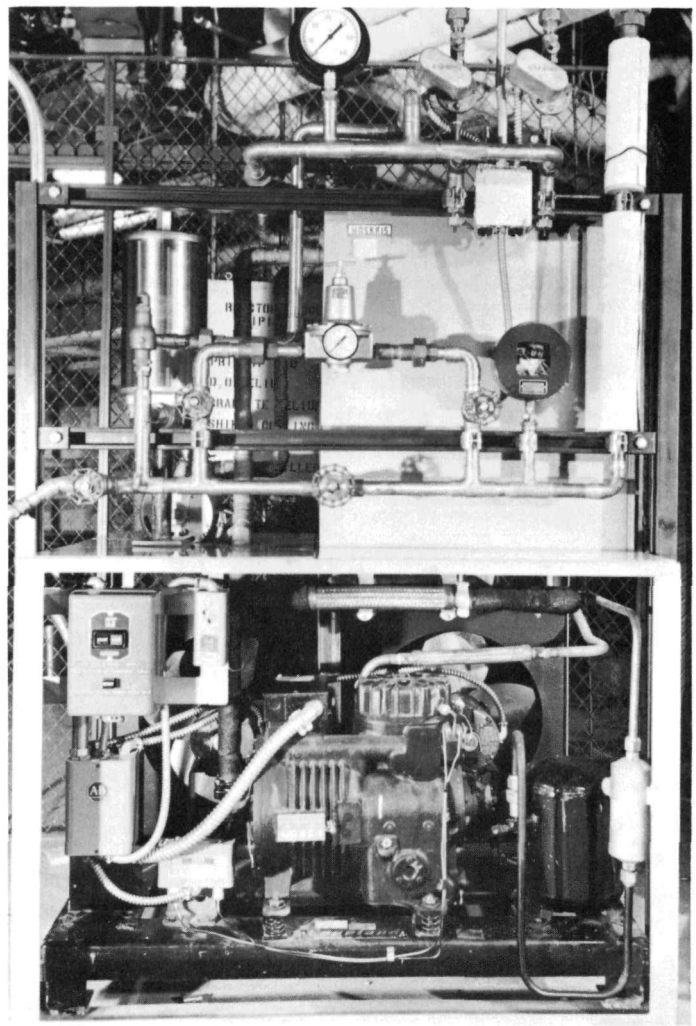
The maximum current is 200 Amp at 100-DC-V input. Hence, the maximum ampere-turn is 9.8×10^4 and the maximum power consumption is 20 kW. The total coil resistance is 0.488 Ω and the temperature rise is 25°C* for the water-cooling rate of 6 gpm at a water pressure of 60 psi.

*In the cryogenic and high-temperature experiments, the input water is cooled below 10°C to reduce the ambient heat radiation (see Chapters 2-7 and 2-11).

Each coil unit is vertically divided into 14 subcoils, and each subcoil is composed of two vertically wound unit-coils. Each subcoil possesses a pair of inlet-outlet water leads which are connected to the master water pipe. This insures equal distribution of pressure and temperature of the cooling water throughout the coils. The DC power supply is a standard silicone-diode rectifying unit with maximum output of 25 kW. The diodes are also cooled by water flowing at a rate of 4 gpm under a pressure of 60 psi. The water-cooling system with the safety devices is shown in Figs. 14 and 15. Here, distilled water in the refrigeratory cycle is used in lieu of city water, for flexible and stable controls of the heat-exchange rates and for assuring the water purity. Copper-constantan thermocouples are embedded into each coil unit, and extra thermocouple connections are provided (see Fig. 13) for measuring the pole-piece temperature in the high-temperature experiment (Chapter 2-11). The total weight of our magnet is only about 900 lb which is just about half the weight of the conventional 20-kOe magnet. Our magnet, in part, resembles the Paris and Uppsala magnets (Hoare et al. 1961, p. 179, and the references therein).



120-8563
 Fig. 14. Block Diagram of the Cooling System and the Safety Devices for the Diffraction Electromagnet

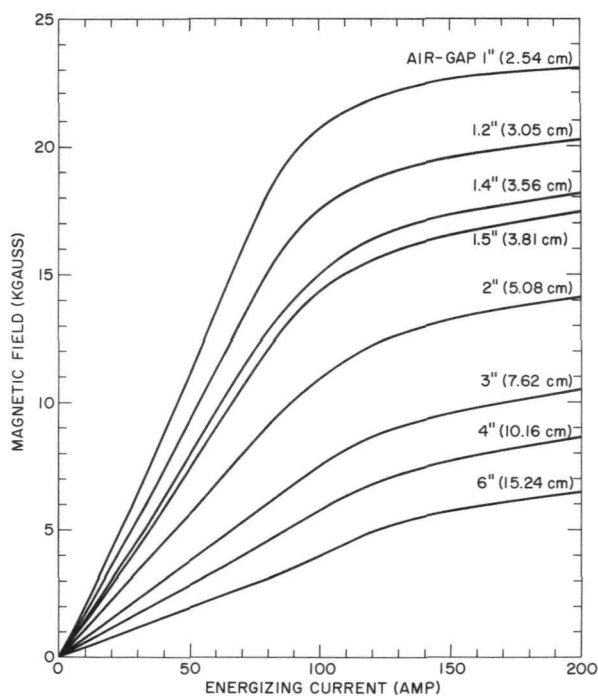


120-6556
 Fig. 15. The Magnet-cooling System and the Auxiliary Safety Devices (below the Reactor Floor)

2-5. Magnet Experimental Data

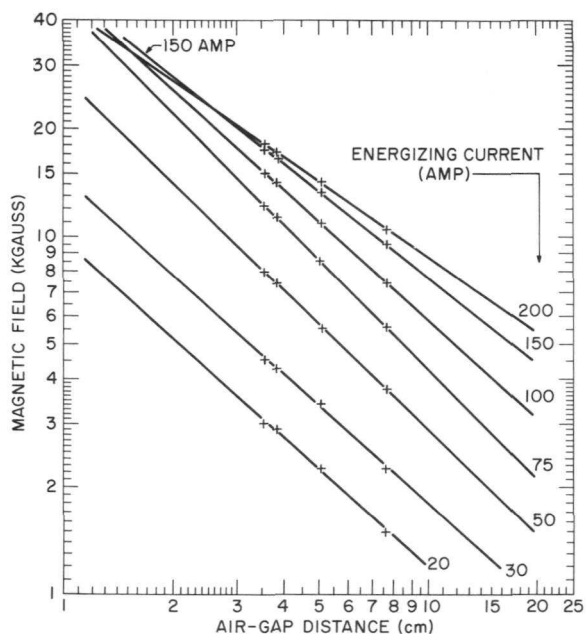
As stated in the preceding chapter, simple equations of the first degree correlate the gap distance and the dimensions of the top cone trustum of the pole pieces. However, these correlations are multinomial. Moreover, the pole-piece face is not circular but is closely approximated by a rectangle. These factors add more complexity to interrelations among the gap distance, the fulx density, and the field homogeneity.

A part of the magnetic-field measurements with the diffraction magnet was carried out by a group at the Spectromagnetic Industries. The magnetic flux densities at the center of the air gaps of 1.4, 1.5, 2, and 3 in. were measured for varying energizing current (see Fig. 16). In Fig. 17, the flux densities are replotted as a function of the air-gap distance for selected coil-current values. Special attention should be paid to the log-log rectilinear relation between the flux density and the gap distance in Fig. 17, since single or double right-cone pole unit suggests a semi-log rectilinear relation with the gap distance in the log scale. By extrapolation, results for gap distances of 1.0, 1.2, 4, and 6 in. were obtained. The data are also shown in Fig. 16. The seemingly adventurous extrapolation was validated from field calculations. The flux densities at the gap center for



120-8568

Fig. 16. The Magnetic Flux Density at the Center of the Gap as a Function of the Energizing Current. The data for the 1.0-, 1.2-, 4-, and 6-in. gaps were extrapolated from the experimental values for 1.4-, 1.5-, 2-, and 3-in. gaps.



120-8570

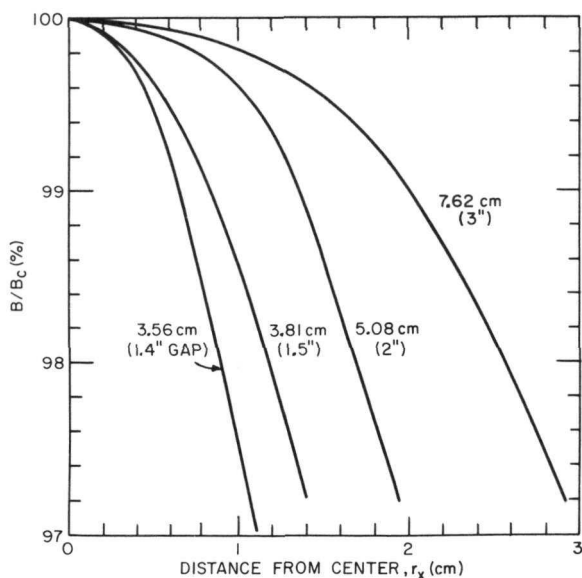
Fig. 17. The Magnetic Flux Density as a Function of the Air-gap Distance and Energizing Current. The crosses represent experimental values. Note intersections among the lines for 200, 150, and 100 Amp.

a maximum current of 200 Amp are 23.1, 20.2, 18.15, 17.45, 14.10, 10.50, 8.6, and 6.5 kGauss for 1.0-, 1.2-, 1.4-, 1.5-, 2-, 3-, 4-, and 6-in. gaps, respectively.

In Fig. 17, there may be noted intersections among the straight lines for higher energizing currents. This implies that at very small gaps the lower current could produce a higher magnetic field. In fact, for the gaps smaller than about 0.8 in., the flux-density dependency on the current is no longer a monotonically increasing function, but possesses a maximum at some current below 200 Amp. This peculiar situation arises because of increasing fringe flux and local saturation in the pole pieces. The discussion on the field homogeneity will further substantiate this.

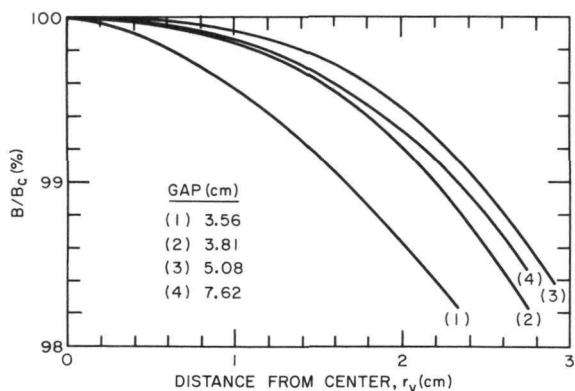
Our interest in the small gaps lies in future experiments for magnetization-orientation of the magnetic spins of the antiferromagnetic and ferrimagnetic substances and for related high-field studies at or near room temperature. External fields exceeding 30 kOe can be obtained with 1.7-cm gaps or smaller, the rapidly decreasing field homogeneity at these higher fields can be overcome by slight improvement of our pole-piece design. The field homogeneity is discussed below.

The percentage flux-density distributions in the midplane normal to the pole axis are shown in Figs. 18 and 19, for the x and y directions, respectively. The 200-Amp cases are cited here. Let the quantity $\Delta(B/B_c)$ represent the



120-8566

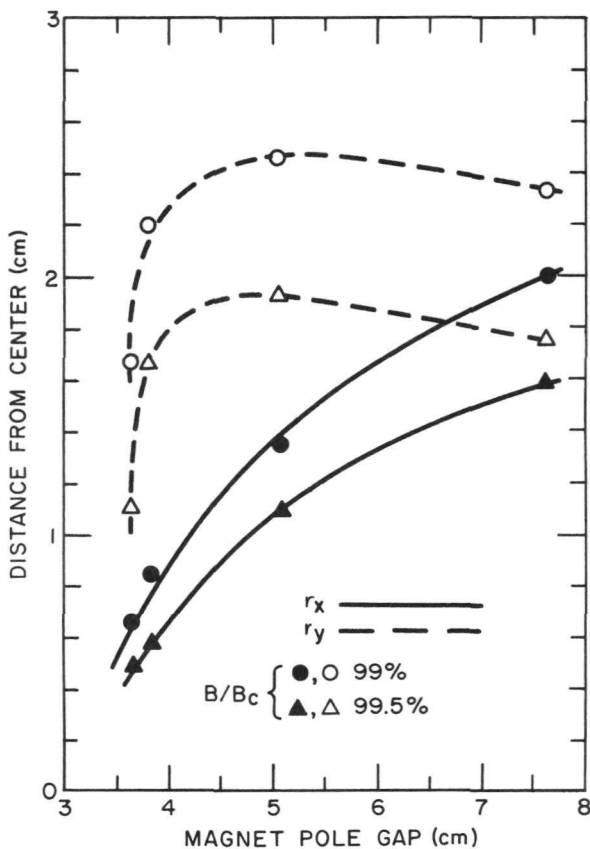
Fig. 18. The Magnetic-field Homogeneity Curves. B_c : the magnetic flux density at the center of the air gap. r_x : the radial-vector component normal to the pole axis and parallel to the chords of the arcs confining the pole-piece face.



120-8564

Fig. 19. The Magnetic-field Homogeneity Curves. r_y : the radial-vector component to the pole axis and parallel to the long edges of the pole-piece face.

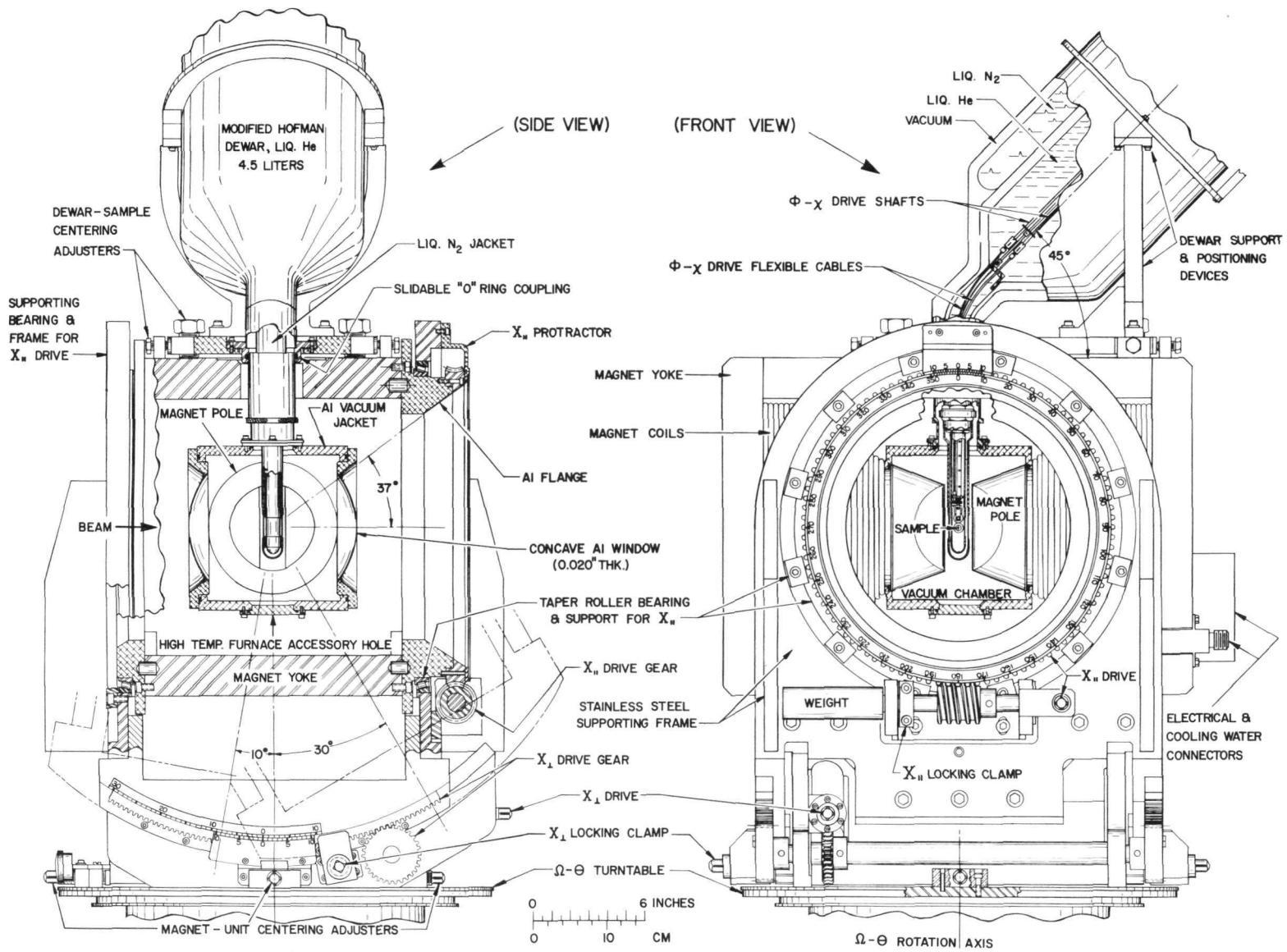
field homogeneity, where $\Delta(B/B_c)$ in % = $100 - (B/B_c)(\text{in } \%)$; B , the flux density at the given point; B_c , the central flux density. The following experimental values for $\Delta(B/B_c)$ in % at $r_x = 0.5$ cm, $r_y = 2.25$ cm, correspond to the largest-specimen cross section 1 cm x 4.5 cm; 0.52% at $r_x = 0.5$ cm and 1.64% at $r_y = 2.25$ cm for the 1.4-in. gap; 0.37 and 1.05% for the 1.5-in. gap; 0.08 and 0.91% for the 2-in. gap; 0.04 and 0.77% for the 3-in. gap. The x-direction homogeneity satisfies our original intention, but along the y-direction it is lower than intended. However, the specimen cross section referred to above is for a powder sample, for which the accuracy of neutron detection is seldom higher than the magnetic-field homogeneities cited above. For most single-crystal studies, the specimen cross section can be made less than 1 cm x 2 cm. The values of $\Delta(B/\Delta B)$ at $r_y = 1$ cm are: 0.44% for the 1.4-in. gap; 0.16% for the 1.5-in. gap; 0.14% for the 2-in. gap; 0.08% for the 3-in. gap. Consequently, highly homogeneous magnetic fields with the specified flux densities are available for single-crystal specimens.



120-8565

Fig. 20. The Curves Representing the Field-homogeneity Dependency on the Air-gap Distance.

The flux-density distribution in the gap is further analyzed in Fig. 20, where a general tendency of increasing field homogeneity for the larger gap is evident along the x-direction. However, along the y-axis direction, when the gap becomes smaller than about 3.75 cm (1.48 in.), the field homogeneity decreases very rapidly. This is due to aggravating flux leakage and to an increasing negative contribution of the pole-piece magnetization to the gap field. Maxima in the field-current curves (see Fig. 16) for very small gaps are based on the same phenomena as described before. For satisfying our field requirements, the gap should be larger than 1.4 in., or a smaller specimen volume should be chosen for the gaps less than about 1.4 in. The y-direction homogeneity decreases slowly for the gaps larger than about 5 cm (2 in.). Further interpretation of these interesting results is in progress.



120-7768

Fig. 21. The Liquid-Helium Angular Dewar with the Cryo-goniometric Device Mounted on the Diffraction Electromagnet. The 1.4-in.-gap pieces are shown in this assembly. The window thickness should read 0.031 instead of 0.020 in.

2-6. Magnet Orienter

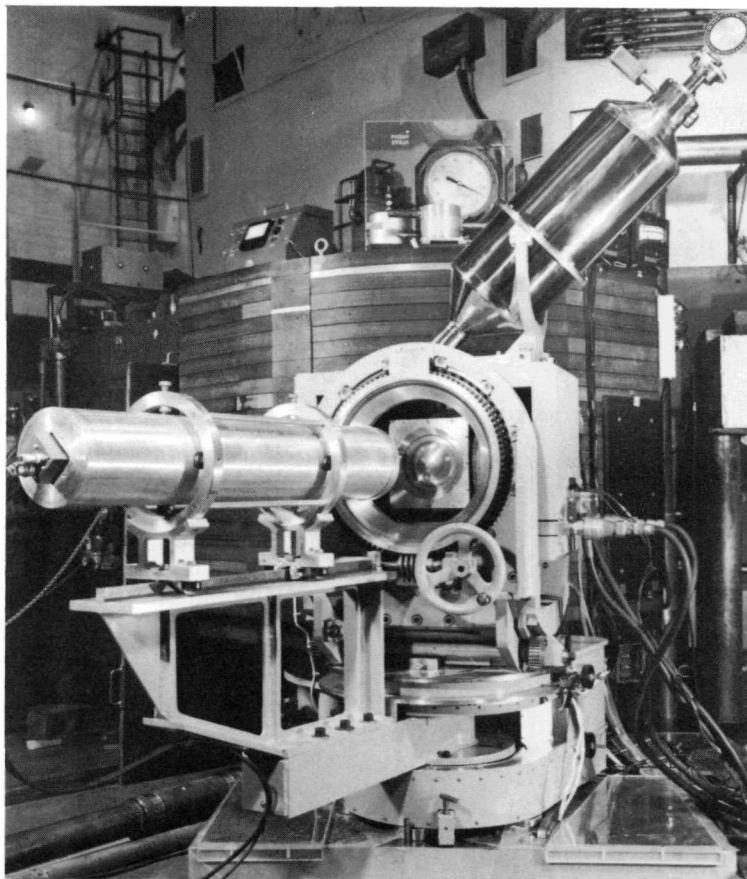
Ordered or partially ordered electronic-spin alignments in magnetic substances are frequently multifold as regards magnitude and direction of the magnetic moment. The variety and complexity of the spin structure are exhibited by the occurrence of antiferromagnetic, ferrimagnetic, and related, yet nonclassifiable, characteristics (see, e.g., the review article by Nathans and Pickart, 1963). Some examples are: order-disorder and multi-twin-domain distributions; multispin-axis structure in a single domain, such as the spiral and related spin configurations; different moment-vector assignments at otherwise equivalent lattice sites; entangled intercorrelations among a variety of the magnetic atoms in a compound; coexistence of localized and delocalized moments. It is obvious that a higher freedom in the selection of the magnitude and direction of the external magnetic field will be conducive to lesser degeneracy of the spin configuration and to more fruitful results in studies of anisotropy and magnetostriction.

The simplest technique for varying the external field direction is a direct mounting of the magnet on the Ω -table. In such a case the magnetizing vector is parallel to the reflection plane or, more specifically, parallel to the scattering vector in the normal-beam equatorial mode. If the dimensions permit, the magnet may be mounted vertically so that the field direction is perpendicular to the reflection plane. However, as stated in the introductory remarks, the field direction should be more variable in order to elucidate the complex spin structures with higher degree of accuracy.

On the other hand, the goniometric orientation of the specimen within the narrow pole gap is severely restricted because of confronting steric hindrance. Higher orientational freedom of the magnet will certainly relieve the steric limitation imposing on the specimen-goniometer design. A magnet orienter to meet with these requirements has been constructed, and its design features are described below.

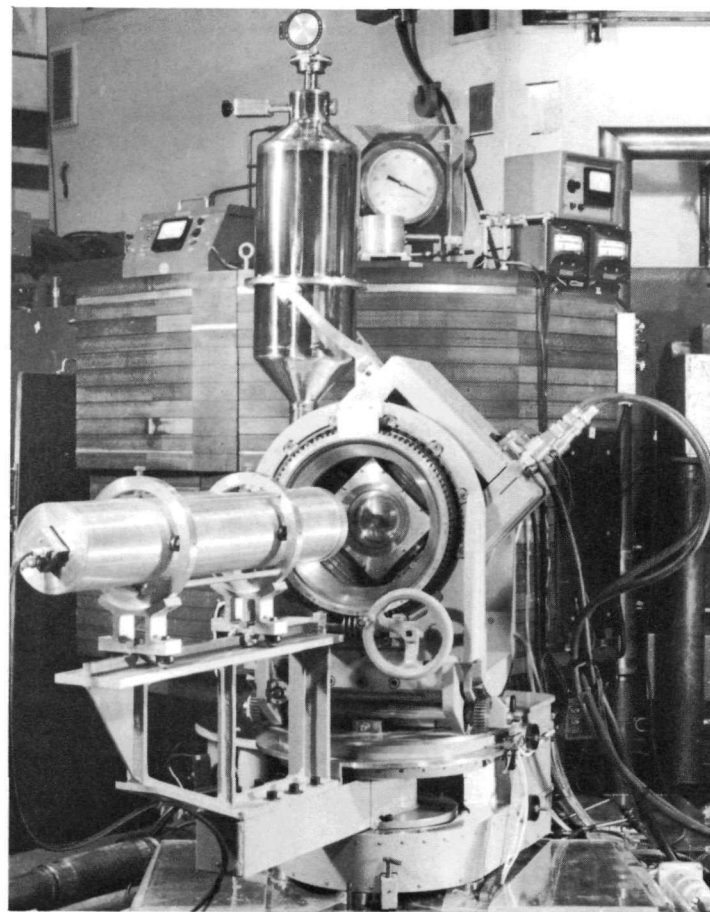
A schematic drawing of the orienter is given in Fig. 21. Photographic illustrations are shown in Figs. 22 to 25. Also shown in these figures is the angular cryo-goniometer assembly which will be delineated in the succeeding chapters.

We take the air-gap center as the goniometric origin and define two azimuth orientations as follows: $X_{||}$, rotation parallel to the magnet-pole axis (xz-plane rotation); X_{\perp} , rocking angle normal to the $X_{||}$ circle and parallel to the $\Omega-2\theta$ axis. The X_{\perp} rocking orientation does not change the direction of the external field vector, but facilitates a goniometric alignment of the specimen with respect to the diffractometer axes. The magnet is supported by a large bearing assembly



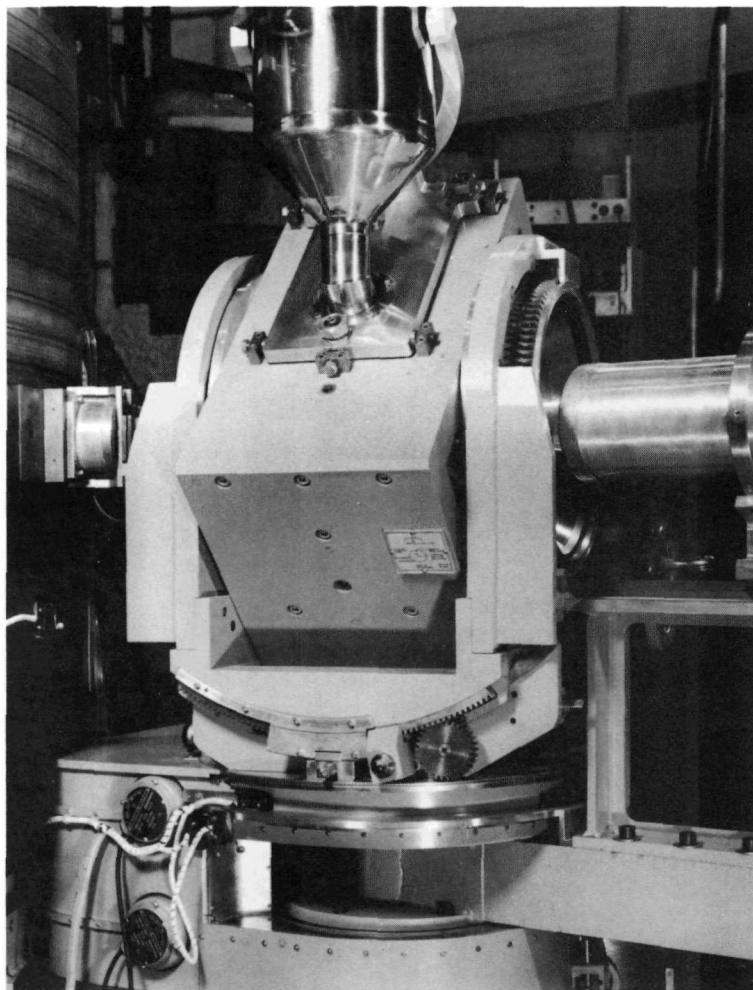
120-8036

Fig. 22. The Diffractometer Assembly with the Liquid-Helium Angular Dewar Mounted on the Electromagnet in the Setting for $X_{\parallel} = 0^{\circ}$. The light-duty counter shield is employed in this assemblage.



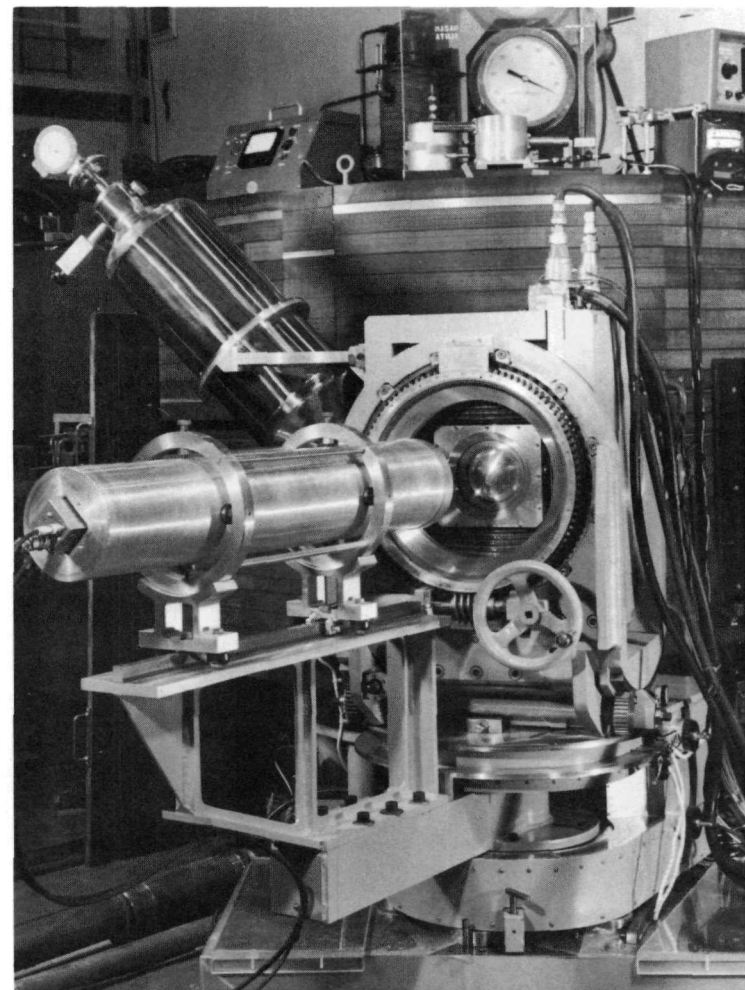
120-8034

Fig. 23. The Setting at $X_{\parallel} = 45^{\circ}$.



120-8040

Fig. 24. The Side View at $X_{||} = 45^{\circ}$. The X_{\perp} setting mechanism and the angular Dewar centering adjusters are seen. Also shown are a side view of the fission counter, the Slo-Syn motors for Ω and 2θ drives, and the limit and reversing microswitches.



120-8035

Fig. 25. The Setting at $X_{||} = 90^{\circ}$.

for a full-circle X_{\parallel} orientation,* and sits on the X_{\perp} cradle. The magnet-orienter unit is subsequently mounted on the Ω -table so that automatic setting and scanning in the Ω and 2θ drives can be made. However, automation of X_{\parallel} and X_{\perp} is not realized. The admissible beam-path is represented by a pair of right cones having a common vertex at the air-gap center and a common cone axis perpendicular to the X_{\parallel} circle. The vertical half-angle of the cone is 37° (see Chapter 2-4).

Materials employed in the orienter construction are, unless unavoidable, nonferromagnetic or of low permeability, for the obvious reason that they do not alter the magnet-flux distribution in any significant way. It is quite probable that the orienter could be designed to improve the magnetic-field properties, particularly for decreasing the fringe flux densities. However, no such attempt was made because of the complexity of the field calculation. The orienter, on the other hand, certainly increases the mechanical strength of the magnet frame against the large strain force due to the magnetostatic attraction between the poles.

For adapting the X_{\parallel} bearings, a pair of aluminum anchor rings with chair-shape cross section is symmetrically fastened to the yoke. These aluminum bearing adapters are 20 in. in OD, 12 in. in ID, and as thick as 2.75 in. in the widest section. A single-row taper-roller bearing is slipped onto the ring seat of each adapter. The circular worm-gear (100 teeth, 16.7-in.-pitch diameter) with a 360° protractor is secured to the outer side-wall of the aluminum adapter on the diffracted-beam side. The bearing and gear, made of hardened steel, do not significantly influence the magnet characteristics. The outer lace of each bearing is inserted into the circular intrados of the arch-gate-shaped bearing plate, which is of stainless steel,** 1.375 in. thick, and is enforced by a pair of stainless steel collateral braces (stainless steel supporting frame in Fig. 21). The bearing plate on the diffracted-beam side is equipped with a rectilinear worm gear to mesh with the large circular X_{\parallel} worm-gear, and also a 0.1° vernier is attached to this bearing-plate. The zero point of X_{\parallel} signifies the pole axis being parallel to the reflection plane. Each bearing is preloaded by means of twelve equally spaced pads fastened to the bearing plate. All mesh surfaces of the gears are coated with a MoS_2 fine-powder paint (moly-coating) in lieu of oil, for better permanent lubrication and anticorrosion purpose. Although the X_{\parallel} gear setting is very stable, a locking clamp is provided in order to prevent accidental manipulation of the crank handle.

*Although the design is aimed at 360° revolution, the electrical-cable and cooling-water connections to the magnet limit the actual orientational freedom to 270° .

**Stainless steel, AISI No. 310, is used here. Other stainless steels having the magnetic permeability of about 1.00 are, in the AISI numbers, 302, 303, 309, 316, 321, and 347. The following types are ferromagnetic: SAE 1020, AISI 410, 416, 420, 430, 440, and 446.

The magnet with the X_{\parallel} assemblage is mounted on the rocker portion of the X_{\perp} cradle. Because of the steric hindrance, the orientation is limited to 30° toward the incoming beam and 10° along the outgoing beam. The body of the rocker is of Meehanite cast iron, with an average thickness of about 2.5 in. The top and bottom sections of the rocker are cylindrically concave and convex, respectively. The radial vector of the concave top is parallel to the X_{\parallel} circle and is designed to allow the full X_{\parallel} revolution of the yoke. The radial vector of the convex bottom is parallel to the X_{\perp} circle.

A pair of arc-shaped spur-rack-gear strips are screwed onto the X_{\perp} rocking parapets (a collateral pair of the convex-arc-bottom braces). A protractor segment is attached to the side wall of the rack gear for the X_{\perp} reading. The cradle base is made of 1.25-in. hardened steel plate and possesses a pair of parapets whose concave rails meet the convex braces located at the rocker bottom through the moly coat. The mesh between the driving spur-gear of the cradle base and the rocker rack-gear is adjustable by means of brass gibs. The vernier strip for 0.1° reading and a locking clamp are attached to the X_{\perp} base. A circular hole is made at the center of the cradle-base platform. The hole is fitted into the spacer hub located at the center of the Ω -table. The diameter of the spacer hub is 0.09 in. smaller than the hole diameter. This difference is allowed for the lateral centering adjustment of the magnet with respect to the Ω -axis. The Ω -axis alignment is carried out by means of four linear-adjusting screws sustained in the thrust blocks which are fastened near the edge of the Ω -table in the orthogonal configuration (see Fig. 36). The lateral displacements of the centering adjustment are measured by two dial indicators (0.0005-in. graduation). They are mounted on the thrust blocks and are activated by a " Σ "-shaped arm whose other lever end contacts the cradle base.

For locating a common centroid of the X_{\parallel} and X_{\perp} circles with respect to the pole-gap center, one of the pole pieces is replaced by a dowel-pin-guided fixture with a small checking metal ball. The checking ball assumes the position of the pole-gap center. By means of precision dial gauges, relative deviations of the common angular centroid from the pole-gap center are determined by setting the orienter at various X_{\parallel} and X_{\perp} angles. Because of large protractor radius, the accuracy in the manual settings of X_{\parallel} and X_{\perp} can be $\pm 0.02^{\circ}$. A counterweight at the end of the X_{\parallel} driving worm-gear shaft is effective for obtaining a smooth counterclockwise rotation of X_{\parallel} with the angular Dewar mount. Extension of the X_{\perp} orientation to a wider angle would lead to prohibitively difficult engineering problems. The total weight of magnet and orienter is about 1800 lb.

Wollan et al. (1960) have constructed a magnet orienter without the X_{\perp} device. There exist other substantial differences between Wollan's and the present orienter. Our design is far more elaborate.

2-7. Angular Dewar Assembly

A variety of instruments to study the temperature dependency of X-ray and electron diffraction has been developed (for X-ray devices, see, e.g., the book of Peiser et al., 1955; E. R. Dobbs in Hoare et al., 1961, pp. 336-343).

A major difficulty with X-ray and electron techniques lies in the fact that there is a highly limited selection of appropriate low-absorbing beam windows, whereas the choice is much greater for neutron methods (see Appendix I). Hence, there is far more flexibility for neutron instrumentation than for the corresponding X-ray and electron techniques.

Apparatus for temperature-dependence studies with neutrons, however, should be designed for longer periods of continuous operation. Moreover, the fabrication material should not perturb the magnetic field.

In particular, in the low-temperature instrumentation, the specimen-enveloping material should not be superconducting because the external field is greatly distorted due to the magnetic-flux exclusion of the superconductor (Meissner effect). The critical magnetic fields for destroying the superconductivity at 0°K of most of metallic elements are smaller than 0.5 kOe and those of other superconductors are not prohibitively high, except for some special alloys such as employed for the superconducting magnet coil. Moreover, the critical field is lower as the temperature approaches the superconducting transition temperature. However, the superconducting temperature and the critical magnetic field are strongly dependent on impurity, annealing process, particle size, etc. (Hulm and Blaugher, 1961). Consequently, it is safer to use nonsuperconductors or materials having very low superconducting transition temperature, i.e. lower than 1.5°K in our case (equivalent to less than about 0.15 kOe in the critical-field value at 0°K). The superconductivity data in this report are taken from excellent reviews of Matthais et al. (1963) and of Roberts (1964). For magnetic susceptibilities of Dewar-construction materials, see Salinger and Wheatley (1961). Values for the thermal contraction of materials at low temperatures are obtainable from Cryogenic Materials Data Handbook (1961) and from the review of Corruccini and Gniewek (1961). In the handbook are also compiled the mechanical and electronic properties as well. A succinct discussion of Dewar-construction material is given by A. J. Croftin (in the book by Hoare et al., 1961, pp. 118-137). Other useful references for these subjects are: the book of Goldsmith et al. (1961); the review of Johnson (1961); the books by McClintock (1964) and by White (1959).

Three cryogenic devices have been constructed: an angular Dewar to be mounted on the diffraction magnet; a straight Dewar for general

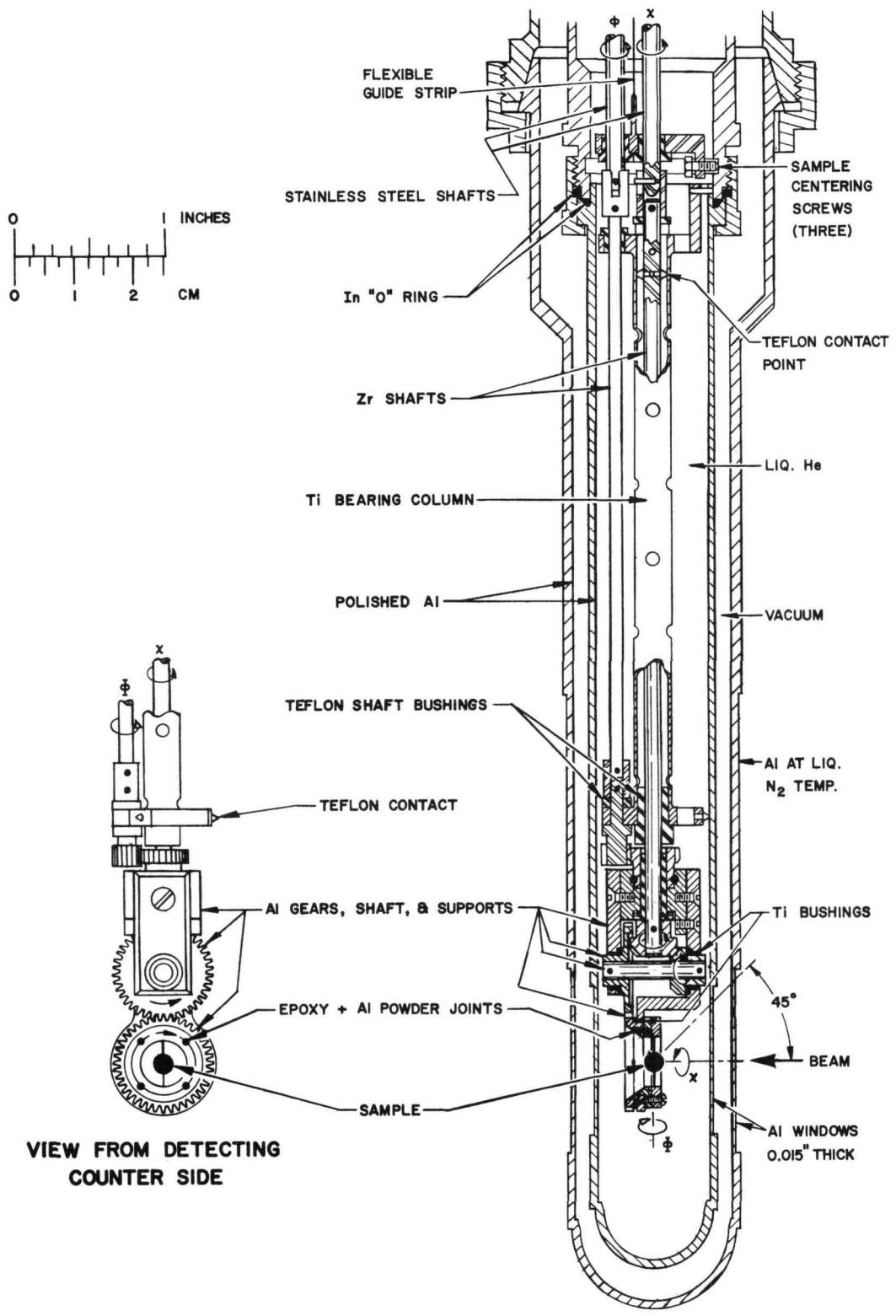
purposes; a liquid-nitrogen vapor-stream cooling unit. The latter two are described in Chapter 2-9, and the temperature control and associated instrumentations are discussed in Chapter 2-10.

The general principle of the angular Dewar designed for the magnet-orienter unit is based on the inventive concept of Wollan *et al.* (1960). The upper portion of the Dewar (the refrigerant-reservoir section) is inclined 45° relative to the specimen-capsule section. In the magnet-mount assembly, the inclining direction of the Dewar is set parallel to the X_{II} circle, so that the orientation range of up to about 100° can be carried out without spilling the liquid refrigerant. Three typical X_{II} settings are illustrated in Figs. 21 to 25.

The liquid-helium Dewar was constructed by Hofman Laboratories, New Jersey, following our dimensional specifications. The capacity of the inner reservoir is 4.5 and that of the outer reservoir 8 liters. The Dewar is of highly polished stainless steel (thin wall and nonmagnetic), except for the thermal-link sheet, which is high-lustre gold-plated copper. The flange with the O-ring sleeve is welded on to the lower neck of the Dewar. The nitrogen- and helium-temperature walls are extended out further and are terminated with the threaded sockets which mate with the specimen-encasing capsules (see Figs. 21 and 26).

The Dewar-positioning plate is laid over the top of the magnet yoke (see Fig. 24). The plate is equipped with three leveling screws for ± 0.2 -in. height adjustment, and these screws possess independent-action pocket screws which fasten the plate to the yoke. Four laterally positioning screws are provided for the cross-translational adjustment of up to ± 0.2 in. The U-shaped support holding the slant section of the Dewar is mounted on the positioning plate. The U-supporter alignment is also adjustable independently or cooperatively in relation with the positioning plate. The bottom flange of the Dewar is screwed onto the positioning plate. At the center of the top yoke, a through hole, 3.4 in. in diameter, is bored as an access to the extended lower section of the Dewar. This hole is slightly less than that for maximum tolerable yoke-loss, whereas it is larger than the flange-sleeve diameter so as to allow lateral adjustment of the positioning plate.

An aluminum box encloses the pole-gap area, and a telescoping sleeve conduit is channeled between the box and the vacuum chamber of the Dewar (see Fig. 21). The side walls of the aluminum box are hollowed out for intercalating the pole pieces and for mating with O-ring grooves circumscribed at the bases of the pole pieces. On the top center of the box, a conduit-access hole and the flange-fitting O-ring are provided for the telescoping sleeve. Another access hole and two cooling-water leads are made at the bottom plate for adapting the high-temperature furnace assembly (see Chapter 2-11). The aluminum box sections surrounding the sides, top,



120-7771

Fig. 26. The Design Detail of the Single-crystal Cryo-goniometer in the Liquid-Helium Angular Dewar. The dark and white arrowheads follow the χ and ϕ drive chains, respectively. The double indium O-ring seal has been replaced by a single aluminum O-ring. The incident beam direction chosen here is for illustrative purpose.

and bottom of the pole-gap area are welded together and set into the air-gap section following removal of the pole pieces. The dowel-pin-guided pole pieces with O-rings are then restored to secure the box position and also the vacuum seal. The wall thickness of these box-sections is about 0.5 in., and the box is approximately an 8-in. cube. The assembly enforces the magnet framework against the interpolar force and, of course, does not interfere with the neutron-beam geometry of concern. Hence, this box segment spanning the pole pieces is normally left in its place regardless of vacuum or nonvacuum experimentation unless the gap distance is altered. The front and back sections of the box are covered lenticularly by a pair of spherical aluminum caps with the square-fringe base for "square O-ring" seal. The spherical cap is 0.031 in. thick and subtends 74° at the center of the pole gap.

After mounting the Dewar on the positioning plate, the telescoping sleeve is slid upward, exposing the threaded terminals of the nitrogen and helium jacket prolongations, to which the aluminum capsules are joined by aluminum lock nuts (see Fig. 26). Aluminum is best suited for enveloping the low-temperature specimen, because of its high neutron transmissibility and low superconductivity transition temperature (1.14°K). The outer aluminum capsule is 1 in. in ID, with a 0.05-in. wall thickness, and the beam-window section is 1.75 in. high and has a 0.015-in. wall thickness (see Fig. 26). The outer aluminum capsule contacts the nitrogen jacket extension through matching tapered surfaces to provide efficient thermal conduction. The inner aluminum capsule is similar, except for the following: a 0.75-in. ID in the main section; a 1-in. beam-window height; an O-ring groove near the top of the capsule; guide slots for suspending the cryogoniometer (see Chapter 2-8). These capsules are designed for the single-crystal study with the cryogoniometric device and for the pole gap of 1.4 in. or larger.

The vacuum O-ring seal of the inner capsule, which is cooled down to near 0°K , has been a major impediment. Among prevalent metal O-ring materials, high-purity Ag, Al, Au, Cu, In, Pb, Pb with a few percent Sn, In, and Al (see the book by White, 1959, pp. 275-276), were subjected to the test. The gold and silver seals are probably best suited for the semi-permanent seal, but are too costly if frequent replacement is required. The thermal contraction of indium is appreciably larger than most of the construction metals,* and under stress it continues to flow like a paste, even at very low temperatures. Consequently, the amount of indium should be slightly larger than the O-ring cavity volume, and the O-ring coupling should be "leak proof" so as to trap the indium within the cavity. In other

*If the thermal contraction is unidirectional, the differential linear-thermal contraction between indium and aluminum is about 0.003 in. per inch over the region from 300°K to 0°K .

words, indium should be in a compressed state at room temperature. The O-ring coupling shown in Fig. 26 is designed for the indium O-ring, and the upper O-ring is fitted into the thread-end cavity as a subservience to the main lower seal.

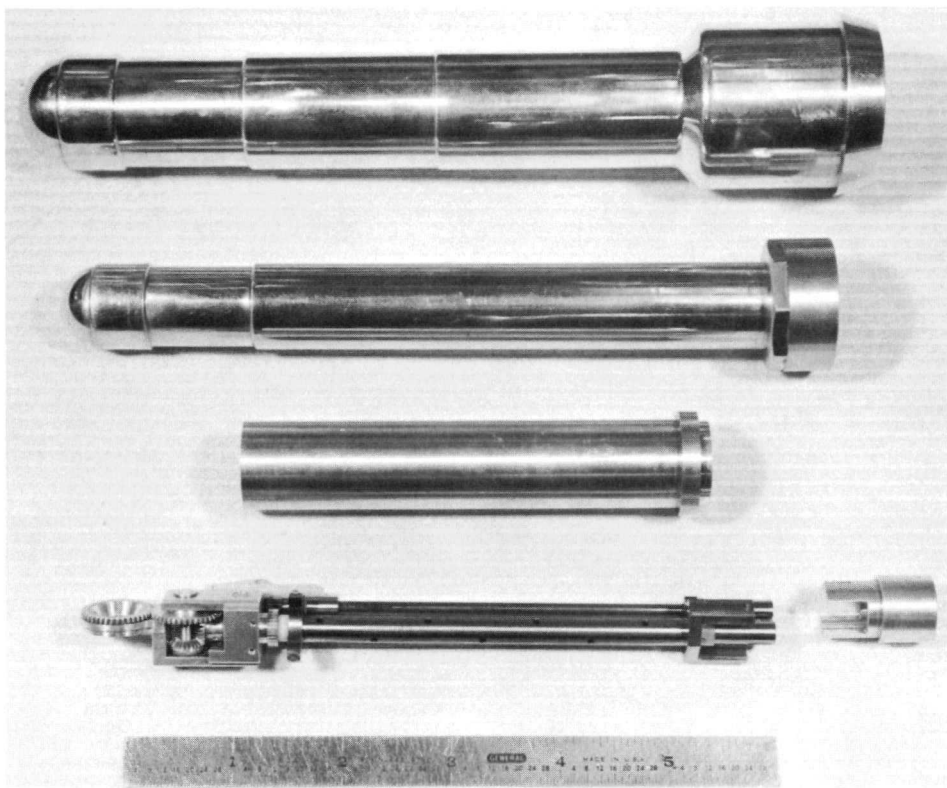
The indium O-ring is prepared as follows. The indium wire is fitted into an O-ring groove made on Teflon sheet. The split ends are spliced together with indium solder and a pen soldering iron. Extra indium around the soldered joint is scraped off with a scalpel. A 45°-cut press-joint without solder splicing did not form a good seal even under flow stress, contrary to several reports recommending this technique. Our indium seal was, however, not always successful unless exceedingly overcautious preparation and handling of indium ring were provided.

The annealed pure-aluminum O-ring with circular or rectangular cross section was tried. A single O-ring scheme was eminently successful. Here, because aluminum is far less ductile than indium, the surface of the aluminum ring and that of the O-ring cavity had to be highly polished in order to eliminate any transverse microgroove, or either or both of the surfaces should be machined to have multi-circular microgrooves. On the other hand, work hardening of aluminum helps in ceasing the stress flow, and the thermal expansion is also favorable in eliminating the laborious procedures required for the indium O-ring. The evacuation of the angular Dewar assembly is carried out through the pumping tee located near the top of the Dewar.

2-8. Angular Cryo-goniometer

Ideally, a full two-circle goniometric device should be provided for the crystal in the external magnetic field with the $2\pi-X_{||}$ modulation, and the Ω -setting of the crystal should be independent of that of the magnet (three Eulerian angles for the specimen crystal, and the Ω and X variations for the external magnetic field vector, i.e., five independent angular settings in total). However, such a complete device is virtually hypothetical in the low- and high-temperature instrumentations with the magnetic device.

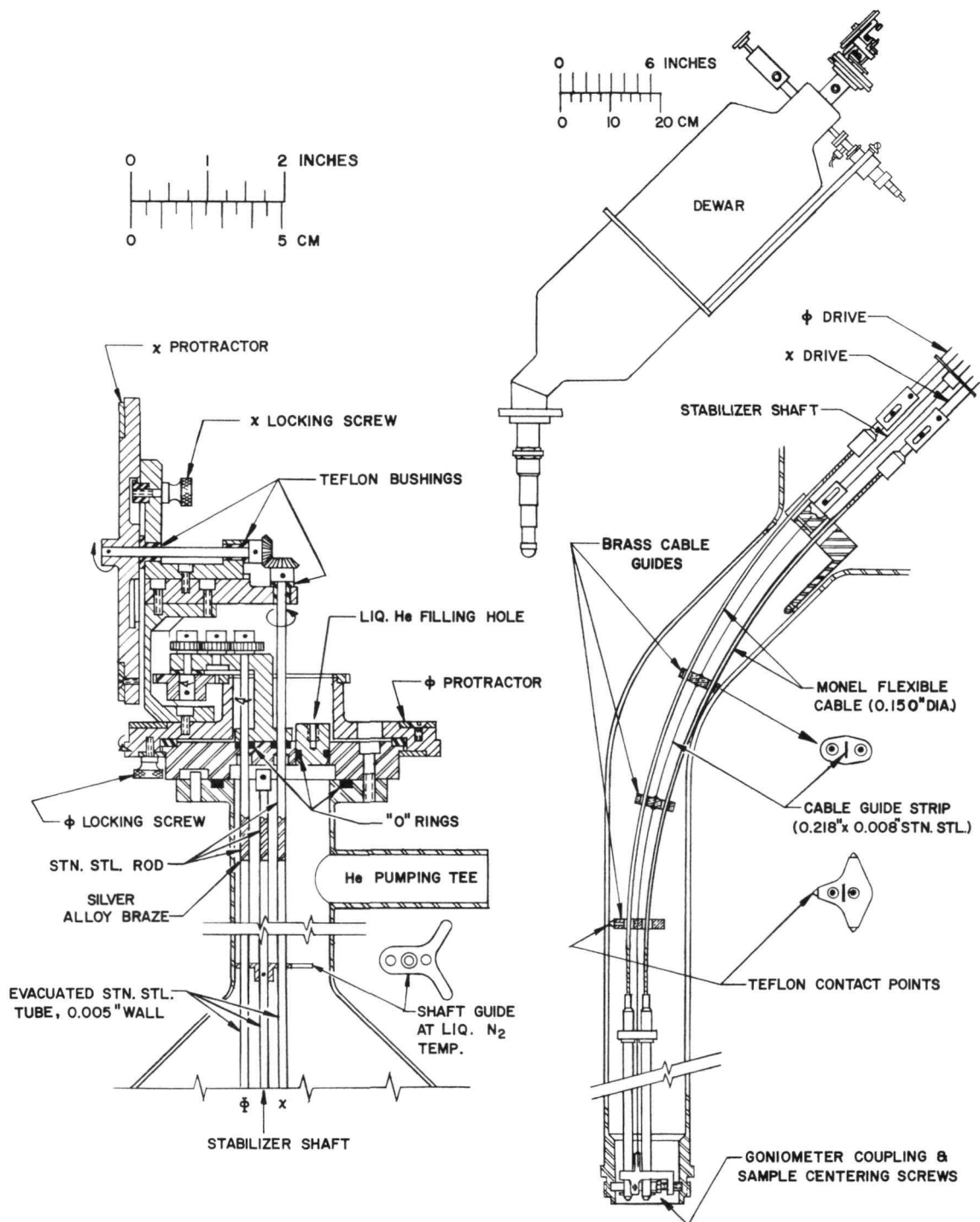
A goniometer for the angular Dewar has been constructed to facilitate a limited crystal-plane orientation in the cryo-magnetic environment. The angular cryo-goniometer comprises two parts: the lower segment for the crystal mount, which is termed here as a cryo-goniometer (see Figs. 26 and 27); the remote goniometric control to fit into the angular Dewar (see Fig. 28).



210-692

Fig. 27. Photographs of the Goniometer and Related Components for the Liquid-Helium Angular Dewar Assembly. From top to bottom; aluminum outer capsule, aluminum inner capsule, dummy inner capsule for the sample alignment, and the cryo-goniometer with the shaft-coupling alignment tool.

The cryo-goniometer provides a two-circle setting of the specimen crystal: a 2π rotation around the axis coinciding with the y axis of the magnet; another full circle parallel to the y axis. The former angle is denoted by the lower case Greek letter ϕ , and the latter by lower case χ . As illustrated in Fig. 26, the crystal is mounted at the bored center of a 40-tooth aluminum spur-gear for the χ rotation. The bore diameter for the spherical crystal mount is 0.342 in. (0.87 cm), and smaller crystals are set in the thin aluminum washer which is agglutinated to the χ -circle. The adhesive used for the specimen mounting is General Electric varnish No. 7031. The one side of the χ -bore is conically hollowed out, and the ϕ -axis lies on the opposite face of the χ -circle. The vertical half-angle of the admissible beam cone is about 55° for the conical opening and is nearly 90° in the opposite direction. The rim thickness of the χ -circle was made to be as thin as possible in accommodating the gear-support framework. The χ -gear is driven by the identical aluminum gear, which is steered by the central shaft through a bevel-gear coupling. One revolution of the χ -shaft results in one revolution of the χ -circle. The χ -shaft slips in the Teflon bushings without transferring its motion to the ϕ -gear train. Nevertheless, the ϕ -shaft is locked stationary during the χ -modulation, since foreign material, such as solidified air, often plugs up the bearing interstices.



120-7774

Fig. 28. Design Features of the Remote-control Mechanism for the Cryo-goniometer. The thermocouples and other temperature-measurement attachments are omitted in this drawing.

The ϕ -shaft revolves the specimen-gear assembly around the χ -shaft through aluminum pinion-gear meshing. Two clockwise revolutions of the ϕ -shaft correspond to one counterclockwise ϕ -revolution of the specimen-gear assembly. Simultaneously, the χ -shaft makes one revolution counterclockwise. In other words, the χ -shaft and the specimen-gear assembly turn together so that the χ -setting of the specimen is kept unaltered. This can be carried out rather easily by means of the compensating gear-coupling in the remote-control gear train described later.

Besides aluminum and Teflon components, bushings, dowel pins, and screws made of titanium or stainless steel comprise the specimen-gear assembly. The χ - and ϕ -shafts are made of zirconium and are supported and guided by the titanium bearing support. A pair of small guide pins are provided at the hook-shaped notch of the bearing column. A Y-shape guide plate attached to the bottom end of the bearing column and three Teflon arrow pins are inserted at the Y-finger tips. The top guide pins are inserted into the slots made on the top of the inner capsule, and the Teflon arrow pins insure the axial and centering alignments of the goniometer. The stainless steel shaft-links of key-slot type join the goniometer and the remote-control device.

The superconducting transition temperatures of titanium and zirconium are 0.39° and 0.55°K , respectively, and the critical magnetic fields for destroying the superconductivity at 0°K are 0.1 and 0.05 kOe, respectively. AISI 310 stainless steel is presumably a nonsuperconductor, at least above 1°K .

Among the suitable materials, zirconium and titanium undergo least thermal contraction. As regards thermal contraction, titanium and zirconium behave almost identically. The differential linear thermal contraction in the range from room temperature to near 0°K is about 0.003 in. per inch for Al-Ti and Al-Zr, and 0.001 in. for aluminum vs. stainless-steel, aluminum contracting more in all cases. Teflon shrinks as much as 0.02 in. per inch in cooling, from 0°C to 0°K .

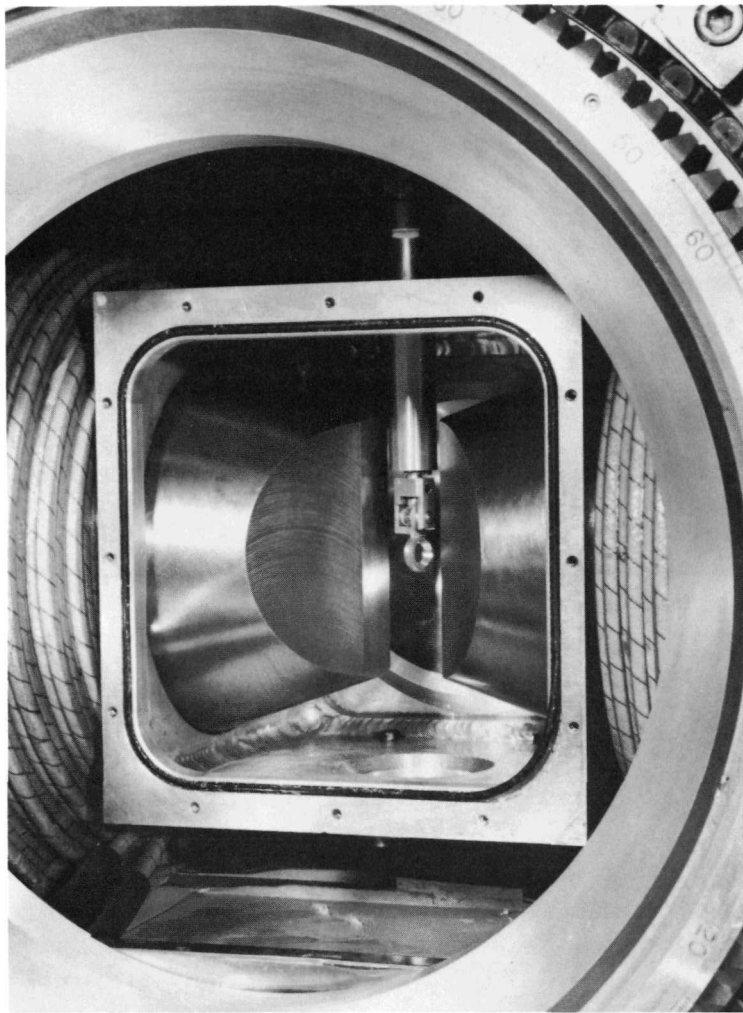
Our design for the small components is such as to decrease the fitting friction at the lower temperatures. Actually, because of the small dimensions, the differential contraction between the Teflon bushing and bracing metal is less than 0.0005 in. in cooling through 300° . For larger or longer parts, such as the drive shafts, the afore-cited slidable linkage is employed for compensating the contraction difference. These principles were also applied to the remote-control device.

The cryo-goniometer is operated from the top of the angular Dewar as follows: outset drive-gear assembly, rigid drive shafts, and flexible cables (see Fig. 28). The O-ring cover plate closes off the mouth of the liquid-helium chamber. On the cover plate, we have a port-plug hole with

an O-ring seal, for filling the liquid-helium chamber with refrigerant, and two shaft-guide holes, also with individual O-ring seals. The ϕ -handwheel is then mounted over the cover plate by means of a circular flange and a Teflon friction ring. A 120-tooth spur-gear, which is coaxially attached to the ϕ -handwheel, is coupled with the 60-tooth side-gear. Three identical pinions, including a mediating lazy pinion, propagate the above 2:1 gear conjugation into the ϕ -shaft, so that one clockwise revolution of the ϕ -handwheel corresponds to two counterclockwise revolutions of the ϕ -shaft. Since the ϕ -shaft rotates the ϕ specimen axis through the 1:2 pinion coupling of the cryo-goniometer, the handwheel motion becomes identical with the specimen motion. The χ -handwheel is vertically fastened on the ϕ -handwheel. A pair of bevel gears joins the horizontal χ -wheel axis to the χ -shaft. The gear connections in the χ -drive channel are all in 1:1 ratio, and the clockwise rotation of the handwheel looking toward the center of the Dewar axis corresponds to the clockwise rotation of the specimen looking from the vertex side of the χ -circle cone opening. A 360° protractor, with 0.1° vernier, and a locking screw are provided for both χ - and ϕ -wheels. The χ -wheel has to be locked stationary during the ϕ -motion, and this conjoins the motion of the χ -shaft and the specimen-gear assembly as described before.

The drive shafts near the outset gear assembly and those near the bottom neck of the Dewar are of stainless steel rod, and the long mid-sections are evacuated stainless steel tubes of 0.125-in. OD and 0.005-in. wall. The rod and the tube are joined by means of a silver-alloy brazing. The stabilizer shaft is made similarly and holds four shaft-guide plates stationary. The bottom shaft-guide plate is a prong type whose three figures are fitted into the bottom neck of the Dewar. The Monel flexible cables of 0.15-in. diameter extend the drive shafts, and a stainless steel guide strip is connected to the stabilizer shaft at the bottom shaft-guide plate. The guide strip is equipped with the cable-guide plates, and these are fitted into the 45° -bend tube extension of the inner chamber of the Dewar. Near the end of the inner tube, the cables are replaced by the rod shafts, which are accurately positioned at the termination guide-prong equipped with three centering screws. The modulus of elasticity of the Monel alloy is very insensitive to temperature variation down to near 0°K (see Cryogenic Materials Data Handbook, 1961).

The remote-control section is preassembled before insertion into the Dewar. The shaft linkage between the remote control and the cryo-goniometer is made with help of the shaft-coupling alignment tool (see Fig. 27). For coinciding the cryo-goniometer center with the magnet-orienter center, a dummy inner capsule is used to expose the χ -circle (see Figs. 27 and 29). The lining up is carried out at room temperature with the Dewar-sample centering adjusters located at the top of the magnet (see Figs. 21 and 24, and Chapter 2-7). For the powder study, the inner capsule and the cryo-goniometer are replaced by variable-temperature sample holder, described in Chapter 2-10.



120-8038

Fig. 29. The Cryo-goniometer in the Sample-aligning Assembly. The dummy inner capsule is being used to align the goniometer and the sample. This assembly is also used for the sub-room-temperature experiment above 100°K with the liquid-nitrogen vapour-stream technique. The 1.4-in.-gap pole pieces are shown.

Because of the thermal contraction of the supporting materials, the specimen position moves up about 0.3 mm upon cooling to near 0°K . This is detectable by the collimation method, but can be neglected in the wide-open collimation. A slight backlash occasionally develops also at low temperatures; hence a unidirectional rotation is employed in manipulating the handwheels. Cooling and warming have to be carried out as slowly as possible in order to avoid thermal shock to and quenching of the intricate parts. The refrigerant-filling plug is usable only at certain ranges of the ϕ -wheel setting, but this does not hinder the experiment appreciably. Liquid helium (4.5 liters) lasts about 6 days, and under the reduced vapor pressure of 6 mm Hg (1.6°K), starting liquid of 4.5 liters at 4.2°K lasts

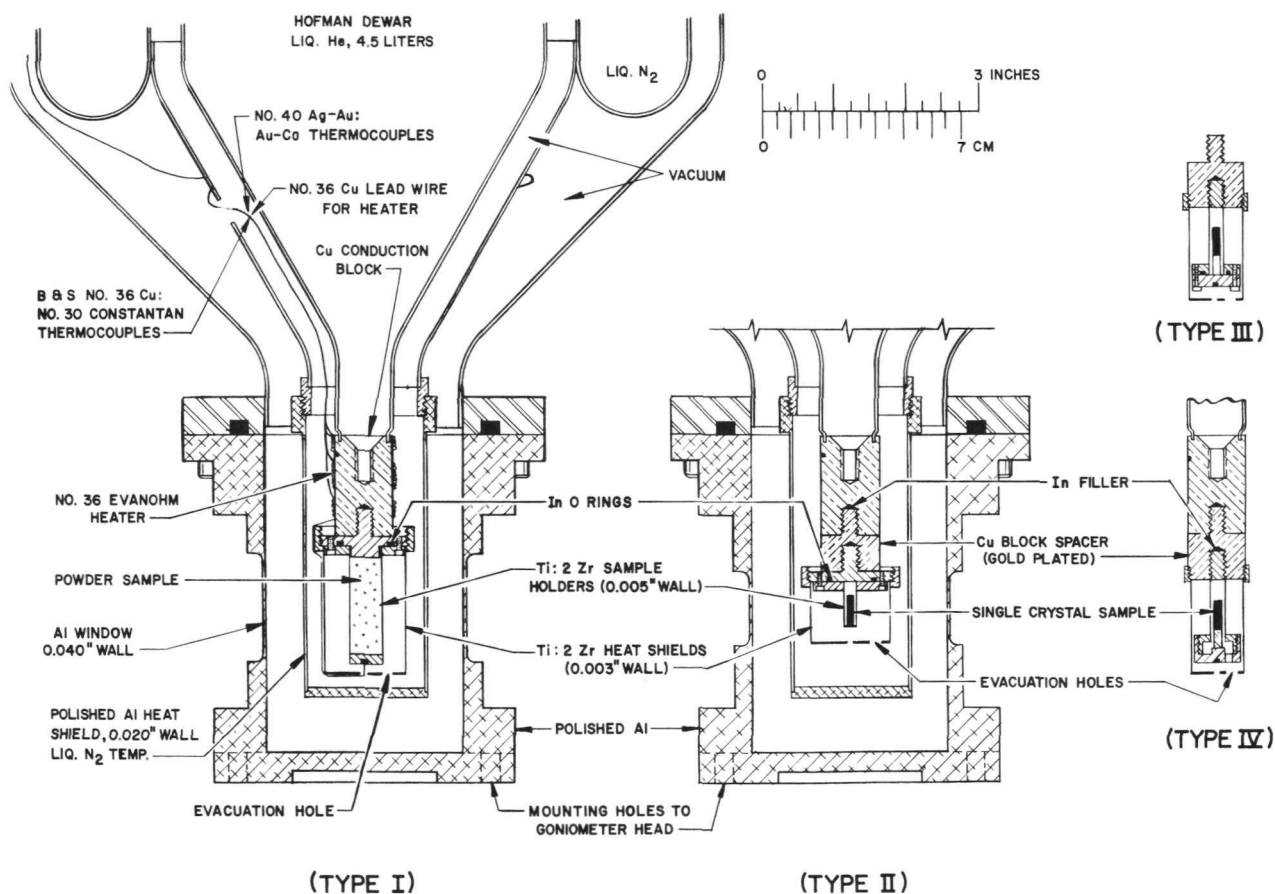
nearly two days. The temperature-measuring and control devices are described in the following chapter.

As stated in Chapter 2-3, the magnet cooling is enforced to reduce the heat radiation to the low-temperature environment of the specimen. The beam-path components in the cryo-goniometer assembly on the magnet are all of aluminum when the specimen and the refrigerant are excluded. The total thickness of these aluminum components is 0.122 in. (0.31 cm), which attenuates about 3.0% of the 0.1-eV neutrons.

2-9. Auxiliary Cryogenic Devices

A straight Dewar with a conduction-type specimen mount has been employed primarily for the neutron studies without use of external magnetic field. In this case, scattering angles are not restricted by the magnet geometry; hence the straight Dewar has been frequently used for the crystallographic studies and also for extending the cryo-magnetic data to high scattering angles. It is based on Abrahams' design (1960),* and hence the description here emphasizes our modifications and functional data.

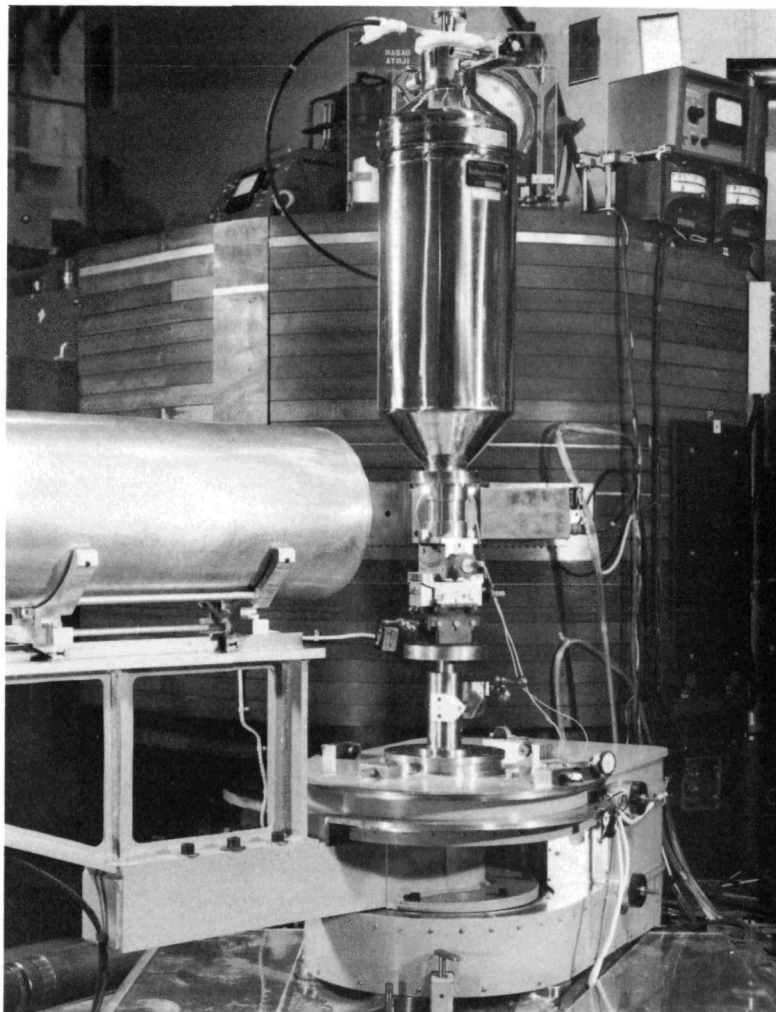
The Dewar, constructed also by the Hofman Laboratories, Inc., may be described as the angular Dewar without the 45°-bend extension (see Chapter 2-7). The helium chamber is terminated by a copper block to which the specimen is appended in a cold-finger configuration. The specimen-housing designs are depicted in Fig. 30, and the goniometric mount on the diffractometer is shown in Fig. 31. An aluminum vacuum cup



120-7772

Fig. 30. The Sample-housing Construction in the Liquid-Helium Straight Dewar. The powder-specimen mount is illustrated as type I, and other types are designated for the single-crystal study. The specimen is in the vacuum environment in type IV, and all others are in the helium-gas atmosphere. The thermocouples are omitted in the single-crystal drawings. Au/Co: Ag/Co thermocouple has been replaced by Au/Co: Cu. The indium O-ring has occasionally been replaced by an aluminum O-ring.

*Kogan *et al.* (1960) has described the USSR diffraction cryostat.



120-8037

Fig. 31. Liquid-Helium Dewar Mounted on the Universal Goniometer Head. Also seen in the photograph are: on the top of the biological shield, a part of the vapor pressure regulator for the refrigerant, the power supply for an ion-getter vacuum pump to be used with the high-temperature furnace, the thermocouple controller for protecting the magnet coils; on the left of the shield, a removable Masonite section for the auxiliary beam output; on the right of the shield, the monochromator remote-control entry-door; near the central portion of the shield, the angle-selecting wedge plug and guide-plate. The heavy-duty counter shield is employed in this experiment.

encloses the bottom cutout of the Dewar through an O-ring joint. The total height of the aluminum cup is 4.75 in., and its inner diameter is 2.75 in. All surfaces of the aluminum cup are highly polished using the optical-glass fine-finish procedure. The aluminum cup supports the Dewar, weighing 35 lb without refrigerant and about 50 lb with filled refrigerants, liquid helium (4.5 liters; 1.3 lb) and liquid nitrogen (8 liters; 14.3 lb). The

beam-window dimensions safely sustaining these weights are: 0.040-in. thickness and 1.625-in. height for the powder specimen where goniometric tilting adjustment is usually very small; 0.040-in. thickness and 1-in. height for the single crystal mounting, for which tilting alignment of up to $\pm 20^\circ$ can be made. The flange base of the aluminum cup is mounted on the goniometer head through the dowel-pin guide (see Chapter 2-2).

The powder-specimen holder is sealed off by the O-ring cap which is screwed into the copper-block cold finger (Type I in Fig. 30). Optional indium filler is used to fill up the thread-end void for eliminating dead-evacuation space and for improving the thermal conduction. The beam-impinging segment of the holder is 0.394 in. (1 cm) in ID, has a 0.005-in. wall thickness, and is 1.5 in. high. The powder is filled in the holder under dry helium and the cap compresses down the powder to insure good thermal contact of the sample. The O-ring material is either indium or aluminum; the latter is most frequently employed (see Chapter 2-7). The O-ring is designed so that it does not destroy the thermal contact between the cap and body of the holder. The holder currently in use is constructed of disordered $Ti_{2,13}Zr$ alloy whose superconducting transition temperature is $1.32^\circ K$ (Hulm and Blaugher, 1961). Hence, a Weiss-type magnet can be used for low-magnetic-field applications at temperatures above $1.32^\circ K$ or with magnetic fields higher than the critical value, which is about 0.5 kOe at $0^\circ K$. Here, the pole gap should be larger than 3.5 in., and the pole-piece surface should be smaller than 3.5×3.5 in.

The single-crystal encapsulations (Types II to IV in Fig. 30) are similar. The cold-finger tip is situated 1 in. above the beam center and hence the copper-block spacer is used to bring the small crystal down to the beam. In Types II and III, the crystal is in a helium-gas atmosphere which acts as a transfer gas for thermal conductivity. In Type IV, the crystal is in the vacuum environment and fillings of $Ti_{2,13}Zr$ for thermal contact are inserted between the crystal and the holder wall.

The inner capsule made of $Ti_{2,13}Zr$ of 0.003-in. wall is held at the liquid helium temperature, and the mirror-finished aluminum outer capsule of 0.02-in. wall extends to the liquid nitrogen wall. Evacuation and thermocouple-access holes are provided in the inner capsule. A small dent for placing the thermocouple junction is made on the cold finger and also at the bottom of the specimen holder. The thermocouple winds around the cold finger and then the nitrogen jacket before leading out to the room-temperature environment, so that the heat gradient and leak are reduced. General Electric varnish No. 7031 is used to adhere the thermocouple wires to the Dewar walls and, although the thermocouple junction contacts the Dewar metals, silicon grease is applied in and around the access dent. Currently, two different types of thermocouple are led into the Dewar: Cu:constantan (0.005:0.01 in. in diameter) for the higher-temperature region, and Au + 2.1 a/o Co:Ag + 0.37 a/o Au (0.003 in. : 0.003 in.) for

measuring the lower temperatures. A Au + 2.1 a/o Co:Cu thermocouple has been substituted for the latter. The thermocouple extending to the bottom of the specimen holder is subjected to the neutron beam, but its scattering effect is negligibly small. To obtain small temperature rise, Evanohm* wire (of 0.005-in. diameter and about 310- Ω resistance) is wound around the cold finger. Of course, the temperature control of this configuration is very primitive and uneconomical.** Because of rapid boiling off of the refrigerant, a temperature rise of only about a few degrees is a practical limit at 4.2°K and about 10° rise near 77°K. Further discussions on the temperature measurement and control are given in the following chapter.

The rate of the liquid-helium evaporation averages 0.45 and 0.32 liter/day at the top and bottom half of the reservoir, respectively. Hence, a 4.5-liter filling lasts nearly 12 days. The liquid nitrogen in the outer chamber vaporizes at a rate of 3 to 4 liters/day. Under an equilibrium vapor pressure of 6 mm Hg (at about 1.6°K), the 4.5-liter filling of liquid helium lasts nearly 3 days. The components, 0.3-cm aluminum and 0.04-cm Ti_{2.13}Zr, in the beam path attenuate about 4.3% of the 0.1-eV neutrons.

A conventional nitrogen-stream cooling technique is employed primarily in conjunction with the full two-circle goniometer (see Chapter 2-2) or with other bulky specimen-mounting techniques for which the Dewar encasement is unsuitable. This technique is occasionally used to cool the specimen mounted in the magnet air gap (see Fig. 29). The nichrome-wire-wound heater which is controlled through the variable autotransformer is immersed in the liquid-nitrogen reservoir which is refilled automatically. (Greater advantage would be obtained in long, continuous operation if the reservoir capacity were as large as 100 to 200 liters.) The cold nitrogen vapor is led to the specimen through the vacuum-jacketed transfer tube with another heater coil in the vapor path. The temperature is controlled by varying the heating rates of these two heaters.

For the higher temperature range (about 150°K and up), dry nitrogen running through an optional heater path is mixed with the main stream in order to maintain a high stream strength. Even with a constant heating rate, the temperature changes slightly, depending on the amount of the reservoir nitrogen. Hence, for high-precision temperature control in a long-range experiment, an automatic thermocouple-temperature controller should be

*Evanohm: Wilbur B. Driver Co., Newark, New Jersey. 75% Ni, 20% Cr, and 0.5% Al and Cu, in weight percent. This material has high electrical resistance and very small resistance change with temperature. The wire can withstand up to 300°C.

**The rate of vaporization of liquid helium in the Dewar is accelerated to about 1 ℓ /hr for an external energy input of 1 W.

incorporated into the system. Our unit, without such device, possesses a temperature constancy of about $\pm 1^\circ\text{C}$ in the range from 80°K to 250°K , although this requires relatively frequent modulation of the manual controllers. The specimen is partially enveloped by an encasement of aluminum, quartz glass, or Mylar, which acts also as the stream reflector.

H. A. Levy's group at Oak Ridge has developed a low-temperature encasement for the Φ -goniometer of the two-circle goniometer in conjunction with the nitrogen-stream method. This device is equipped with a universal joint and a flexible path in the coolant channel so that the Φ , χ , and Ω settings can be made without large angular restriction. The cryogenic device needed for the two-circle goniometer becomes exceedingly involved at temperatures below 77°K , and no such device has yet been developed.

2-10. Discussion of Cryogenic Instrumentation

We now discuss current and possible future improvements of our Dewar devices. Special emphasis is placed on the temperature measurement and control [see the books by Dahl (1962), Hoare et al. (1961) and White (1959)].

In addition to the use of Cu:constantan and Au + Co:Cu thermocouples (Chapters 2-8 and 2-9) for measuring temperature, a mercury or silicon-oil manometer is employed in the controlled vapor-pressure technique. A resistance thermometer is usually bulkier than the thermocouple junction and hence was not particularly suitable for our configuration. A gallium-doped germanium resistance thermometer of diameter smaller than 0.5 mm is now available, but its resistance is influenced by the magnetic field. As is well known, in the lower sub-room-temperature region, it is better to place the thermocouple reference junction in boiling liquid nitrogen or the like instead of in the ice point. Also, the via medium section connecting the measuring and reference junctions should not be exposed to a temperature higher than that of the reference junction. This was, however, not readily adaptable with our Dewar design. Our accuracy of temperature measurement is no better than $\pm 0.1^\circ\text{C}$, but this suffices for our present research objective.

The vapor-pressure regulation of the refrigerant is being carried out with a Cartesian monostat capable of regulating ± 0.1 mm Hg for 0- to 30-cfm flow.

Selection of a refrigerant for temperature variation is highly limited in experiments in or near reactors. A refrigerant that generates explosive, inflammable, reactive, or toxic gases requires a separate, special exhaust system incorporating elaborate safety devices, particularly since a slightly reduced atmospheric pressure is maintained inside the CP-5 reactor. Liquid

hydrogen is an example of such a refrigerant, as is liquid oxygen. The temperatures available through use of these must be obtained by other means.

The liquid refrigerants suitable for our reactor experiments are, with regulation from 760 to 1 mm Hg, helium for the range from 4.2°K to 1.3°K, nitrogen for the range from 77.4°K to 63.2°K (94.0 mm Hg, triple point), CF₄ for the range from 145.2°K to 88.5°K, CClF₃ for the range from 191.8°K to 119.5°K, CCl₂F₂ for the range from 243.4°K to 152.5°K, and CCl₃F for the range from 296.9°K to 187.9°K. Currently, CF₄ and CClF₃ are more costly than helium. Solid refrigerants (see Table III) and freezing mixtures exhibit large temperature drift unless careful provisions are made for maintaining them at thermodynamic equilibrium. They are, however, sometimes handy to use in an experiment in which a relatively large temperature fluctuation may be tolerated.

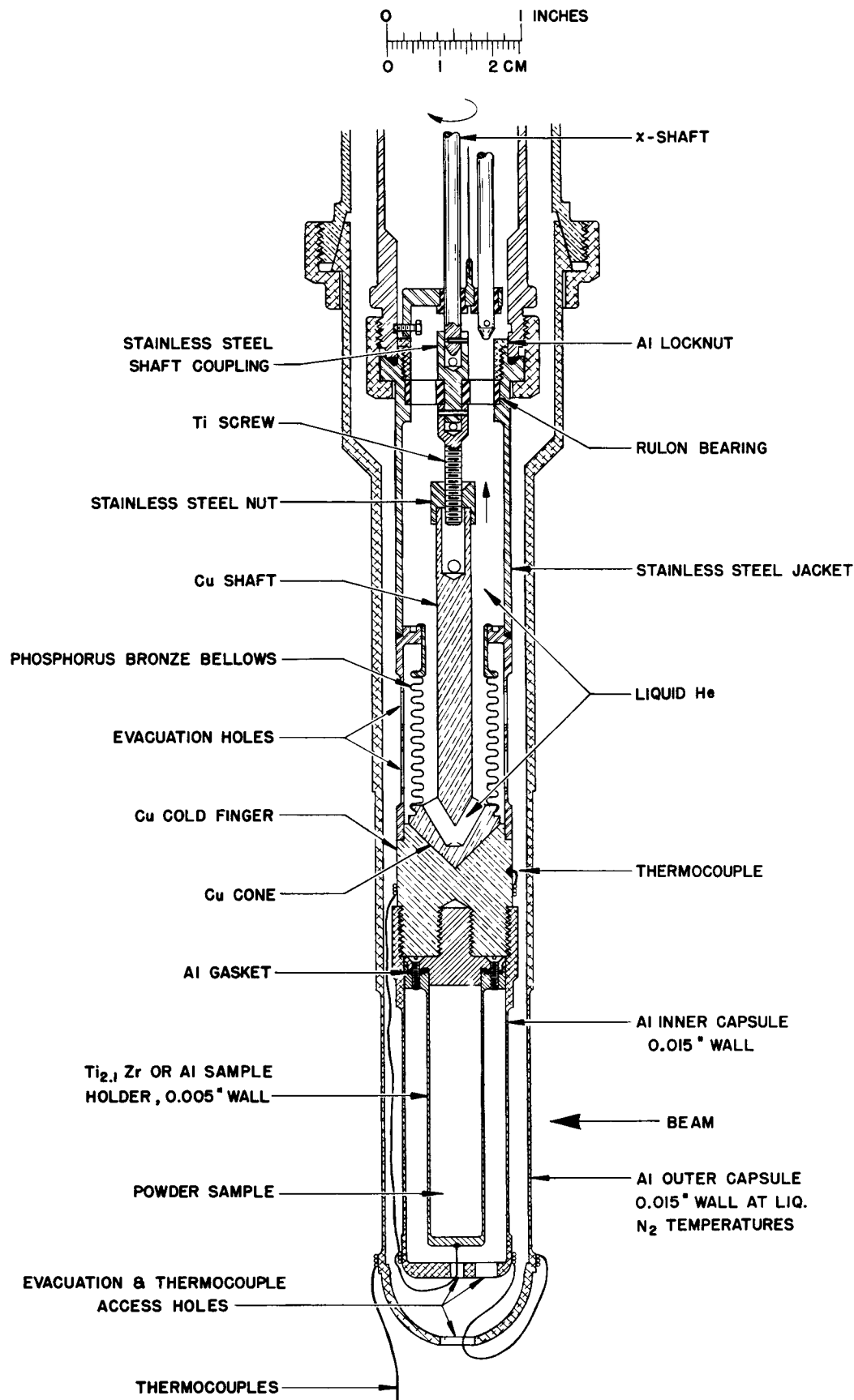
In the angular Dewar with the cryo-goniometer, the specimen is immersed in the refrigerant whose neutron-attenuation path length is, neglecting the specimen crystal, about 0.75 in. or 2 cm. The 2 cm of liquid helium attenuates only about 3% of the thermal neutrons. However, as seen from Table III of Appendix I, the total cross sections of other conceivable refrigerants are too large to be used for the direct cooling technique. Solid refrigerant cannot be used because it interferes with the goniometric mechanism.

The following instrumentations on the angular Dewar are currently underway to permit wider temperature variation:

Two aluminum, hollow hemispheres whose equatorial planes have been shaped to encase the specimen and to fit into the χ -circle may be used to cut down the effective beam path of the refrigerant to about 2 mm or less. Nitrogen and most of Freons can be employed in this manner. However, the temperature region from 4.2°K to 63.2°K, is still unattainable by this technique.

A transfer-tube technique is under consideration. The liquid-helium transfer-tube with several flexible sections is inserted into the Dewar through a pumping tee and is extended down to near the specimen. The in-Dewar section of the tube is about 0.125 in. in diameter, and its near-specimen segment is not vacuum jacketed. The liquid helium in a storage Dewar is forced into the specimen section by means of a small vacuum pump with a needle-valve control in a return-gas cycle. If higher temperatures are wanted, liquid nitrogen is used in place of liquid helium. The difficulty here is to facilitate a wide modulation of the X_{\parallel} and Ω settings without transpositioning of the transfer-tube assembly.

The cold-finger sample mount with a thermal valve (see Fig. 32) is perhaps of more elegant design than provided by the aforementioned



120-8652

Fig. 32. A Variable-temperature Sample Holder for the Angular Dewar. The single-crystal encasements are similar to those shown in Fig. 30.

techniques. This angular-Dewar attachment is now under construction, so that operational data are not yet available. The inner capsule, made of stainless steel, is terminated by a copper cold finger whose refrigerant side is machined out to form a conical well. The lower 1-in. section of the 0.05-in. capsule wall is thinned out to 0.01 in., and eight staggered holes, each 0.25 in. in diameter, are made on the thin-wall section to provide evacuation channels. Heat leakage through this thin-wall section is expected to be relatively insignificant. A phosphorus-bronze bellows is suspended from the midsection of the capsule, and the bottom opening of the bellows is enclosed by the conical top of the copper valve shaft. Two pairs of mutually orthogonal V-tunnels are drilled in the conical top for introducing the refrigerant near the vertex. A stainless steel nut is brazed on the neck of the copper shaft. The nut is engaged on a titanium screw at the χ -shaft terminal, which is guided by a Rulon* bearing. The χ -shaft revolution regulates the height of the copper shaft, and thereby modulates the conductive and radiative heat transfer from the copper conical top to the cold finger. With the use of this assembly, practically all sub-room temperatures are expected to be attainable with the use of liquid helium and nitrogen. The specimen housing is similar to that for the straight Dewar. The χ - and ϕ -goniometries of the specimen are of course not operational with this device.

Incorporation of the bellows-type temperature control to the straight Dewar is not considered because of unexchangeable cold-finger construction, and hence the transfer-tube technique may be adapted to the straight Dewar for the temperature region from 4.2° to 63.2°K. Fortunately, the warming-up rates of all of our Dewar assemblies are exceedingly slow. For instance, about 3 to 6 hr are required to warm the empty inner chamber at 4.2°K to the outer chamber temperature of 77°K. A number of rocking curves with temperature measurement of sufficient accuracy can be obtained during this long warming-up period.

Finally, perhaps the most suitable Dewar construction for variable temperature control over the entire range of sub-room temperatures is that based on the variable helium-gas heat-link technique. Such a Dewar is now available from, for instance, Andonian Associates, Waltham, Massachusetts. The cryo-goniometer or other devices can readily be adapted in this type of Dewar.

*Rulon is a product of Dixon Corporation, Bristol, Rhode Island, and is Teflon impregnated with inorganic or metallic powder, such as graphite, mica, or silver. Some Rulons possess excellent bearing properties over a wide temperature range, including that near 0°K.

2-11. Diffraction Furnaces

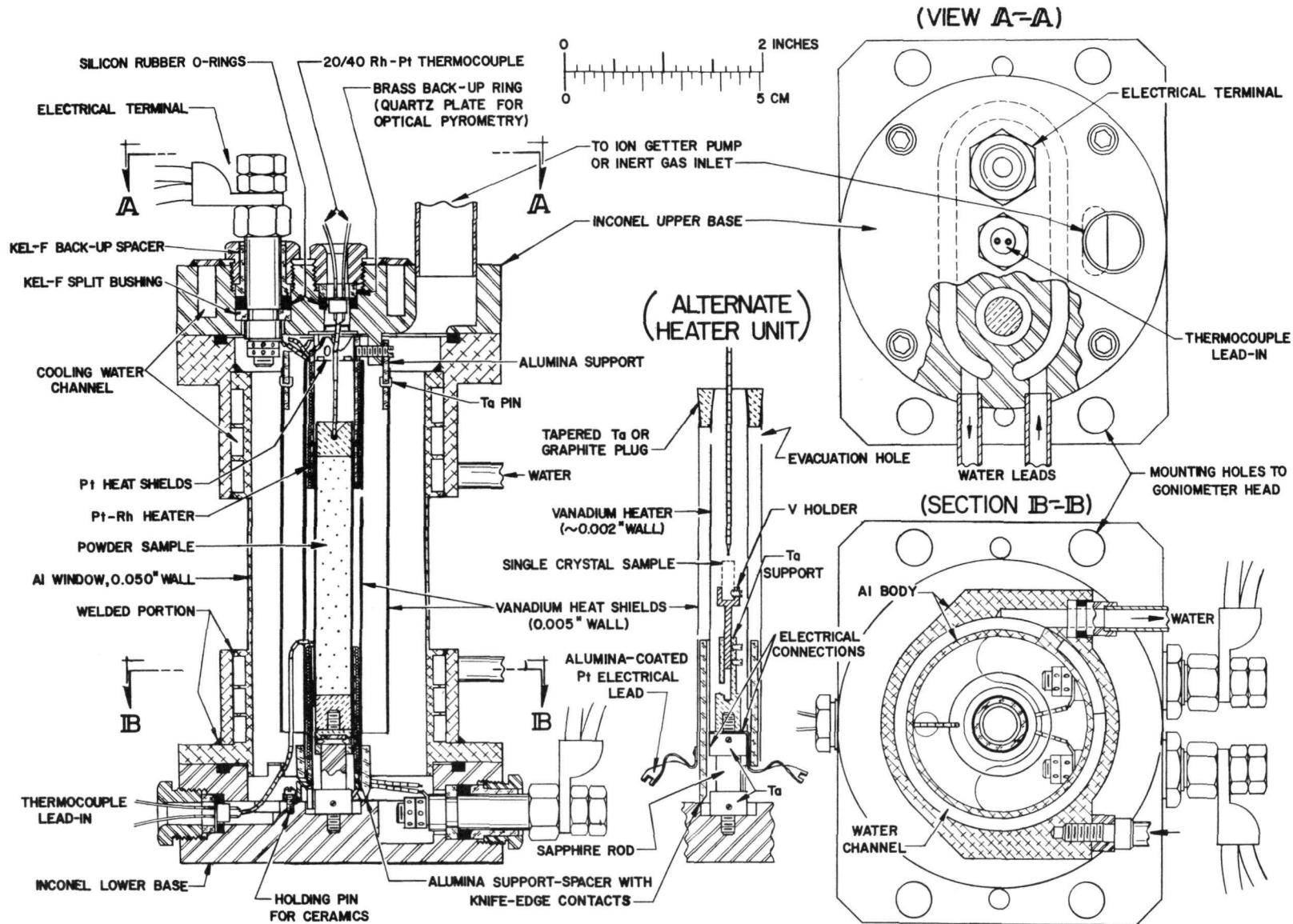
Numerous types of X-ray high-temperature cameras for both counter and film techniques have been developed, and more than a score are available commercially (see, e.g., the books by Campbell, 1956, and Peiser et al., 1955). Progress in this area is exponentially expanding; even the use of plasma jets and laser beams is under development. X-ray cameras can readily be adapted for neutron studies, especially since the components in the X-ray beam-path, such as beryllium, are usually sufficiently thin enough to have small neutron attenuation.

As stated in Chapter 2-7, the diffraction furnace for the neutron diffractometer is far easier to design on account of a wider choice of beam-path components (see Table III of Appendix I). A survey shows that at least a dozen furnaces designed solely for the neutron diffraction have been in use at various laboratories, although, only a few have been described in the literature (Abrahams, 1963; Willis et al., 1962). Our neutron diffraction furnaces, one mounted on the large goniometer head for a full scattering-angle study and the other for the magnet mount, possess some unique features described below. The first is denoted as M-1 and the latter as M-2 or magnetodiffraction furnace.

The M-1 furnace is illustrated in Figs. 33 through 36 and the magneto-furnace in Figs. 37 and 38. Some components, such as heating element, heat shield, sample holder, and electric terminals, are common to the two furnaces, thus avoiding unnecessary duplication in fabrication. Although the furnaces are particularized here as high-vacuum high-temperature devices, they can also be employed in an inert atmosphere.

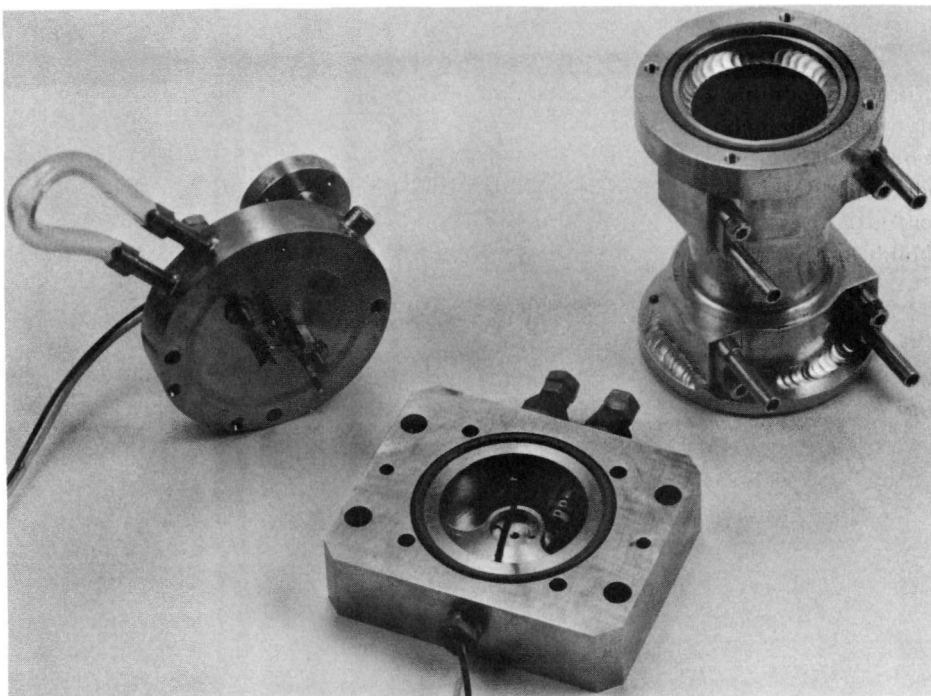
The furnaces are of the resistor-heater type and a temperature of about 2000°C maximum is expected. (The highest attainable temperature is dependent on the heater element, which is readily exchangeable.) Both single-crystal and powder studies can be accommodated in these furnaces.

The basic principles in design of the laboratory furnaces are concisely yet comprehensively described by Start and Thring (1960). Recent advances in high-temperature measurement and control have been compiled by Dahl (1962). The physical properties of various materials at high temperatures are given in books by Campbell (1956), Goldsmith et al. (1961), Samsonov (1964), and Shaffer (1964). References previously cited for the low-temperature materials (see Chapter 2-7) frequently include high-temperature properties also.



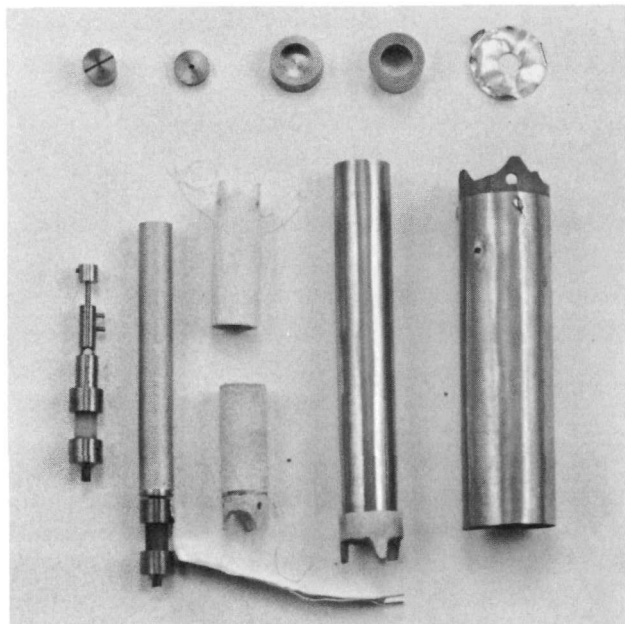
120-7773

Fig. 33. The High-temperature Diffraction Furnace (M-1) to be Mounted on the Large Goniometer Head. Two typical assemblies of the furnace elements are shown.



120-8496

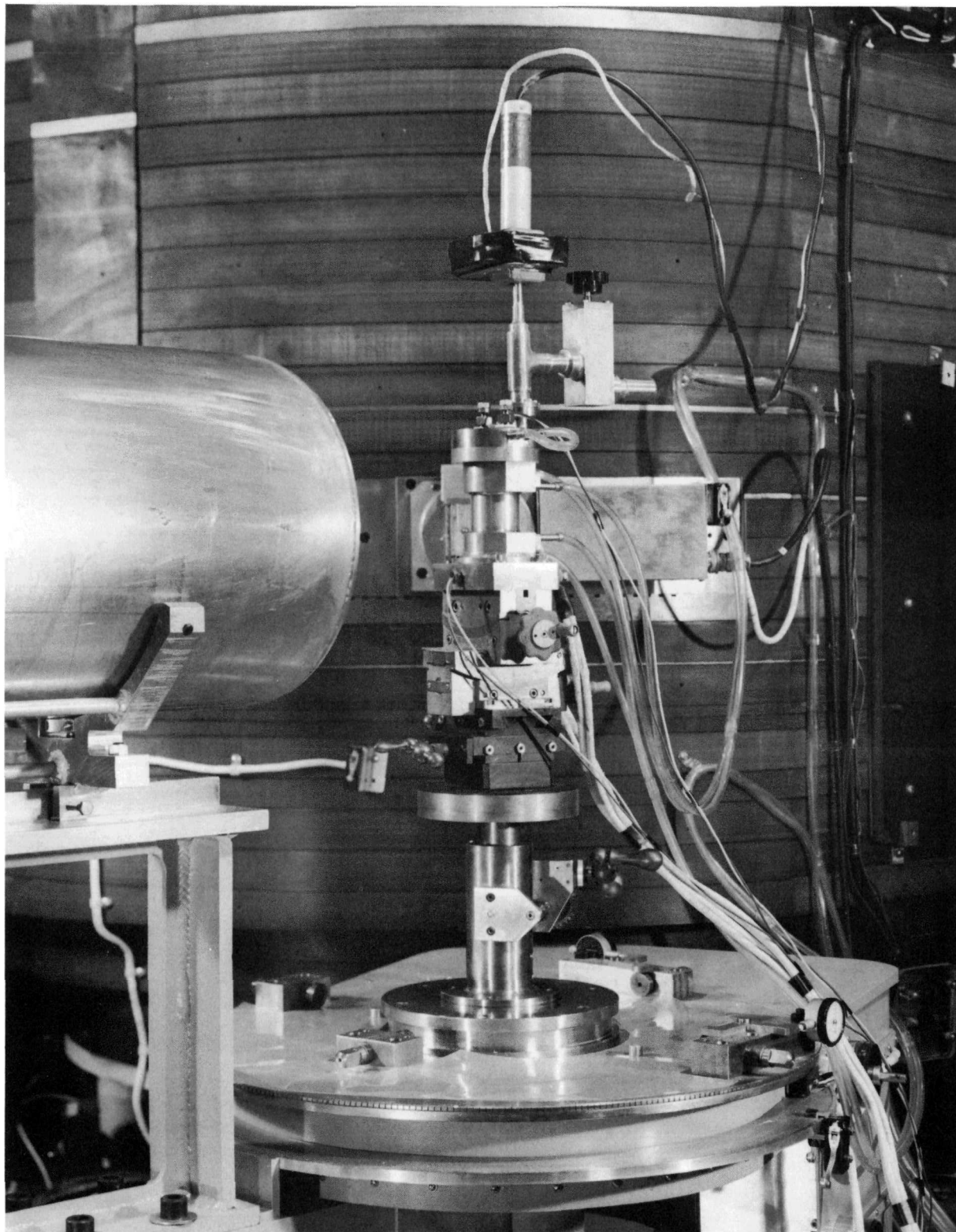
Fig. 34. The Low and Upper Inconel Bases and the Aluminum Mantle of the M-1 Furnace



120-8497

Fig. 35.

Examples of Furnace Elements. Top row (from left to right): two tapered, tantalum cover plugs to be used with the wire-resistor heater; two types of tantalum or graphite spacer plugs for the tube heater; platinum heat-shield. Main row: single-crystal holder; the holder-heater for the powder specimen; the wire/resistor heater; the inner heat shield; the outer heat shield.



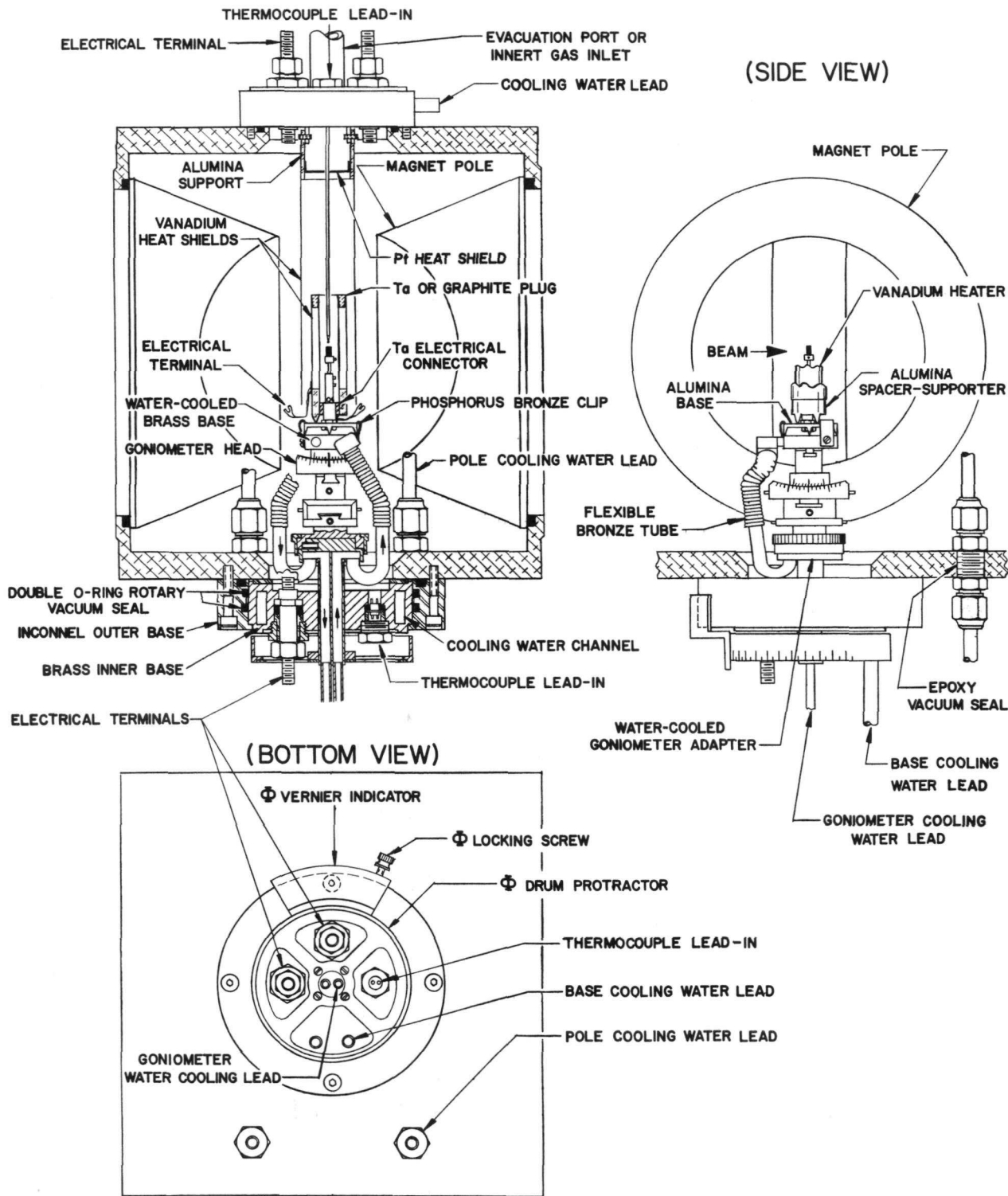
120-8039

Fig. 36. The M-1 Diffraction Furnace with the Ion-getter Vacuum Pump Mounted on the Goniometer Head. The centering adjusters for the magnet unit are also clearly seen on the Ω -table.



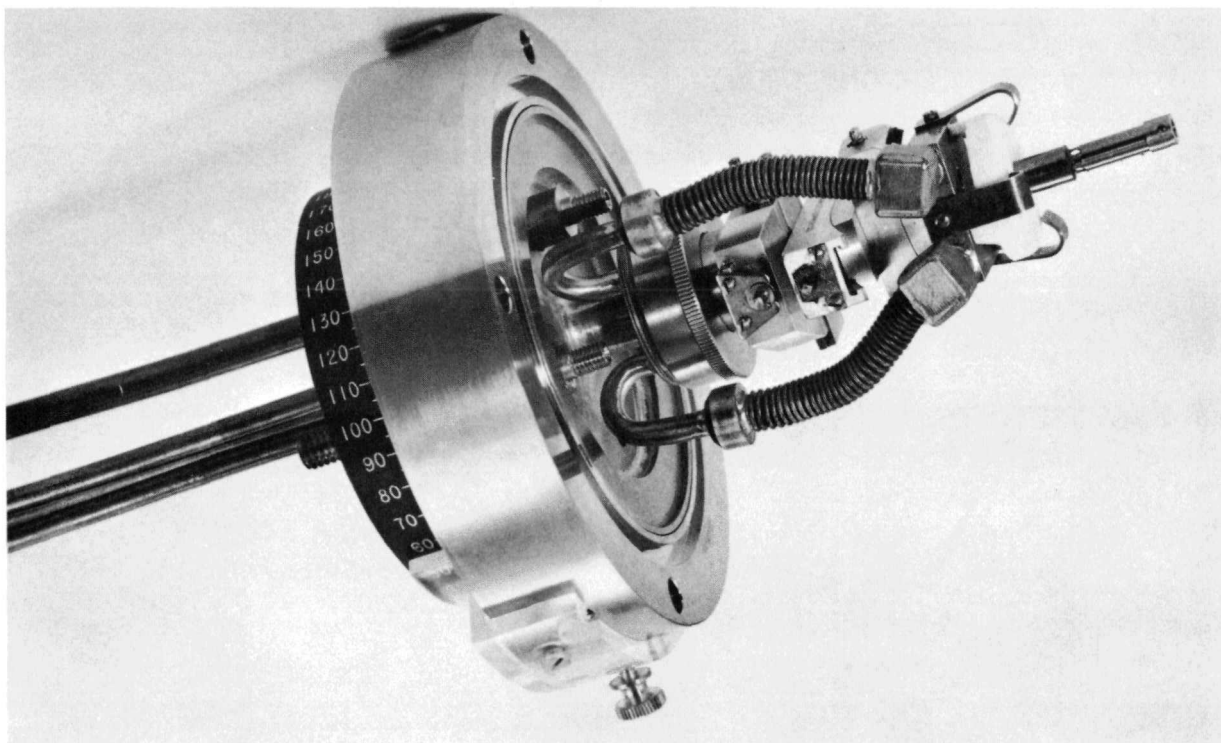
(FRONT VIEW)

(SIDE VIEW)



120-7770

Fig. 37. The Magneto-diffraction Furnace. The heat-shield sheet covering the goniometer-head is omitted in this drawing.



120-8495

Fig. 38. The Magneto-diffraction High-temperature Goniometer

The vacuum housing of the M-1 furnace consists of three parts: upper and lower Inconel* bases, and an aluminum central mantle (see Figs. 33 and 34). The three-part construction permits easy manipulation and interchange of the furnace components. The outer shape of the furnace is that of a symmetrically stepping cylinder. The cylinder diameter ranges from about 3.25 to 1.85 in. (the latter being the outer diameter of the aluminum beam window); the cylinder is 1.5 in. high and has a 0.05-in. wall. The overall height of the furnace is 6 in., excluding the electrodes and the like on the upper base. The center of the specimen is situated 2.875 in. from the furnace base, so that the specimen position coincides with the azimuth-rocker center of the large goniometer head (see Chapter 2-2). As implied by these dimensions, the furnace is indeed small and compact, and it can be placed in the Weiss-type magnet with the pole gap of about 2 in.

The vacuum-housing parts are screwed together with silicone-rubber O-rings** and evacuation is through the 0.56-in.-ID port tube on the

*Inconel used here has the approximate composition (w/o), 76 Ni, 16 Cr, and 8 Fe. This material is highly resistant to oxidation and other corrosion at elevated temperatures, except under sulfidizing atmosphere. The solidus temperature is about 1400°C. The thermal conductivity is very low, slightly higher than that of the stainless steel. It is paramagnetic above -40°C.

**All of the O-rings in the furnace are made of silicone rubber whose maximum continuous-service temperature is about 200°C. Apieson-H grease, which can be used up to 250°C, is used with the rubber O-ring. Occasionally, Teflon O-ring (max service temp of 260°C) is employed instead.

upper base. Two copper electric terminals and one thermocouple lead-in are provided for each of the upper and lower bases. The diameter of the narrowest section of the electrode is 0.325 in.; hence its allowable carrying capacity is 127 Amp in the rubber-covered wire standard. The O-ring compression seal with the Kel-F* spacers is employed for the vacuum-tight insertion of the electrode. The thermocouple is led into the vacuum chamber through a stuff cavity containing Stupakoe (or Fusite) and O-ring compression seals. Triadic sprigs with tantalum screws are projected down from the upper base; they are primarily used for hanging the outer heat shield and the wire-resistor heater element. The upper base and aluminum mantle are equipped with a cooling-water channel. Heat dissipation of the lower base is by conduction through a large area of contact with the aluminum mantle and with the goniometer head.

The sample holder is supported by a tantalum-sapphire spacer which is screwed into the lower-base center. The spacer is composed of tantalum screw cups and synthetic sapphire rod (0.75 in. high and 0.25 in. in diameter), and tantalum screw pins are used to fasten them together. The powder-sample holder is a tube of vanadium, 3 in. high, of 0.375-in. OD, and with a 0.005-in. wall. Both ends of the vanadium tube are enclosed by a tantalum or vanadium plug which is slightly tapered inward to meet with the tube-diameter variation, ± 0.005 in. The single-crystal Ta-V holder is height-adjustable, and its near-spacer section is bored out for minimizing the heat leak and to facilitate evacuation of the screw void of the holder (see Figs. 33 and 35). As discussed later, a variety of the holder material can be used in lieu of those mentioned above.

The resistor-heating element can be in the form of either a wire or cylindrical thin-wall tube. The former consists of a pair of upper and lower heaters. The resistor wire is wound on recrystallized alumina tube, 1.625 in. high, 0.5 in. in OD, and 0.4 in. in ID, for close fitting to the sample holder and to the inner heat shield. The wire is threaded through twin holes near the top of the tube, and double wire-threads are wound down so that both wire terminals are about 0.3 in. above the tube bottom. Three equally spaced holes, each 0.094 in. in diameter, are drilled around the tube wall just above the tube bottom, which is ground out to an arch-tripod shape with knife-edged feet. The lower heater sits on the Inconel lower base through the knife-edge contacts, and a tantalum holding pin keeps the heater stationary. Another heater is hung upside-down from the upper base by means of the triadic sprigs and tantalum screws. Pt or Pt-Rh alloy wires of B & S No. 36 to 32 (0.005- to 0.008-in. diameter) are most frequently employed as resistor elements. Although the winding area is small, a resistor with up to 15 Ω can be made. In order to reduce vaporization and to insure electrical insulation, refractory cement is coated on the wound wire.

*Kel-F: polytrifluorochloroethylene; max service temp of 200°C.

The vanadium inner heat shield, 4 in. high, 0.6 in. in ID and with a 0.005-in. wall, encases the Pt-Rh heater and is positioned by the alumina support spacer, whose bottom portion is also shaped into an arch-tripod with knife-edge contacts to the lower base. The outer heat shield, also of vanadium, hangs from the upper base and is 4 in. high, of 1-in. ID, and with a 0.005-in. wall. The heat zone for the neutron-impinging section is created through conduction heating of both the sample holder and the inner heat shield by the Pt-Rh heater. A Pt-sheet disk is inserted into the top opening of the heat zone so as to abate radiative heat toward the upper base.

The alternative heater unit uses the vanadium sample-holder as a resistor. The holder wall is thinned out to about 0.0015 in. by use of dilute HNO_3 . The resistance of the holder then increases to about 0.005Ω at 20°C . The height of the inner heat shield in this case is 3.5 in., and its wall thickness is thinner than 0.005 in. A tapered spacer plug made of tantalum or graphite is press-fit into the annulus space between the holder and the inner shield, and an alumina-tube spacer similar to that for the Pt-Rh heater supports the inner shield. Platinum ribbon is arc-welded to the inner shield as electrical lead. Another platinum electrical lead is connected to the sample-holder base, so that the holder, the inner shield, and the spacer plug constitute an electric continuum. It should be noted that the inner shield here plays the dual-role of secondary heater and heat shield. This holder-heating module is employed both for the powder and single-crystal mounts, except when powder samples have appreciable electric conductivity.

The Pt-Rh* heater can serve up to about 1600°C in extended operation. The vanadium holder or heater, can be used to about 1300°C ; above this the vapor pressure of vanadium is higher than 4×10^7 mm Hg** (see the book by Nesmeyanov, 1963, for vapor pressures of elements). Under an inert gas atmosphere, the vanadium components may be used up to near the melting point, 1710°C .

For the wire-resistor furnace, tungsten spirals† may be used up to a maximum service temperature of 2600°C in vacuum and to 3200°C (just below melting point of 3377°C) in a helium atmosphere. For the tube-resistor type, Mo (mp 2617°C), Pt,†† Ta (mp 2997°C), and W possess higher service temperatures than does vanadium. Preferably, the heater and heat shield should be prepared from the same material so as to simplify

*Melting or solidus points: Pt, 1769°C ; 10% Rh/Pt, 1845°C ; 20% Rh/Pt, 1900°C ; 40% Rh/Pt, 1945°C . The vapor pressure of platinum is 3×10^{-7} mm Hg at 1400°C , which is the recommended maximum service temperature.

**The vapor pressures of vanadium are 7.1×10^{-8} , 9.0×10^{-7} , 8.5×10^{-6} , 6.2×10^{-5} , and 3.6×10^{-4} mm Hg at 1227, 1327, 1427, 1527, and 1627°C , respectively.

†Tungsten-wire windings sag appreciably at high temperatures.

††Rh has a relatively high neutron cross section; hence Pt-Rh alloys are not recommended for the beam-path material (see Appendix I).

the scattering effect due to the furnace components. The cumulative neutron attenuation of one 0.002-in. holder-tube, two 0.005-in. heat shield, and aluminum windows is, for 0.1-eV neutrons: 6.3% for V; 5.0% for Mo; 8.2% for Pt; 7.5% for Ta; 7.7% for W. Similarly, thin-walled tubes of Al_2O_3 , BeO , graphite, MgO , SiC , ThO_2 , and ZrO_2 may be employed for the beam-path furnace elements; their melting points are, respectively, 2015-2050°C, 2530°C, 3000°C (service temperature), 2800°C, 2200°C (service temperature), 3035°C, and 2700-2980°C. Here, the oxide resistors with low neutron attenuation, $\text{ThO}_2\text{-Y}_2\text{O}_3$ and $\text{ZrO}_2\text{-Y}_2\text{O}_3$, are of potential use for temperatures in excess of 2000°C, even under an oxidizing atmosphere (R. F. Geller in the book by Campbell, 1956, pp. 263-268). The inner heat shield may be used as an auxiliary or startup heater for the oxide heater.

The furnace has been successfully employed up to about 1700°C. The lower pair of the electrodes were warmed to over 100°C in the 1700°C operation; hence, a copper capillary tube for leading cooling water was wound around the lower electrodes. The thermocouples, B & S No. 36 (0.005-in. diameter), were placed as illustrated in Fig. 33. Commonly used thermocouples are: Pt-10% Rh/Pt for up to 1760°C; 20% Rh/Pt-40% Rh/Pt for 1850°C; 60% Ir/Rh-Ir for 2300°C. For other high-temperature thermocouples, see the book by Dahl (1962).

Optical pyrometry can be accommodated by the present design, by replacing the upper-thermocouple lead-in seal by a silica-glass window.

In view of lengthy experimental period and radiation hazard, automatic temperature control is highly desired. For this, a stepless, proportional, auto-feedback controller is most ideal. However, tentatively, a manual auto-transformer control has been employed in our experiment. The input of 110 V AC is fed into the step-down transformer through the auto-transformer. The output is 6 to 12 V, with maximum power of about 1.5 kW. In the normal high-vacuum operation, the furnace assembly is degassed at the operation temperature under high vacuum obtained through the conventional vacuum station. The evacuation route will then be diverted to the ion-getter pump of 1-l/sec or 8-l/sec capacity (see Fig. 36). This enables an Ω -setting of the furnace without large restriction.

The design of the magneto-furnace is very unique as regards the sample-holder construction, which is illustrated in Figs. 37 and 38. The Inconel flange is adapted to the bottom opening of the aluminum vacuum box of the magnet (see Chapter 2-7). The flange, termed outer base in Fig. 37, holds up the water-cooled inner base through a double-O-ring rotary vacuum seal. The inner base is equipped with two electrodes, a thermocouple lead-in, and the water-cooled spindle column. On the top of the spindle column, a standard small goniometer head is mounted. The upper rocker of the goniometer head is a brass base which is water cooled via the spindle water channel and flexible bronze tubes. A small alumina table

is then fastened to the brass base by means of phosphorus-bronze clips. The sample holder is mounted on the alumina table. The top opening of the aluminum vacuum box is covered with the upper base of the M-1 furnace. The designs of the heater elements, sample holder, electrodes, and thermocouple lead-in are identical with those for the M-1 furnace. The copper tube is wound on the magnet poles for additional water cooling of the magnet core. The Φ -rotation together with the χ_{\parallel} and χ_{\perp} settings of the magnet facilitate the directional modulations of the sample and the external magnetic-field.

APPENDIX I

Transmission Reference Data

The linear absorption coefficients μ in the transmission ratio, $\exp(-\mu t)$, and related data are given in Table III for customary or potential materials for use in neutron-diffraction instrumentation. Unless otherwise noted, the following general guides are applicable to the tabulated values.

Table III

TRANSMISSION DATA FOR SELECTED MATERIALS

The Thicknesses for a Transmission Ratio of 10^{-9} Are Marked with an Asterisk; Otherwise They Are Given for 10% Attenuation

Substance	$\mu(\text{cm}^{-1})$		t(cm)		Remarks
	0.025 eV	0.1 eV	0.025 eV	0.1 eV	
Ag	3.88	2.14	0.027	0.049	Special application.
Al	0.0904	0.0964	1.165	1.092	Encloser. Monochromator.
Au	6.14	3.33	0.017*	0.032*	Special application.
B	98.2	49.7	0.211	0.417	Attenuator.
α -Be	0.981	0.718	0.118	0.147	Use of beryllium windowed X-ray instrument Monochromator.
Cd	119	162	0.174*	0.128*	Attenuator.
Cr	0.601	0.480	0.175	0.219	Special application.
Cu	0.914	0.796	0.115	0.132	Copper foil encloser. Monochromator.
α -Fe	1.12	1.02	18.5*	20.3*	Soller component. t=1.03 for 10% at 0.1 eV.
Gd	1389	387	0.015*	0.054*	Attenuator.
Ge	0.269	0.353	0.391	0.298	Monochromator.
In	7.52	4.29	0.014	0.025	Photo-sensing.
Mg	0.133	0.147	0.791	0.717	Al-Mg alloy encloser.
Mo	0.481	0.449	0.219	0.235	High-temp application.
Ni	1.96	1.83	10.6*	11.3*	Soller component. Fluorine-compd encasement. 0.054 and 0.058 cm for 10%.
Pb	0.264	0.353	0.399	0.299	Monochromator.
Pt	1.09	0.995	0.096	0.106	High-temp application.
Si	0.115	0.112	0.918	0.939	Monochromator. High-temp application.
Ta	1.38	0.884	0.076	0.119	High-temp application.
V	0.711	0.533	0.148	0.197	Encloser.
α -W	1.452	0.915	0.073	0.115	High-temp application.
Zn	0.270	0.276	0.390	0.381	Monochromator.
α -Zr	0.269	0.269	0.392	0.392	
Brass	0.689	0.616	0.153	0.171	Wt %, Cu:Zn = 67:33.
Bronze	0.828	0.727	0.127	0.145	Wt %, Cu:Sn:Zn = 88:10:2.
Monel	1.56	1.43	0.067	0.074	Wt %, Ni:Cr:Fe = 60:33:6.5.
Nichrome	1.64	1.50	0.064	0.070	Fluorine-compd encloser.
PtRh _{0.211}	2.68	1.87	0.039	0.057	Wt %, Ni:Cr:Mn = 79:20:1.
PtRh _{0.633}	4.65	2.95	0.023	0.036	10 w/o Rh. mp 1845°C. High-temp application.
Stainless Steel	1.00	1.00	20.7*	20.7*	25 w/o Rh. mp 1915°C. High-temp application.
Ti _{2.13} Zr	0.472	0.355	0.224	0.296	Type 304. Soller component. 0.10 cm for 10%.
Al ₂ O ₃	0.372	0.348	0.283	0.303	Zero-coherent scattering. Encloser.
B ₄ C	82.5	41.9	0.251*	0.495*	High-temp application.
B ₇ C	89.1	45.2	0.233*	0.458*	Attenuator.
BeO	0.838	0.706	0.126	0.149	High-temp application.
C (graphite) ^a	0.569	0.546	0.185	0.193	High-temp application. Moderator.
CaB ₆	61.0	30.9	0.340*	0.670*	Attenuator.
Hg ₂ Cl ₂	8.30	4.38	2.50*	4.73*	Neutron and γ -ray attenuator.
Glass, Pyrex ^b	4.68	2.76	0.023	0.038	SiO ₂ 80.82%; B ₂ O ₃ 12.86%; Na ₂ O and K ₂ O 4.5%; Al ₂ O ₃ 1.8%. Density, 2.231 g cm ⁻³ .
Li ₂ CO ₃	2.78	1.52	7.45*	13.6*	Low scatterer.

Table III (Contd.)

Substance	μ (cm ⁻¹)		t(cm)		Remarks
	0.025 eV	0.1 eV	0.025 eV	0.1 eV	
MgO	0.393	0.388	0.268	0.271	High-temp application. Borax. Attenuator.
Na ₂ B ₄ O ₇ 10H ₂ O	8.60	4.49	2.41 ^a	4.61 ^a	
NaCl	1.15	0.823	0.091	0.128	Standard crystal.
SiC	0.353	0.341	0.298	0.309	High-temp application
SiO ₂	0.237	0.219	0.444	0.482	Fused silica. Enclosurer. Filter.
ThO ₂	0.636	0.538	0.166	0.196	High-temp application.
ZrO ₂	0.438	0.414	0.241	0.255	High-temp application.
Cellulose	2.44	1.89	8.48 ^a	10.97 ^a	(C ₆ H ₁₀ O ₅) _p . Attenuator. Moderator.
Masonite	2.19	1.69	9.48 ^a	12.27 ^a	Benelex 70. Attenuator. Moderator.
Neoprene	2.11	1.59	9.83 ^a	13.00 ^a	Polychloroprene (C ₄ H ₅ Cl) _p . Soller component.
Paraffin	3.09	2.36	6.71 ^a	8.79 ^a	(CH ₂) _n . Attenuator. Moderator.
Polyethylene	3.09	2.36	6.71 ^a	8.79 ^a	(CH ₂) _p . Attenuator. Moderator.
Teflon	0.349	0.317	0.302	0.332	(CF ₂) _p . Enclosurer.
Liq CCl ₃ F	1.00	0.707	0.105	0.149	Freon 11. Refrigerant.
Liq CCl ₂ F ₂	0.807	0.614	0.131	0.171	Freon 12. Refrigerant.
Liq CClF ₃	0.559	0.417	0.188	0.253	Freon 13. Refrigerant.
Liq CF ₄	0.214	0.192	0.492	0.549	Freon 14. Refrigerant.
Liq He	0.0137	0.0137	7.67	7.67	At 4.2°K. Below 2.2°K, $\mu = 0.0161$.
Liq D ₂	0.0821	0.0821	1.28	1.28	Possible refrigerant.
Liq H ₂ ^c	1.27	1.09	0.087	0.097	Ortho:para = 3:1.
Liq H ₂ ^c	0.544	1.09	0.194	0.097	Para only.
Liq N ₂	0.445	0.396	0.237	0.266	Refrigerant.
Liq O ₂	0.180	0.163	0.584	0.645	Refrigerant.
Solid D ₂	0.105	0.105	1.28	1.28	Refrigerant.
Solid H ₂ ^c	1.52	1.37	0.069	0.077	Ortho:para = 3:1.
Solid H ₂ ^c	0.684	1.37	0.154	0.077	Para only.
Solid N ₂	0.565	0.503	0.187	0.209	Refrigerant.
Solid O ₂	0.226	0.204	0.467	0.516	Refrigerant.
Solid CO ₂	0.286	0.265	0.368	0.397	Refrigerant.

^aEgelstaff (1957) for the cross-section values.

^bWajima *et al.* (1960) for the density and the composition.

^cWhittemore (1962) for the cross-section values.

The μ values were computed from the total cross-section data contained in the review articles by Buckingham *et al.* (1961), Hughes and Schwartz (1958), and Hughes *et al.* (1960) and are based on the following relations:

$$\mu t = n \sigma_t; \quad n = N_A \rho' t / M; \quad \sigma_t = \sum_j q_j \sigma_{tj} = \frac{M}{N_A} \sum_j w_j \left(\frac{\mu}{\rho} \right)_j;$$

$$\sigma_{tj} = \frac{A_j}{N} \left(\frac{\mu}{\rho} \right)_j; \quad M = \sum_j q_j A_j,$$

where n is the number of atoms or molecules per cm² in the direction of the incident beam; N_A , Avogadro number; ρ' , the crystal density or the packing density of the powder sample; M , the chemical formula weight; σ_{tj} , the total cross section of the j -th element with the atomic weight A_j ; w_j , the weight fraction of the j -th element and $\sum w_j = 1$; $(\mu/\rho)_j$, the mass absorption coefficient.

In the neutron-energy region of concern, it is assumed that the following structure-sensitive contributions are insignificantly small: the scattering due to the magnetic electrons; the diffraction-interference effect (book by Bacon, 1962, p. 43; Placzek and Van Hove, 1955); the target-nucleus-recoil and chemical bonding effects on the light atoms (book by Mott and Massey, 1949, pp. 329-334; review article by Ringo, 1957; Rush et al., 1961; Whittemore and McReynolds, 1959). Strictly speaking, σ_t in the above equations should be denoted as the transmission cross section, μ_{eff} , so that the aforementioned subordinate effects would be implicated.

The data for metals, alloys, and inorganic and organic materials used for neutron filters are listed in this order in Appendix II (for boral, see Chapter 1-3). Solid materials are assumed to be in polycrystalline form. The room-temperature state for polymorphous substances is cited, but the phase transitions do not alter the listed values by more than a few percent. The μ values are calculated for neutron energies of 0.025 and 0.1 eV (1.809 and 0.9044 Å); those for other energies can be obtained by multiplying the total cross-section ratio, σ_t/σ'_t , by the listed μ value, where σ_t is the total cross section at the energy in question and σ'_t that at 0.025 or 0.1 eV. Also, intermediate values of μ are obtainable by means of the linear interpolation with good accuracy, since none of the listed substances (except cadmium) possess effectual resonance in or near our energy range, 0.025 to 0.1 eV.

For the substances of low cross section which are usable as components in the beam-path (e.g., the specimen-enclosing material), the thicknesses which remove 10% of the incident neutrons from the beam path are listed. For those of high cross section and Soller-slit materials, the t values for the transmission ratio 10^{-9} are given, since they are commonly used to attenuate all of the incoming neutrons. The thicknesses for other transmission ratio can readily be converted from the table values. Typical ratio values are: $\mu t = 0.1053, 0.2876, 0.6931, 16.12, 20.72, 29.93,$ and 36.84 for $\exp(-\mu t) = 0.9, 0.75, 0.5, 10^{-7}, 10^{-9}, 10^{-13},$ and 10^{-16} , respectively. Reference characteristics with emphasis on the instrumental application are briefly described in the "remarks" column. Table III is also useful in interpretation of the neutron radiography (see Chapter 1-12).

APPENDIX II

Neutron Filters

Neutron filters may be classified into three categories: diffraction cut-off filter; single-crystal filter; resonance filter. The diffraction cut-off filter is used to obtain the neutrons of wavelengths near and longer than $2d_{\max}$, where d_{\max} is the largest interplanar spacing of the filter crystal. Polycrystalline materials with large scattering-to-capture ratio (e.g., Be, BeO, Bi, Cu, Pb, Th, Y) are employed for obtaining a wavelength of about 4 Å or longer; hence, they are of limited application in the diffractometry.

The single-crystal filter (Brockhouse, 1959) utilizes the wavelength dependency of the thermal diffuse scattering and gives a good fast-neutron discrimination in favor of thermal neutrons, provided that the crystal possesses the following characteristics: small cross sections for capture, incoherent scattering, and paramagnetic diffuse scattering; high Debye-temperature or small Debye-Waller temperature factor, leading to a small ratio, thermal diffuse to coherent; readily available in a large size. Among the crystals suggested by Brockhouse (1959), i.e., quartz, calcite, fluorite, bismuth, and cerium, the quartz crystal is most commonly used for discrimination of neutrons having wavelengths shorter than about 2 Å (see Schermer, 1960, for the "total" cross-section curve.) The single-crystal filter for suppressing the higher-energy neutron contamination in the monochromatic beam has to be oriented so that the attenuation due to the Bragg-Laue coherent scattering is insignificantly small. It is obvious that both diffraction cut-off and single-crystal filters are more effectual at lower temperatures and hence are often cooled down to the liquid-nitrogen temperature.

The resonance filter is an essential item in suppressing the higher-order-harmonics contamination in the crystal-monochromated neutrons. Such a filter utilizes a sharp cross-section peak due to the resonance absorption of the constituent isotope of the filter, in contrast with the gradually changing attenuation curve of the single-crystal filter. In Table IV, characteristics of isotopes used for resonance filters employed to diminish the $\lambda/2$ contamination are tabulated, together with their functional data. The chemical compound or mixture containing the filter and low-attenuating elements may be employed when thin metal foil is not readily obtainable. In Fig. 39, the resonance-filter wavelengths are indicated in the correlative curves of wavelength-velocity-temperature for thermal and near-thermal neutrons. These filters can also be usable near the resonance values; an example, Pu²³⁹ is illustrated in Fig. 40.

A balance filter, a combination of two or more resonance filters, may have to be used for some intermediate wavelengths.

Table IV

CHARACTERISTICS OF THE RESONANCE FILTERS COMPUTED FOR THE NATURALLY OCCURRING ELEMENTS EXCEPT FOR Pu²³⁹

Element	Mass Number ^b	E ₀ ^d (eV)	λ ₀ ^d (Å)	E for λ (eV)	α _t (λ ₀) ^e (b)	α _t (λ) ^e (b)	g cm ⁻² for λ ₀ -component to ^f			Transmission Ratio of 2λ ₀ ^g			Metal Thickness (mm) ^h		
							2%	5%	10%	2%	5%	10%	2%	5%	10%
Cd	113	0.178	0.678	0.0445	7800	2430	0.0936	0.0717	0.0551	0.295	0.393	0.488	0.108	0.083	0.064
Er	167	0.47	0.417	0.1175	2430	119	0.447	0.342	0.263	0.826	0.864	0.893	0.494	0.378	0.290
Er	167	0.58	0.376	0.1450	1850	120	0.587	0.449	0.346	0.776	0.823	0.861	0.648	0.496	0.381
Eu	151	0.327	0.500	0.0817	3500	1890	0.282	0.216	0.166	0.121	0.199	0.289	0.546	0.418	0.321
Eu	151 ^c	0.461	0.421	0.1153	11200 ^c	1050	0.0881	0.0675	0.0519	0.693	0.755	0.806	0.171	0.131	0.100
Ir	191	0.654	0.354	0.1635	4850	182	0.257	0.197	0.152	0.864	0.894	0.917	0.115	0.088	0.068
Lu	176	0.143	0.756	0.0358	355	95	3.20	2.45	1.88	0.351	0.449	0.540	3.25	2.49	1.91
Pu ^a	239	0.296	0.526	0.0740	5170	700	0.300	0.230	0.177	0.589	0.667	0.732	0.152	0.116	0.089
Sm	149	0.0976	0.916	0.0244	15800	5550	0.0618	0.0473	0.0364	0.253	0.349	0.445	0.082	0.063	0.048
Yb	168	0.597	0.370	0.1493	165	44	6.81	5.21	4.01	0.352	0.450	0.541	9.79	7.49	5.76

^a Computed for 100% Pu²³⁹.

^b Mass number of isotopes responsible for the resonance.

^c Overlapped with Eu¹⁵³ resonance at 0.457 eV.

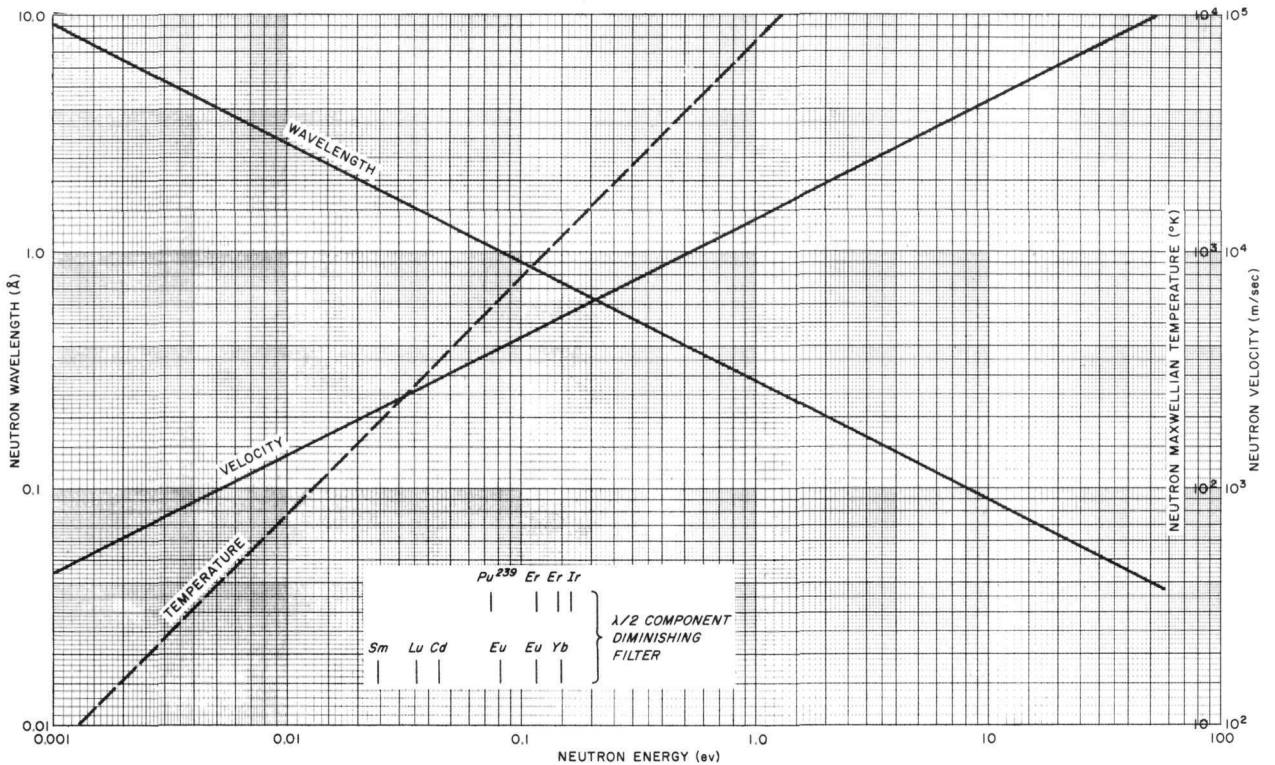
^d λ₀ the neutron wavelength at the resonance energy E₀.

^e Total cross sections at λ₀ and λ = 2λ₀ (for Lu and Yb, see Atoji, 1961a).

^f Weight concentration of the element for diminishing λ/2-component to 2%, 5% and 10% of the original intensity.

^g e.g., Cd of 0.0936 g cm⁻² reduces the λ-component intensity to 29.5% of the unfiltered value.

^h e.g., Cd of 0.108 mm thick is used to filter out 98% of the λ/2 component.



120-8561

Fig. 39. Variations of Neutron Wavelength, Temperature, and Velocity with the Energy in Thermal and Near-thermal Regions. The λ/2-component diminishing filters are placed at the λ-component energies.

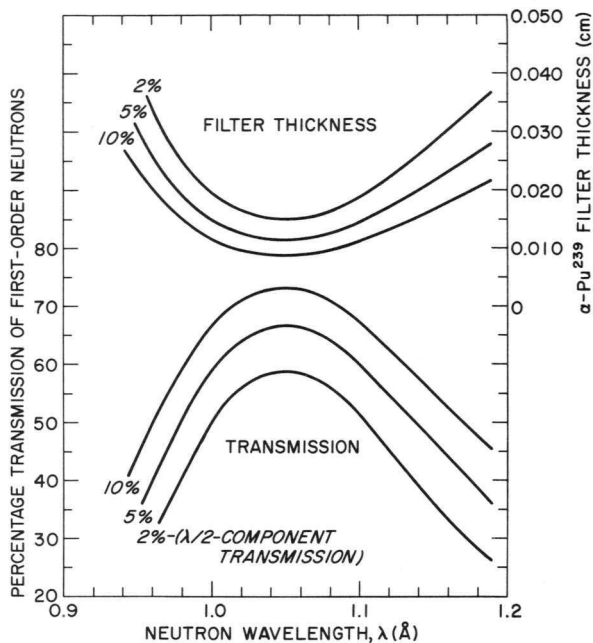


Fig 40

A Reference Diagram for Selecting the α -Pu²³⁹ Resonance Filter. The figures 2, 5 and 10% refer to the percentage transmission values of the $\lambda/2$ component. For example, suppose the first-order wavelength is $\lambda = 1.09 \text{ \AA}$. The thicknesses of the Pu²³⁹ filters for cutting the second-order contamination down to 2, 5, and 10% are 0.0174, 0.0133 and 0.0102 cm, respectively. These filters will decrease the first-order intensity to 53.7, 62.1, and 69.4% of the no-filter value, respectively.

120-8567

In the coherent-scattering study, once the $\lambda/2$ -component intensity is obtained from the standard-sample data with help of the resonance-filter method, the differentiation of the $\lambda/2$ contribution in the specimen data may be carried out without using the filter. However, in the diffuse-scattering study, where the wavelength dependency of the scattering process is difficult to evaluate, the filter technique has to be incorporated in a refined experiment, in some instances, together with a single-crystal filter. In the epi-cadmium neutron spectrometry, practically all of the heavy isotopes serve as the resonance filter (e.g., Hay, 1959; book by Hughes, 1953, pp. 143-146).

SPECIAL TOPIC

SYMMETRY OPERATORS OF MAGNETIC GROUPS

Graphical representations of the 36 three-dimensional Bravais-Shubnikov lattices and the symmetry operators of the axial-vector space groups are given in Figs. S-1 and S-2 and Figs. S-3 to S-7, respectively. The former drawings are essentially facsimiles of those given by Belov *et al.* (1957),* although correlations between the crystallographic axes and the symmetry symbols are more clarified in the present drawings. A partial graphical representation of the latter has been given by Donnay *et al.* (1958). Except for the left-handed enantiomorphic screw-operators, our figures include all of the symmetry operators. The graphical symbols for the antisymmetry elements are tentatively proposed here. The present drawings would be instructive in the systematic analysis on the spin structure of the magnetic substance. Representative references on this subject are given below.

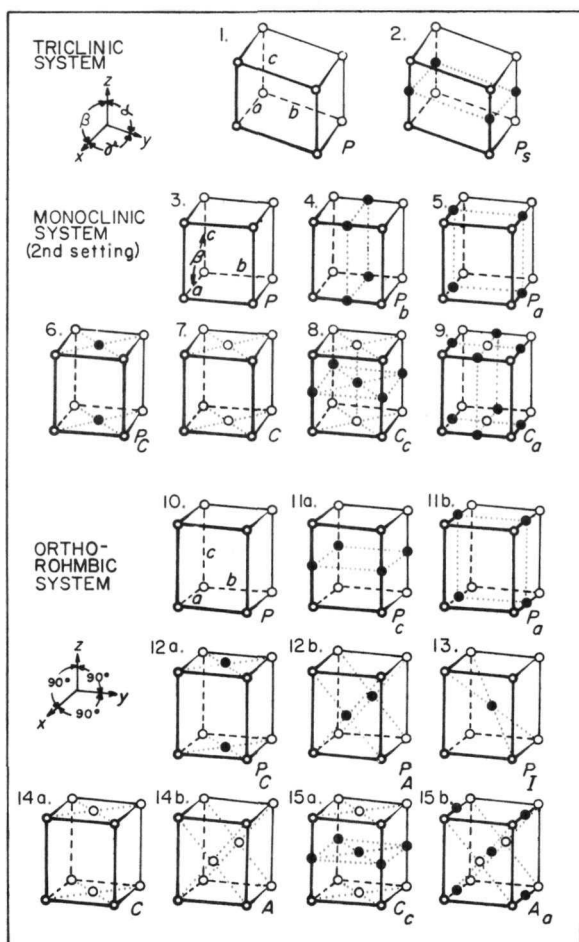


Fig. S-1

Bravais-Shubnikov Lattices

*References to this section immediately follow.

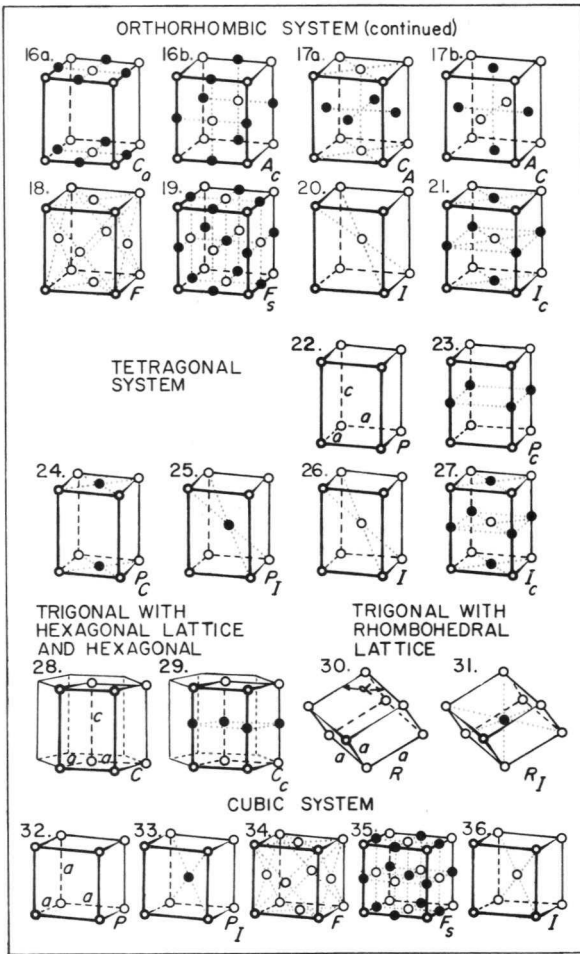



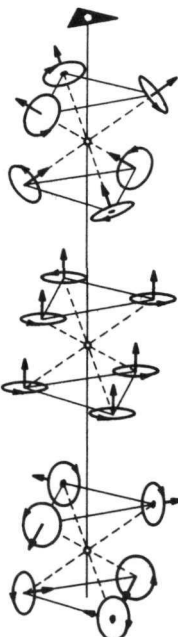
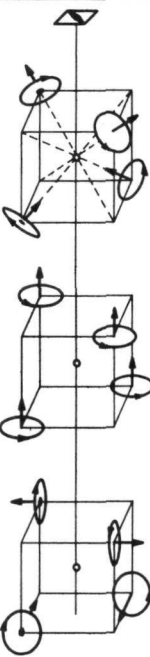


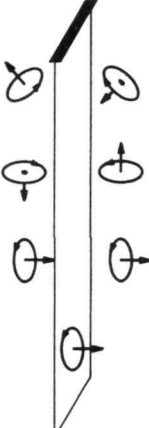
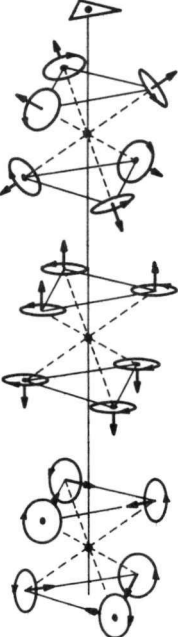
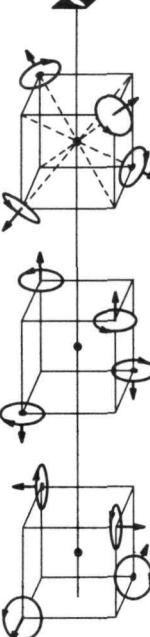
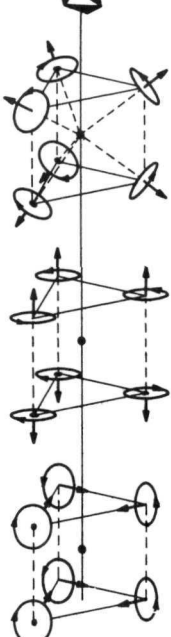
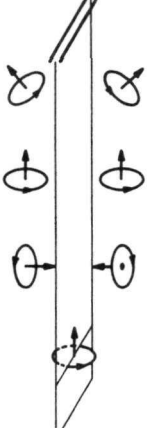
Fig. S-2
Bravis-Shubnikov Lattices (Continued)

120-8129

Fig. S-3
Symmetry Operations of the Axial-vector Space Groups

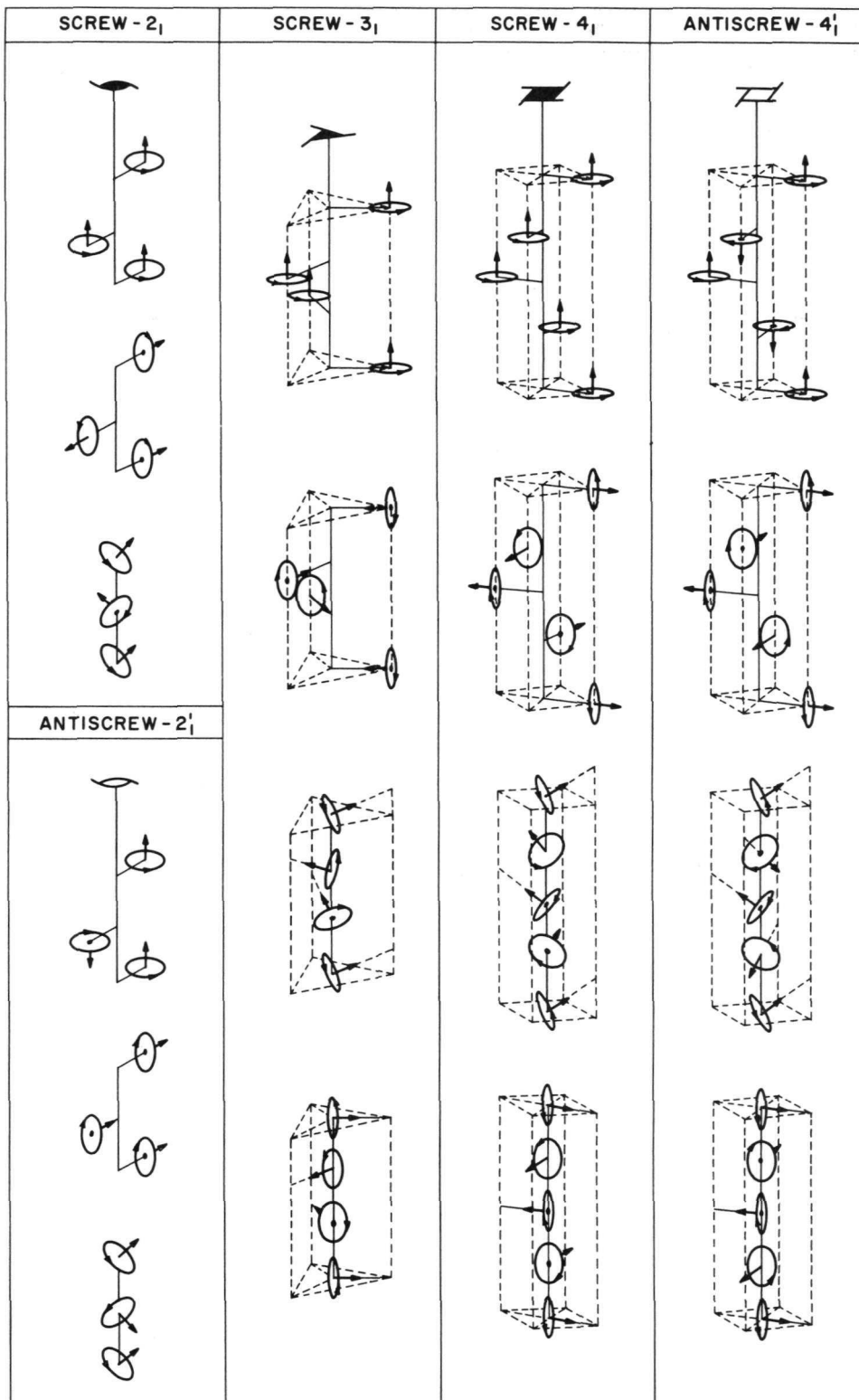
OPERATIONS OF THE FIRST KIND			
TRANSLATION - t	ANTIROTATION - $2'$	ROTATION - 4	ROTATION - 6
ANTITRANSLATION - t'			
ROTATION - 2		ANTIROTATION - $4'$	ANTIROTATION - $6'$

120-7182

OPERATIONS OF THE SECOND KIND			
INVERSION - T	ROTATORY INVERSION - $\bar{3} = 3 \times \bar{1}$	ROTATORY INVERSION - $\bar{4}$	ROTATORY INVERSION - $\bar{6} = 3/m$
			
ANTIINVERSION - $\bar{1}'$			
			
ROTATORY INVERSION - $\bar{2}$ MIRROR PLANE - m $2 \perp m$			
			
	ROTATORY ANTI-INVERSION - $\bar{3}' = 3 \times \bar{1}'$	ROTATORY ANTI-INVERSION - $\bar{4}'$	ROTATORY ANTI-INVERSION - $\bar{6}' = 3/m'$
			
ROTATORY ANTI-INVERSION - $\bar{2}'$ ANTIMIRROR PLANE - m' , $2' \perp m'$			
			

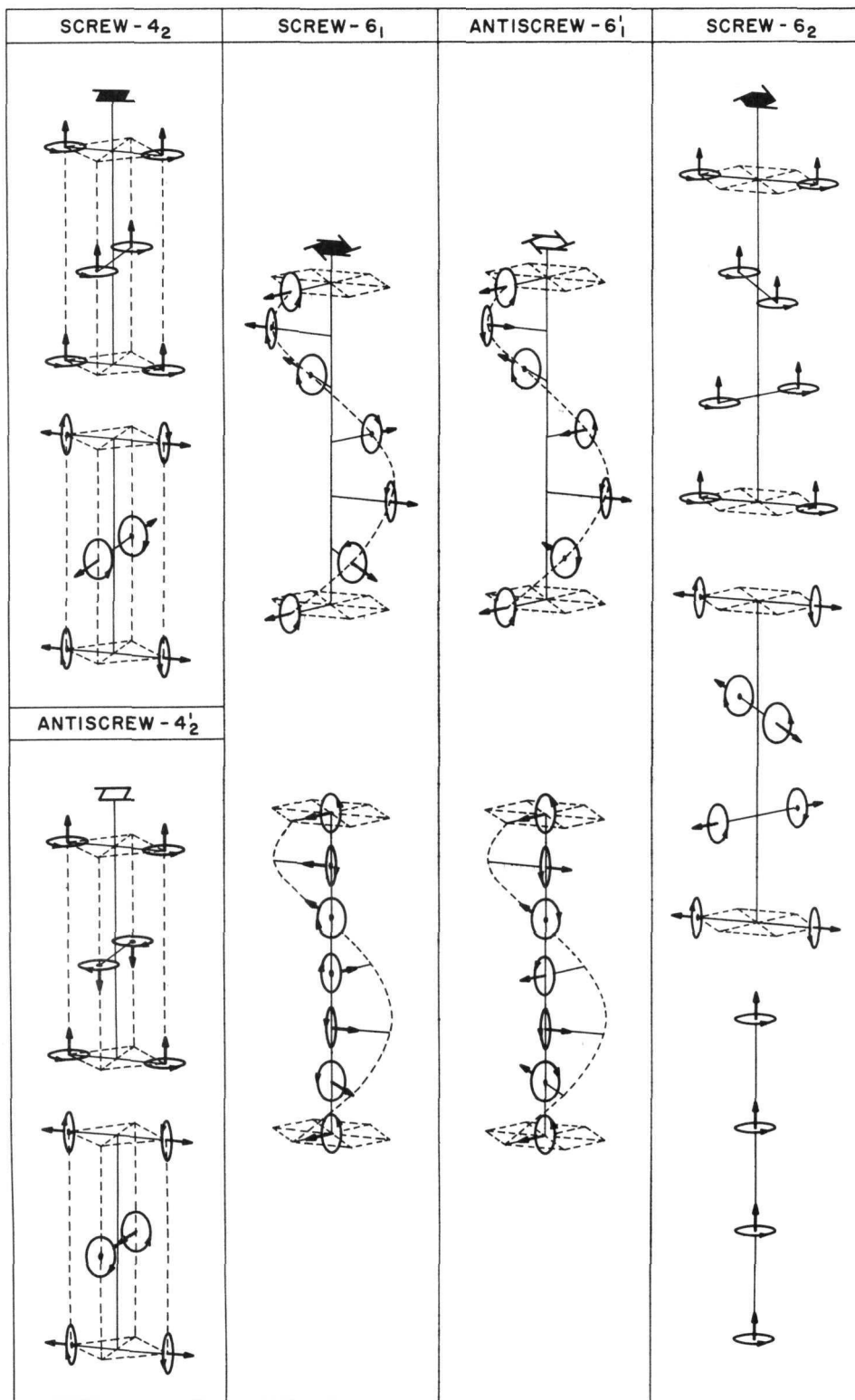
120-7184

Fig. S-4. Symmetry Operators of the Axial-vector Space Groups (Continued)



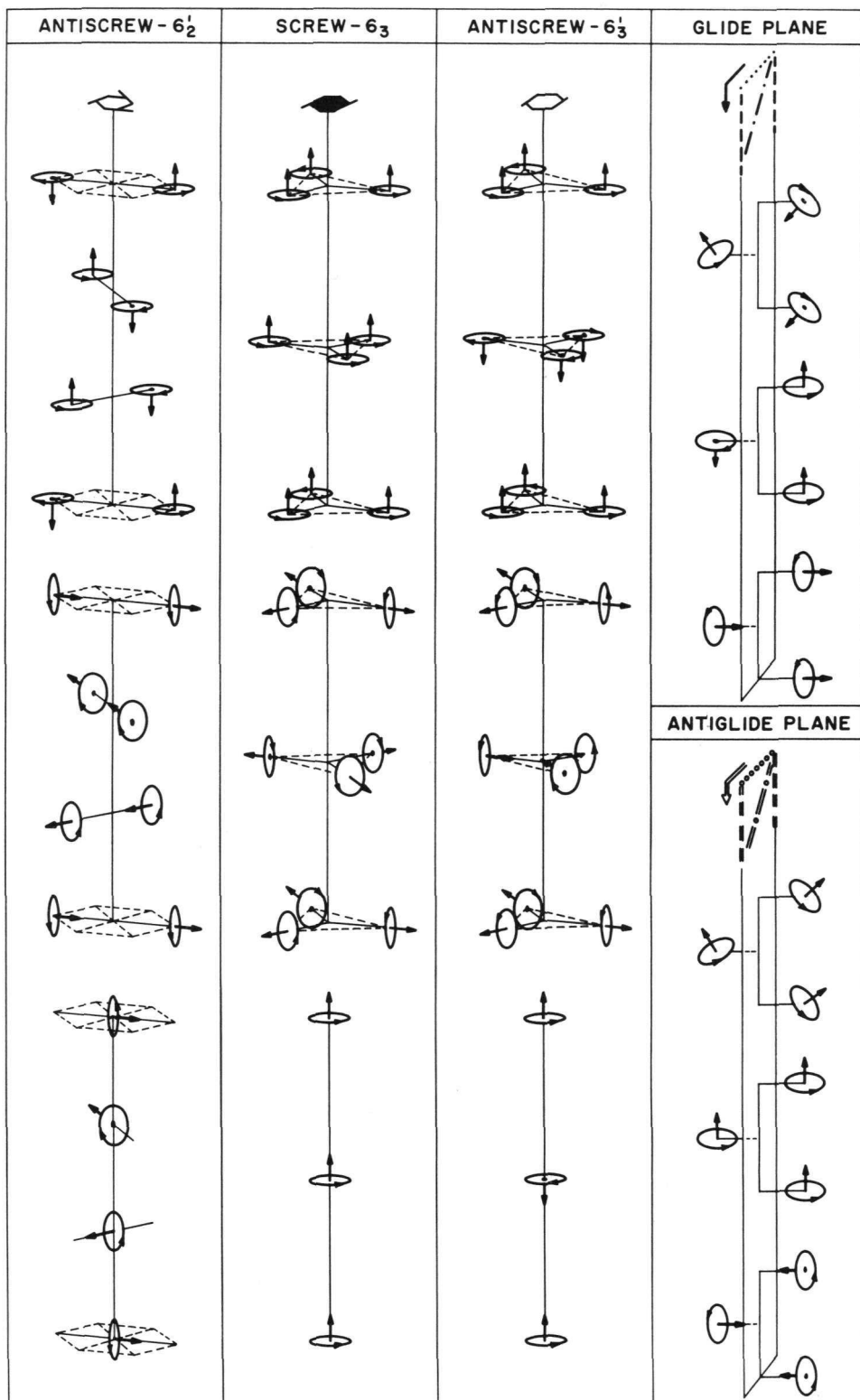
120-7183

Fig. S-5. Symmetry Operators of the Axial-vector Space Groups (Continued)



120-7180

Fig. S-6. Symmetry Operators of the Axial-vector Space Groups (Continued)



120-7181

Fig. S-7. Symmetry Operators of the Axial-vector Space Groups (Continued)

References for Magnetic Groups

Belov, N. V., Neronova, N. N., and Smirnova, T. S., Shubnikov Groups, Soviet Phys.-Cryst. 2, 311 (1957).

Belov, N. V., and Neronova, N. N., Ferromagnetic Groups, J. Phys. Soc. Japan, 17, Suppl. B-II, 330 (1962).

Belov, N. V., Neronova, N. N., and Donnay, G., Tables of Magnetic Space Groups II. Special Positions, J. Phys. Soc. Japan, 17, Suppl. B-II, 332 (1962).

Bertaut, E. F. in Rado, G. T., and Suhl, H. ed., Spin Configuration of Ionic Structures: Theory and Practice. Magnetism, Vol. III, pp. 149-209, Academic Press, New York (1963)

Curien, H., and Donnay, J. D. H., The Symmetry of the Complete Twin, Amer. Mineralogist, 44, 1067 (1959).

Donnay, G., Corliss, L. M., Donnay, J. D. H., Elliott, N., and Hastings, J. M., Symmetry of Magnetic Structures: Magnetic Structure of Chalcopyrite, Phys. Rev. 112, 1917 (1958).

Indenbom, V. L., Relation of the Antisymmetry and Color Symmetry Groups to One-dimensional Representations of the Ordinary Symmetry Groups. Isomorphism of the Shubnikov and Space Groups, Soviet Phys.-Cryst, 4, 578 (1960).

Indenbom, V. L., Belov, N. V., and Neronova, N. N., The Color-Symmetry Point Groups, Soviet Phys.-Cryst., 5, 477 (1961).

Niggli, A., Zur Systematik und gruppentheoretischen Ableitung der Symmetrie-, Antisymmetrie- und Entartungssymmetriegruppen, Z. Krist., 111, 288 (1959).

Niggli, A., and Wondratschek, H., Die einfachen Kryptosymmetrien., Z. Krist., 114, 215 (1960).

Van der Waerden, B. L., and Burckhardt, J. J., Farbgruppen, Z. Krist., 115, 231 (1961).

Wittke, O., The Colour-Symmetry Groups and Cryptosymmetry Groups Associated with the 32 Crystallographic Point Groups, Z. Krist., 117, 153 (1962).

Wondratschek, H., and Niggli, A., Die mehrfachen Kryptosymmetrien., Z. Krist., 115, 1 (1961).

ACKNOWLEDGMENTS

The author wishes to express his sincere appreciation and thanks to the following collaborators, without whose generous help and untiring efforts the project would not have been well-crystallized.

J. Terandy and L. Mapalo are largely responsible for the engineering development of the basic diffractometer and some of its auxiliary devices. F. J. Simanonis, A. E. Schmidt, and other members of A. J. Rogers' engineering group have also participated in the design study. A. P. Hryn was a planner for the machinery fabrication group, and E. E. Klocek and G. M. Lobell coordinated the shop work for the special items. The installation of the basic unit was assisted by R. Mogil's group, and the heat-exchange unit with safety devices for the magnet were completed through collaboration of the members of Plant Engineering and Plant Service Divisions. The Datex Corporation put the automatic-electronics design into effect, and E. W. Johanson and W. C. Kaiser of the Electronics Division constructed a part of the neutron counting system. D. R. Klein and C. T. Rockhold of the Spectromagnetic Industries helped with the magnet design and construction, and the following reactor-operation personnel have closely associated with various stages of the instrumentation: F. H. Martens, H. C. Stevens, J. J. Hartig, J. H. Talboy, R. J. Fanella, J. E. Slattery, and their associates.

The author would like to convey his gratitude to his colleagues in various laboratories for stimulating discussions and for valuable suggestions, particularly to M. K. Wilkinson, W. C. Koehler, and H. A. Levy of Oak Ridge, to C. G. Shull of M. I. T., to J. M. Hastings and L. M. Corliss of Brookhaven, and to D. W. Osborne of Argonne. Grateful thanks are also due to Mrs. Iris Atoji for her efficient secretarial assistance.

REFERENCES

General References*

- Abrahams, S. C., Liquid-helium Goniometer-mounted Cryostat for a Single Crystal Automatic Diffractometer, Rev. Sci. Instr., 31, 174 (1960).
- Abrahams, S. C., Goniometer-mounted Evacuated Furnace for Single Crystal Neutron Diffractometry, Rev. Sci. Instr., 34, 113 (1963).
- Alexander, L. E., and Smith, G. S., Single-crystal Intensity Measurements with the Three-circle Counter Diffractometer, Acta Cryst., 15, 983 (1962).
- Allenden, D., and Winkworth, R., A Programmed Control System for an Automatic Neutron Spectrometer, Nucl. Instr. Methods, 23, 181 (1963).
- Ang, Wang-shon; Chang, Huang-chio; Yang, Tsi-len; Chu, Tia-shen; and Li, Kuang-ting, "Operation and Characteristics of Neutron Diffractometer," Wu Li Hsueh Pao, 17, 222 (1961).
- Arndt, U. W., and Willis, B. T. M., Automatic Neutron Diffractometer for Three-dimensional Structure-factor Determination, Rev. Sci. Instr., 34, 224 (1963); A Programmed Multi-channel Neutron Diffractometer Installation, Nucl. Instr. Methods, 24, 155 (1963).
- Atoji, M., Slow-neutron Scattering Cross Sections of Terbium, Ytterbium and Lutecium, Phys. Rev., 121, 610 (1961a).
- Atoji, M., Neutron Diffraction Studies of CaC₂, YC₂, LaC₂, CeC₂, TbC₂, YbC₂, LuC₂, and UC₂, J. Chem. Phys., 35, 1950 (1961b).
- Bacon, G. E., and Dyer, R. F., A Spectrometer for Single-crystal Neutron Diffraction, J. Sci. Instr., 32, 256 (1955).
- Bacon, G. E., and Dyer, R. F., Neutron Diffraction Instruments at a High-flux Reactor, J. Sci. Instr., 36, 419 (1959).
- Bacon, G. E., Smith, J. A. G., and Whitehead, C. D., Some Mechanical Features of a Double-crystal Neutron Spectrometer, J. Sci. Instr., 27, 330 (1950).
- Barstad, G. E. B., and Andresen, A. F., Single Crystal Goniometer for X-ray and Neutron Diffraction, Rev. Sci. Instr., 28, 916 (1957).
- Belson, H. S., Sphere Grinding and Polishing, Rev. Sci. Instr., 35, 234 (1964).
- Berger, H., Photographic Detectors for Neutron Diffraction, Rev. Sci. Instr., 33, 844 (1962a).
- Berger, H., Comparison of Several Methods for the Photographic Detection of Thermal Neutron Images, J. Appl. Phys., 33, 48 (1962b).
- Berger, H., Resolution Study of Photographic Thermal Neutron Image Detectors, J. Appl. Phys., 34, 914 (1963).

*The translated titles are indicated by quotation marks.

Berger, H., A Polaroid Film Method for Transfer Neutron Radiography, Nucl. Sci. Engineer., 18, 137 (1964).

Betzl, M., and Kleinstück, K., Über Einige Neuartige Elemente zur Steuerung und Registrierung für Ein Neutronendiffraktometer, Fortschr. Mineral., 39, 327 (1961); Die Automatisierte Messeinrichtung des Neutronendiffraktometers am Rossendorfer Forschungsreaktor, Kernenergie, 4, 923 (1961).

Blinowski, K., and Sosnowski, J., Parasitic Reflections of Neutrons in Crystal Monochromators, Nucl. Instr. Methods, 10, 289 (1961).

Boutron, F., and Mériel, P., Correction de Porte-échantillon en Diffraction de Neutrons, Bull. Soc. Franç. Minér., Crist., 83, 125 (1960).

Bowes, H., and Dyer, R. F., A Neutron Crystallography Rig Design Manual, AERE-R-4305 (1963).

Breton, C., Hubert, P., and Mériel, P., Spectromètre à Neutrons pour l'Analyse Cristalline, J. Phys. Radium, 18, 2S-3S (1957).

Brockhouse, B. N., Crystal Filter to Produce Pure Thermal Neutron Beams from Reactors, Rev. Sci. Instr., 30, 136 (1959).

Bykov, V. N., Vinogradov, S. I., Levdik, V. A., and Golovkin, V. S., A Double Crystal Neutron Spectrometer, Soviet Phys.-Cryst., 2, 626 (1957).

Caglioti, G., and Casali, F. F., Rubber Soller Slit Collimators for Neutron Spectrometry, Rev. Sci. Instr., 33, 1103 (1962).

Caglioti, G., de Agostino, E., Marsili, F., Paoletti, A., Pellegrini, U., and Ricci, F. P., "Neutron Diffraction Crystal Spectrometer at the Ispra Center," Nuovo Cimento, 10, 23: Suppl. No. 1, 17 (1962).

Caglioti, G., Paoletti, A., and Ricci, F. P., Choice of Collimators for a Crystal Spectrometer for Neutron Diffraction, Nucl. Instr., 3, 223 (1958).

Caglioti, G., Paoletti, A., Ricci, F. P., and Zocchi, M., Bibliographies on Neutron Diffraction Studies, CN bib-1 (1959).

Caglioti, G., Paoletti, A., and Ricci, F. P., On Resolution and Luminosity of a Neutron Diffraction Spectrometer for Single Crystal Analysis, Nucl. Instr. Methods, 9, 195 (1960).

Caglioti, G., and Ricci, F. P., Resolution and Luminosity of Crystal Spectrometers for Neutron Diffraction, Nucl. Instr. Methods, 15, 155 (1962).

Clayton, G. T., and Heaton, L., A Neutron Diffraction Study of Krypton in the Liquid State, ANL-6112 (1961).

Cole, H., Okaya, Y., and Chambers, F. W., Computer-controlled Diffractometer, Rev. Sci. Instr., 34, 872 (1963).

Corliss, L. M., Hastings, J. M., and Brockman, F. G., A Neutron Diffraction Study of Magnesium Ferrite, Phys. Rev., 90, 1013 (1953).

- Dachs, H., Strahlengang in einem Neutronenspektrometer bei Einkristalluntersuchungen, Z. Krist., 115, 80 (1961).
- Dachs, H., and Stehr, H., "The Use of Flat and Curved Monochromator Crystals in Neutron Spectrometer for Investigating Single Crystals," Z. Krist., 117, 135 (1962).
- de Agostino, E., "A System for the Automatic Control and the Elaboration of Information from a Neutron Spectrometer Utilizing IBM 1620 Computer," RT/EL(63)9 (1963).
- Egelstaff, P. A., The Slow-neutron Cross Section of Graphite, J. Nucl. Energy, 5, 203 (1957).
- Egelstaff, P. A., The Thermal Neutron Cross Sections of Hf, Br, V, Se, Mo, and Bi, AERE N/R 1147 (1958).
- Giacchetti, G., Musci, M., and Paoletti, G., "A Slow Neutron Crystal Spectrometer," Energia Nucl. (Milan), 10, 173 (1963).
- Goedkoop, J. A., and Loopstra, B. O., "Neutron Diffraction and Structure Studies in Kjeller," Ned. Tijdschr. Natuurk., 25, 29 (1959).
- Haas, R., and Shore, F. J., Second-order Contamination in a Neutron Crystal Spectrometer, Rev. Sci. Instr., 30, 17 (1959).
- Hagihara, S., Miyashita, K., Yoshie, T., Ohno, E., and Mogi, M., Three Neutron Diffractometers, Mitsubishi Denki Lab. Rep., 3, 111 (1962).
- Hase, W., and Kleinstück, K., Der Einfluss der Totalreflexion an den Kollimator-Lamellen auf Neutronen-Pulverdiagramme, Z. Krist., 116, 48 (1961).
- Hay, H. J., The Importance of Multiple Bragg Scattering for Neutron Crystal Spectrometers, AERE-R 2982 (1959).
- Hay, H. J., Pattenden, N. J., and Egelstaff, P. A., The Scattering of 4 \AA Neutrons by a Beryllium Crystal, Acta Cryst., 11, 228 (1958).
- Heintzelman, E. F., Stewart, J. G., and Reed, C. G., Simple Machine for Grinding and Polishing Spheres of Ferrimagnetic Materials, Rev. Sci. Instr., 33, 570 (1962).
- Henshaw, D. G., Atomic Distribution in Liquid and Solid Neon and Solid Argon by Neutron Diffraction, Phys. Rev., 111, 1470 (1958).
- Holm, M. W., Scattering of Slow Neutrons by Be and NaCl Crystals, IDO-16115 (1953).
- Hulm, J. K., and Blaugher, R. D., Superconducting Solid Solution Alloys of the Transition Elements, Phys. Rev., 123, 1569 (1961).
- Hurst, D. G., Pressesky, A. J., and Tunnicliffe, P. R., The Chalk River Single Crystal Neutron Spectrometer, Rev. Sci. Instr., 21, 705 (1950).

Ishikawa, Y., and Chikazumi, S., Design of High Power Electromagnets, Japanese J. Appl. Phys., 1, 155 (1962).

Iyengar, P. K., (in Ramachandran, G. N., ed.) Neutron Spectrometer at Trombay. Crystallography and Crystal Perfection, Academic Press, New York: pp. 279-291 (1963).

Joki, E. G., Evans, J. E., and Smith, J. R., A High Resolution Soller Slit Collimator for Use with the MTR Neutron Crystal Spectrometer, IDO-16356 (1956).

Jones, I. R., Calculation of the Optimum Dimensions of Collimators for Neutron Diffraction, Rev. Sci. Instr., 33, 1399 (1962).

Jones, I. R., and Bartolini, W., Suppression of Total Reflection of Neutrons from Collimator Surfaces, Rev. Sci. Instr., 34, 28 (1963).

Kleinstück, K., Das Neutronendiffraktometer für Beugungsexperimente am Rossendorfer Forschungsreaktor, Kernenergie, 4, 913 (1961).

Kogan, V. S., Lazarev, B. G., Zhdanov, G. S., and Ozerov, R. P., A Cryostat for Use at Hydrogen and Helium Temperatures in Neutron Diffraction Studies, Soviet Phys.-Cryst., 5, 297 (1960).

Kraśnicki, S., Pawelczyk, J., and Rapacki, H., The Cracow Neutron Crystal Spectrometer, Nukleonika Polska, 7, 223 (1962).

Kunitomi, N., Hamaguchi, Y., Sakamoto, M., and Komura, S., Neutron Diffractometer JAERI, J. Phys. Soc. Japan, 17, Suppl. B-II, 354 (1962).

Lambe, K. A. D., Rouse, K. D., Valentine, T. M., and Willis, B. T. M., Single-crystal Neutron Diffraction Instruments at DIDO, AERE-R-3709 (1961).

Langdon, F., and Frazer, B. C., Automatic Control and Programming System for Single Crystal Diffractometry, Rev. Sci. Instr., 30, 997 (1959).

Levy, H. A., and Sharrah, P. C., Pattern of Scattering from a Thin Cylindrical Shell Filled with an Absorbing Medium, ORNL-1832 (1955).

Loopstra, B. O., Neutron Beam Experiments, Atoomenergie Haar Toepassing, 4, 253 (1962).

Lowde, R. D., Single-crystal Neutron Diffraction Analysis, Nature, 167, 243 (1951).

Lutz, G., Experimental Technology in Neutron Diffraction, Kerntechnik, 2, 391 (1960).

Maschinen Fabrik Augsburg-Nuremberg A. G. München, German Neutron Diffraction Apparatus, Nucl. Energy, 14, 269 (1960).

McAlpin, W., Design of a Third Axis for the Chalk River Crystal Neutron Spectrometer, Nucl. Instr. Methods, 25, 205 (1964).

- McReynolds, A. W., Neutron Monochromator Crystals - Fe_3O_4 and Ge, Phys. Rev., 88, 958 (1952).
- Mead, W., and Sparks, J. T., The Livermore Neutron Diffraction Spectrometer, Bull. Amer. Phys. Soc., 5, 464 (1960).
- Miyake, S., Hoshino, S., Suzuki, K., Katsuragi, H., Hagihara, S., Yoshie, T., and Miyashita, K., Single-crystal Neutron Diffractometer with Automatic Programming-control System, J. Phys. Soc. Japan, 17, Suppl. B-II, 358 (1962).
- Mueller, M. H., Heaton, L., Sidhu, S. S., and Terandy, J., Argonne Dual Neutron Diffractometers Using a Single Primary Beam, ANL-6537 (1962).
- Mueller, M. H., Heaton, L., and Sidhu, S. S., Full Circle Goniostat for Diffraction Intensity Data, Rev. Sci. Instr., 34, 74 (1963).
- Nathans, R., Shull, C. G., Shirane, G., and Andresen, A., The Use of Polarized Neutron in Determining the Magnetic Scattering by Iron and Nickel, J. Phys. Chem. Solids, 10, 138 (1959).
- O'Connor, D., and Bońkowski, L., A Universal Double-crystal Neutron Spectrometer, Acta Phys. Polon., 18, 265 (1959).
- Ozerov, R. P., Kiselev, S. V., Karpovich, I. R., Goman'kov, V. I., and Loshmanov, A. A., A Remotely Controlled Neutron Diffractometer Based on a GUR-3 Unit, Soviet Phys.-Cryst., 5, 294 (1960).
- Pattenden, N. J., and Baston, A. H., The Construction and Operation of a Single Crystal Neutron Spectrometer, AERE-NP/R-2251 (1957).
- Pepinsky, R., Frazer, B. C., and McKeown, M. L., New Goniometers for Single-crystal Neutron Diffraction Studies, Rev. Sci. Instr., 25, 699 (1954).
- Pepinsky, R., and Frazer, B. C., Modification of General Electric SPG Goniometer for Single-crystal Neutron Diffraction Measurements, Rev. Sci. Instr., 26, 402 (1955).
- Petch, H. E., Brouwer, W., Torrie, B. H., and Brown, I. D., A Neutron Diffractometer for a Pool Reactor, Research Reactor J., 1, No. 1, 8 (1960).
- Peterson, S. W., and Levy, H. A., A Single Crystal Neutron Spectrometer for a High Flux Reactor, Abstract, ACA Annual Meeting, Cornell University (1959).
- Placzek, G., and Van Hove, L., Interference Effects in the Total Neutron Scattering Cross-Section of Crystals, Gennaio Il Nuovo Cimento, 1, 233 (1955).
- Ponce de Leon, J. M., and Diaz, L. M., Construccion y Puesta a Punto de un Espectrometro de Cristal para Neutrones, An. R. Soc. Esp. Fis. Quim. Ser. A., 58, No. 3-4, 119 (1962).
- Prince, E., The NRL Automatic Single Crystal Neutron Diffractometer, NRL-5744 (1961).

- Prince, E., and Abrahams, S. C., Single-crystal Automatic Neutron Diffractometer, Rev. Sci. Instr., 30, 581 (1959).
- Rush, J. J., Taylor, T. I., and Havens Jr., W. W., Proton Motions in Solids by Slow Neutron Scattering Cross Sections, J. Chem. Phys., 35, 2265 (1961).
- Sabine, T. M., Neutron Diffraction Research in Australia, J. Phys. Soc. Japan, Suppl. B-II, 352 (1962).
- Sabine, T. M., An Analytical Treatment of the Geometrical Properties of the Three-circle Goniometer, Aust. J. Phys., 16, 272 (1963).
- Sabine, T. M., and Browne, J. D., A Geometrical Consideration in the Design of Neutron Spectrometers, Acta Cryst., 16, 435 (1963).
- Sabine, T. M., Pryor, A. W., and Hickman, B. S., The Scattering of Long Wavelength Neutrons by Irradiated Beryllium Oxide, AAEC/TM 140 (1962).
- Sailor, V. L., Foote Jr., H. L., Landon, H. H., and Wood, R. E., High Resolution Crystal Spectrometer for Neutrons, Rev. Sci. Instr., 27, 26 (1956).
- Salinger, G. L., and Wheatley, J. C., Magnetic Susceptibility of Materials Commonly Used in the Construction of Cryogenic Apparatus, Rev. Sci. Instr., 32, 872 (1961).
- Santoro, A., and Zocchi, M., Geometrical Properties of a Four-circle Neutron Diffractometer for Measuring Intensities at an "optimum" Azimuth of the Reflecting Planes, Acta Cryst., 17, 597 (1964).
- Sawyer, R. B., Wollan, E. O., Bernstein, S., and Peterson, K. C., A Bent Crystal Neutron Spectrometer and Its Application to Neutron Cross-section Measurement, Phys. Rev., 72, 109 (1947).
- Schermer, R. I., A Crystal Monochromator for Neutron Spectrometry, TID-14863 (1960).
- Shull, C. G., Production of Highly Polarized Neutron Beams by Bragg Reflection from Ferromagnetic Crystals, Phys. Rev., 81, 626 (1951).
- Shull, C. G., Neutron and X-ray Diffraction Studies of Solids, AFOSR TR 60-111 (1960).
- Sikkema, C. P., Elimination of End Effects in Proportional Counters, Nucl. Instr., 1, 148 (1957).
- Smith, H. G., Use of Polaroid Film in Neutron and X-ray Diffraction, Rev. Sci. Instr., 33, 128 (1962).
- Smith, H. G., and Holcomb, D. L., Modified Polaroid Film Holder for X-ray and Neutron Diffraction, Rev. Sci. Instr., 34, 1441 (1963).
- Start, P. L., and Thring, M. W., Design of Laboratory Furnaces, J. Sci. Instr., 37, 17 (1960).
- Stehr, H., Messgenauigkeit und Verkürzung der Messdauer bei der Untersuchung von Einkristallen mit Neutronen, Z. Krist., 118, 263 (1963).

Szabó, P., On the Optimum Dimensions of Collimators for Neutron Diffraction, Nucl. Instr. Methods, 5, 184 (1959).

Szabó, P., On the Effect of Total Reflection on the Optimum Dimensions of Collimators for Neutron Crystal Spectrometers and Diffractometers, Nucl. Instr. Methods, 6, 183 (1960a).

Szabó, P., Optimum Dimensions of Collimators for Neutron Crystal Spectrometers and Diffractometers, Acta Cryst., 13, 988 (1960b).

Szabó, P., and Krén, E., "The Orientation of Large Single Crystals Prepared for the Purpose of Neutron-Monochromatization," Magy Tud. Akad. Kozp. Fiz. Kut. Ins. Kozlemen., 7, 366 (1959).

Szabó, P., Krén, E., and Gordon, J., High Intensity Neutron Diffractometer, Acta Phys. Acad. Sci. Hung., 15, 203 (1963).

Takei, W. J., Frazer, B. C., and Shirane, G., Neutron Diffraction Facility at the Westinghouse Testing Reactor, Bull. Amer. Phys. Soc., 5, 464 (1960).

Thewlis, J., Neutron Radiography, British J. Appl. Phys., 7, 345 (1956).

Wajima, J. T., Rustad, B. M., and Melkonian, E., Germanium Crystal as a Neutron Monochromator and the Determination of Its Higher Order Contaminations, J. Phys. Soc. Japan, 15, 630 (1960).

Wang, S. P., Shull, C. G., and Phillips, W. C., Photography of Neutron Diffraction Patterns, Rev. Sci. Instr., 33, 126 (1962).

Wanic, A., and Riste, T., α -Fe₂O₃ as a Crystal Monochromator, Rev. Sci. Instr., 31, 214 (1960).

Weiss, R. J., Hastings, J. M., and Corliss, L. M., Neutron Crystal Monochromators, Phys. Rev., 83, 863 (1951).

Whittemore, W. L., Differential Neutron Thermalization, GA-3409 (1962).

Whittemore, W. L., and McReynolds, A. W., Effects of Chemical Binding on the Neutron Cross Section of Hydrogen, Phys. Rev., 113, 806 (1959).

Willis, B. T. M., Some Theoretical Properties of the Double-crystal Spectrometer Used in Neutron Diffraction, Acta Cryst., 13, 763 (1960a).

Willis, B. T. M., Use of a Two-circle Device to Obtain Three-dimensional Neutron Diffraction Data, Acta Cryst., 14, 90 (1960b).

Willis, B. T. M., Some Geometrical Properties of the Three-circle Goniometer, AERE-R 3773 (1961).

Willis, B. T. M., Single-crystal Neutron Diffraction Equipment at the DIDO Reactor, J. Sci. Instr., 39, 590 (1962).

Willis, B. T. M., Lambe, K. A. D., and Valentine, T. M., A Neutron Diffraction Study of the Thermal Motions of the Atoms in Urania and Thoria, AERE-R 4001 (1962).

Wollan, E. O., and Shull, C. G., The Diffraction of Neutrons by Crystalline Powders, Phys. Rev., 73, 830 (1948).

Wollan, E. O., Shull, C. G., and Marney, M. C., Laue Photography of Neutron Diffraction, Phys. Rev., 73, 527 (1948).

Wollan, E. O., Wilkinson, M. K., Koehler, W. C., Cable, J. W., and Child, H. R., The ORNL Neutron Diffractometer for Magnetic Studies, Bull Amer. Phys. Soc., 5, 464 (1960).

Wooster, W. A., Geometrical Factors Influencing the Design of Automatic Single-crystal X-ray and Neutron Diffractometers, J. Sci. Instr., 40, 14 (1963).

Wooster, W. A., Wooster, A. M., and Wooster, G. A., (in Ramachandran, G. N., ed.) "An Automatic X-ray Diffractometer." Crystallography and Crystal Perfection, Academic Press, New York: pp. 295-308 (1963).

Yamzin, I. I., Apparatus for Neutron Diffraction Structural Analysis, Soviet Phys.-Cryst., 4, 397 (1959).

Yamzin, I. I., Staritsyn, V. E., and Nozik, Yu. Z., A Small Neutron Diffractometer, Soviet Phys.-Cryst., 7, 58 (1962).

Yamzin, I. I., Kuz'minov, Yu. S., and Staritsyn, V. E., A Neutron Diffractometer, Soviet Phys.-Cryst., 8, 234 (1963).

Zinn, W. H., Diffraction of Neutrons by a Single Crystal, Phys. Rev., 71, 752 (1947).

Živanović, M. D., Jović, D. M., and Konstantinović, J. M., Double-crystal Neutron Spectrometer, Bull. Instr. Nucl. Sci., 11, 59 (1961).

Reference Books

Allen, W. D., Neutron Detection, Philosophical Library, New York (1960).

Bacon, G. E., Neutron Diffraction, 2nd. ed., Clarendon Press, Oxford (1962).

Beck, C. K., ed. (1957). Nuclear Reactors for Research. London, MacMillan.

Blizard, E. P., and Abbott, L. S., ed., Reactor Handbook. Vol. III, Part B, Shielding, 2nd. ed., Interscience Publishers, New York (1962).

Brickwedde, F. G., ed. (1962). Temperature, Its Measurement and Control in Science and Industry. Vol. III. Part I. Basic Concepts, Standards and Methods. Reinhold, New York.

Campbell, I. E., ed., High-temperature Technology, John Wiley and Sons, New York (1956).

Curtiss, L. F. (1959). An Introduction to Neutron Physics. New York, Van Nostrand.

- Dahl, A. I., ed., Temperature, Its Measurement and Control in Science and Industry. Vol. III. Part 2. Applied Methods and Instruments, Reinhold, New York (1962).
- Furnas, T. C., Single Crystal Orienter Instruction Manual, General Electric, Milwaukee (1956).
- Gillespie, A. B., Signal Noise and Resolution in Nuclear Counter Amplifiers, Pergamon Press, London (1953).
- Glasstone, S. (1955). Principles of Nuclear Reactor Engineering. New York, Van Nostrand.
- Goldsmith, A., Waterman, T. E., and Hirschborn, H. J., Handbook of Thermophysical Properties of Solid Materials, MacMillan, New York (1961).
- Goodenough, J. B. (1962). Magnetism and Chemical Bond. New York, Interscience-Wiley.
- Hoare, F. E., Jackson, L. C., and Kurti, N., ed., Experimental Cryophysics, Butterworths, London (1961).
- Hughes, D. J., Pile Neutron Research, Addison-Wesley, Cambridge, Mass. (1953).
- Hughes, D. J. (1954). Neutron Optics. New York, Interscience Publishers.
- Hughes, D. J. (1957). Neutron Cross Sections. New York, Pergamon Press.
- International Tables for X-Ray Crystallography (1952, 1959 and 1962). Vol. I, II and III. Birmingham, Kynoch Press.
- Kolm, H., Lax, B., Bitter, F., and Mills, R., ed., High Magnetic Fields, John Wiley and Sons, New York (1962).
- McClintock, M., Cryogenics, Reinhold, New York (1964).
- Mott, N. F., and Massey, H. S. W., The Theory of Atomic Collisions, 2nd ed., Clarendon Press, Oxford (1949).
- National Bureau of Standards Handbook 63. Protection Against Neutron Radiation up to 30 Million Electron Volts, U. S. Government Printing Office, Washington D. C. (1957).
- Nesmeyanov, A. N., English edition by Gary, R., Vapor Pressure of the Chemical Elements, Elsevier, Amsterdam (1963).
- Peiser, H. S., Rooksby, H. P., and Wilson, A. J. C., ed., X-Ray Diffraction by Polycrystalline Materials, Chapman and Hall, London (1955).
- Price, B. T., Horton, C. C., and Spinney, K. T., Radiation Shielding, Pergamon Press, New York (1957).
- Price, W. J., Nuclear Radiation Detection, McGraw-Hill, New York (1958).

Samsonov, G. V., Plenum Press Handbooks of High-temperature Materials. No. 2. Properties Index, Plenum Press, New York (1964).

Shaffer, T. B., Plenum Press Handbooks of High-temperature Materials. No. 1. Materials Index, Plenum Press, New York (1964).

Tipton, C. R., ed., Reactor Handbook, Vol. I. Material. 2nd. ed., Interscience Publishers, New York (1960).

White, G. K., Experimental Techniques in Low-temperature Physics, Clarendon Press, Oxford (1959).

Wirtz, K., and Beckurts, K. H. (1958). Elementare Neutronen Physik. Berlin, Springer-Verlag.

Wood, E. A., Crystal Orientation Manual, Columbia University Press, New York (1963).

Review Articles

Atoji, M. in Cotton, F. A., ed. (1964). Neutron Diffraction. Progress in Inorganic Chemistry. in preparation. New York, Interscience Publishers.

Bacon, G. E. in Guggenheim, E. A., Mayer, J. E. and Tomkins, F. C., ed. (1963). Applications of Neutron Diffraction in Chemistry. The International Encyclopedia of Physical Chemistry and Chemical Physics. Topic 11. The Ideal Crystalline State. Vol. I. New York, Pergamon Press.

Bacon, G. E., and Lonsdale, K., Neutron Diffraction, Rep. Prog. Phys., 16, 1 (1953).

Bacon, G. E., and Thewlis, J. (1949). Neutron Diffraction. Proc. Roy. Soc., London, A196, 50.

Barschall, H. H. in Flügge, S., ed. (1958). Detection of Neutrons. Handbuch der Physik. Vol. XLV, pp. 437-486. Berlin, Springer-Verlag.

Bertaut, E. F. in Rado, G. T., and Suhl, H., ed. (1963). Spin Configurations of Ionic Structures: Theory and Practice. Magnetism, Vol. III. pp. 149-209. New York, Academic Press.

Bethe, H. A. (1937). Nuclear Physics. Rev. Mod. Physics, 9, 69.

Bollinger, L. M. in Ajzenberg-Selove, F., ed. (1960a). Techniques of Slow Neutron Spectroscopy. Nuclear Spectroscopy, Part A, pp. 342-357. New York, Academic Press.

Bollinger, L. M. in Ajzenberg-Selove, F., ed. (1960b). Slow Neutron Resonances. Nuclear Spectroscopy, Part A, pp. 416-451. New York, Academic Press.

- Buckingham, B. R. S., Parker, K., and Pendlebury, E. D., Neutron Cross Sections of Selected Elements and Isotopes for Use in Neutronics Calculations in the Energy Range 0.025 eV-15 MeV, AWRE 0-28/60 (1961).
- Cassels, J. M. in Frisch, O. R., ed. (1950). The Scattering of Neutrons by Crystals. Progress in Nuclear Physics, Vol. I, pp. 185-215, London, Butterworth-Springer.
- Corliss, L. M. in Francombe, H. M. and Heeger, A. J., ed. (1963). Magnetic Structures and Neutron Diffraction. Magnetic Materials Digest. The Literature of 1962. pp. 29-35. Philadelphia, M. W. Lads.
- Corruccini, R. J., and Gniewek, J. J., Thermal Expansion of Technical Solids at Low Temperatures, National Bureau of Standards, Monograph 29, U. S. Government Printing Office, Washington D. C. (1961).
- Cryogenic Materials Data Handbook (1961, Quarterly hereafter). U. S. Department of Commerce, Series 171809-1, -2 etc. Washington D. C., U. S. Government Printing Office.
- deGennes, P. G. in Rado, G. T. and Suhl, H., ed. (1963). Theory of Neutron Scattering by Magnetic Crystals. Magnetism, Vol. III, pp. 115-147. New York, Academic Press.
- Feld, B. T. in Segré, E., ed. (1953). The Neutron. Experimental Nuclear Physics, Vol. II, pp. 208-586. New York, John Wiley and Sons.
- Goedkoop, J. A., Neutron Diffraction, Philips Tech. Rev., 23, 69 (1961/62).
- Goodenough, J. B. in Rado, G. T. and Suhl, H., ed. (1963). Magnetism and Crystal Structure in Nonmetals. Magnetism, Vol. III, pp. 1-62. New York, Academic Press.
- Harris, P. M. and Erickson, R. A. in Williams, F. D., ed. (1962). Diffraction Methods of Molecular Structure Determination. Methods of Experimental Physics, Vol. III, pp. 265-358. New York, Academic Press.
- Hastings, J. M. and Corliss, L. M. in Weissberger, A., ed. (1960). Neutron Diffraction. Technique of Organic Chemistry, Vol I, Part 2, pp. 1763-1797. New York, Interscience Publishers.
- Hughes, D. J., and Schwartz, R. B., Neutron Cross Sections, BNL-325, 2nd. ed. (1958).
- Hughes, D. J., Magurno, B. A., and Brussel, M. K., Neutron Cross Sections, BNL-325, 2nd. ed., Suppl. I. (1960).
- International Atomic Energy Agency (1962). Pile Neutron Research in Physics. Vienna, IAEA.
- Johnson, V. J., ed., Properties of Materials at Low Temperature (Phase I). A Compendium, Pergamon Press, New York (1961).
- King, N. M. in Frisch, O. R., ed., Semiconductor Counters, Progress in Nuclear Physics., 9, pp. 27-69. MacMillan, New York (1964).

Landolt-Börnstein (1962). Vol. II, Part 9. Chapters 29-1 to 29-3, Berlin, Springer-Verlag.

Matthias, B. T., Geballe, T. H., and Compton, V. B., Superconductivity, Rev. Mod. Phys., 35, 1 (1963). Errata: Rev. Mod. Phys., 35, 414 (1963).

Nathans, R., and Pickart, S. J., in Rado, G. T., and Suhl, H., ed., Spin Arrangements in Metals, Magnetism, Vol. III, pp. 211-269. Academic Press, New York (1963).

Netherlands'-Norwegian Reactor School (1962). Advanced Course on Neutron Crystal Spectrometry. Kjeller, Institutt for Atomenergi.

Porter, C. E. (1963). Statistical Properties of Spectra. Physics Today, 16, No. 2, 26.

Ringo, G. R., in Flügge, S., ed., Neutron Diffraction and Interference, Handbuch der Physik, Vol. XXXII, pp. 552-642. Springer-Verlag, Berlin (1957).

Riste, T. (1961). Neutron Diffraction Studies of Spin Fluctuations in Magnetic Substances. KR-5.

Roberts, B. W., in Mendelssohn, K., ed., Superconductive Materials and Some of Their Properties, Progress in Cryogenics, Vol. 4, pp. 159-231. Academic Press, New York (1964).

Selove, W., in Ajzenberg-Selove, F., ed. (1960). The Interactions of Neutrons with Matter. Nuclear Spectroscopy, Part A, pp. 335-341. New York, Academic Press.

Shull, C. G., and Wollan, E. O. (1948). X-Ray, Electron and Neutron Diffraction, Science, 108, 69.

Shull, C. G., and Wollan, E. O. in Seitz, F. and Turnbull, D., ed. (1956). Applications of Neutron Diffraction to Solid State Problems. Solid State Phys. Vol. II, pp. 138-217. New York, Academic Press.

Sidhu, S. S., Heaton, L., and Mueller, M. H. in Finniston, H. M. and Howe, J. P., ed. (1961). Some Applications of Neutron Diffraction. Progress in Nuclear Energy, Ser. V, Vol. III, pp. 419-450. New York, Pergamon Press.

Wilkinson, M. K. (1954). Techniques and Applications of Neutron Diffraction. Amer. J. Phys., 22, 263.

Wilkinson, M. K., Wollan, E. O. and Koehler, W. C. in Segré, E., ed. (1961). Neutron Diffraction. Ann. Rev. Nucl. Sci. Vol. XI, pp. 303-348. Palo Alto, Annual Reviews.